Historical Faulting, Chronostratigraphy, and Paleoseismicity of the Central Nevada Seismic Belt

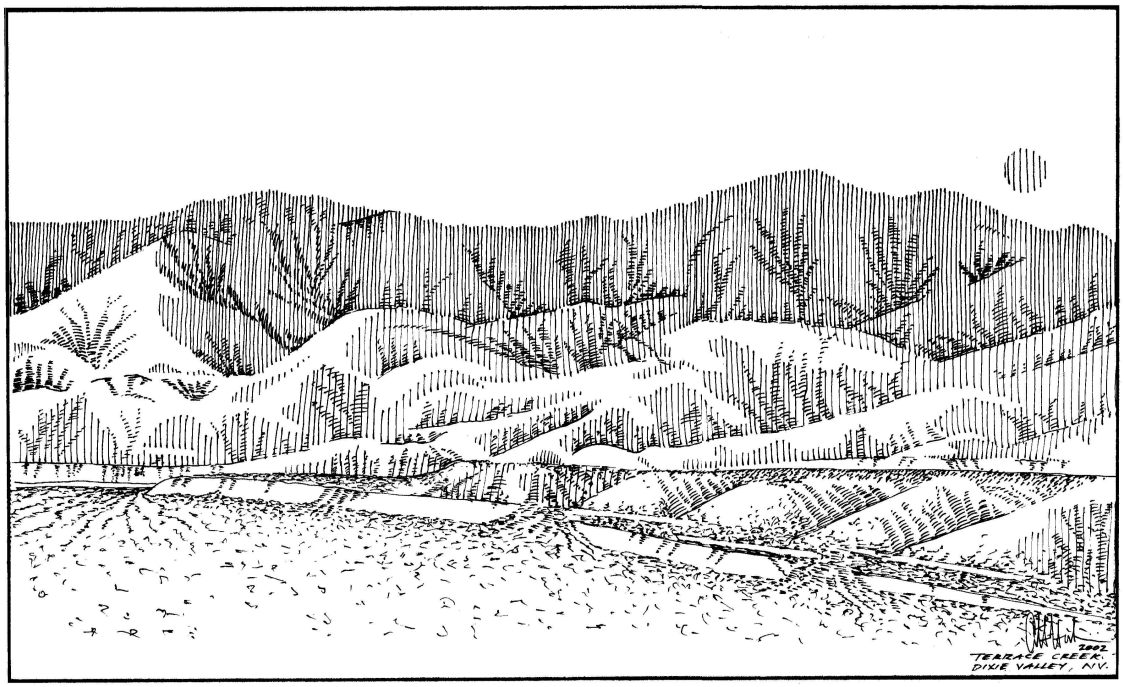

Field Guide
2002 Pacific Cell Friends of the Pleistocene Field Trip
September 20-22, 2002

Historical Faulting, Chronostratigraphy, and Paleoseismicity of the Central Nevada Seismic Belt

Friends of the Pleistocene
Pacific Cell

2002 Fall Field Trip
September 20-22, 2002

Field Trip Guidebook

Organized by:
John Caskey

Edited by:
John Caskey

Trip Leaders:

John Caskey, *San Francisco State University*
John W. Bell and Alan R. Ramelli, *Nevada Bureau of Mines and Geology*
Mackay School of Mines, University of Nevada, Reno
Kenneth D. Adams, *Desert Research Institute, Reno, Nevada*
Marith C. Reheis, *U.S. Geological Survey, Denver, CO*

Other Contributors:

D. Burton Slemmons, *2905 Autumn Haze Lane, Las Vegas, NV*
Steven G. Wesnousky, *Center for Neotectonic Studies, University of Nevada, Reno*
Eric W. Ford, Carolyn J. Domrose, Gary Schneider, Michael W. Goebel, Nathan W. Smith, Tandis S. Bidgoli, and Anne Marie Scherer, *San Francisco State University*

Sponsored by:
Department of Geosciences
San Francisco State University

Table of Contents

List of Figures

List of Contributing Articles and Stop Descriptions

DAY 2

DAY 3

Introduction

Welcome to the 2002 Pacific Cell FOP! This year's trip brings us to the central Nevada seismic belt named by Wallace (1984) for the belt-like clustering of multiple, large-magnitude, historical earthquakes. The central Nevada seismic belt is defined by a north-trending zone of concentrated seismicity that includes a half dozen major surface rupturing earthquakes (see Road Log, Figure 1, inset) including: the 1915 Pleasant Valley (M_s7.7); 1932 Cedar Mountain (M_s7.2); the 1954 Rainbow Mountain (M_s6.3); 1954 Stillwater (M_s7.0); 1954 Fairview Peak (M_s7.2); and 1954 Dixie Valley (M_s6.8) earthquakes. Recent GPS studies by Thatcher et al. (1999) and Svar et al. (2001) show that levels of modern crustal strain across the central Nevada seismic belt continue to be elevated with respect to adjacent regions. Many of the results and ideas from recent and ongoing research presented on this trip are geared toward understanding contemporary tectonic processes in the western Basin and Range by focusing on the historical faulting, chronstratigraphy, and paleoseismicity in the vicinity of the 1954 earthquake sequence (Road Log, Figure 1).

The trip begins in the Rainbow Mountain area (Road Log, Figure 1), where the 1954 earthquake sequence initiated in July and August of 1954. We then follow the 1954 earthquake sequence to Fairview Peak, site of the December 16 event, and then northward into Dixie Valley where the culminating Dixie Valley earthquake followed on the heals of the Fairview Peak event by only 4 minutes and 20 seconds.

Rainbow Mountain lies on the eastern side of the Lahontan Mountains where Roger Morrison conducted his seminal research on the stratigraphy of the pluvial Lake Lahontan basin (e.g., Morrison, 1964, 1991). The chronostratigraphy defined by Morrison is the basic framework for not only unraveling the structural relations exposed in our fault trenches at Rainbow Mountain (Stop 1-1), but also for developing a regional stratigraphic chronosequence that extends beyond the Lahontan basin and into Dixie Valley (Stops 1-3 and 2-3). On Day 1 we will examine evidence for smaller late Holocene pluvial lakes in the Lahontan basin (Stop 1-2) that bears on our understanding of the paleoclimate record, archaeology of the Great Basin, and recent paleoseismicity of the Carson Desert region. We will also discuss the regional evidence for very large pre-late Pleistocene lakes of the Great Basin (Stop 1-4).

The large 1954 earthquakes, dramatic surface faulting, and classic Basin and Range structure and tectonic geomorphology in the Fairview Peak and Dixie Valley region has drawn the attention of other renown geologists. Burt Slemmons (1957) conducted his initial pioneering work in the field of active faulting in this area. His paper "Geologic Effects of the Dixie Valley-Fairview Peak, Nevada, Earthquakes of December 16, 1954" studying the contemporary tectonics of the Basin and Range province. At Stops 1-3 and 2-2 we will visit some of the spectacular 1954 scarp exposures and features described by Burt in his original report.

Bob Wallace, another great pioneer in the field of neotectonics, was inspired by the record of late Pleistocene to recent of faulting that is so well-preserved in the high desert of central Nevada. His ideas on the morphology and ages of scarps and their application to paleoseismology and patterns and timing of late Quaternary tectonics of the Great Basin represent some of the great contributions to the field of neotectonics (e.g., Wallace, 1977, 1984a, 1984b; Wallace and Whitney, 1984). Days 2 and 3 take us

northward to the Stillwater seismic gap where Wallace developed and applied many of his original ideas on geomorphic characteristics and ages of fault scarps (Stop 2-1).

The classic Basin and Range architecture of Dixie Valley has motivated geologists and geophysicists alike to explore the valley's geology from bottom to top. George Thompson and colleagues at Stanford led an intensive, multifaceted geophysical survey of the valley in the 1960's aimed at an understanding its 3-dimensional structure (Thompson et al., 1967). They also recognized that the pluvial lake record offered the opportunity to characterize Holocene deformation across the Dixie Valley fault (Thompson and Burke, 1973). Our more recent studies in the valley have built on the observations and data of Thompson and others to further our understanding of both the subsurface structure (Stop 2-2) and the Holocene tectonic and isostatic signals of deformed pluvial lake shorelines (Stop 3-1).

The research and ideas presented on this trip are largely inspired and made possible by a solid foundation of original ideas put in place by some of the truly great geologists of our time. Our work has been primarily to fill in the details.

John Caskey
San Francisco, CA
September, 2002

Acknowledgements

This year's FOP was made possible by the help of many people. Warm gratitude goes out to all the trip leaders and guidebook contributors for their enthusiasm and support; Alan Ramelli, Gary Schneider, and Rick Ford for finding the time to help with some eleventh hour fieldwork to help fill a large gap in the shoreline rebound data; Gary Schneider, Ken Adams, and Maria Ducey for helping to dig those last-minute soil pits and for sacrificing their backs for road maintenance; Carolyn Domrose for field assistance, editorial assistance on the guidebook, and help with trip logistics; Tom Sawyer for field assistance and helping out with trip logistics; Bud Burke for sharing advice and for his never-ending support and enthusiasm; Ken Adams, John Bell, Craig dePolo, and Alan Ramelli for all the thought provoking discussions over the years; Burt Slemmons and Steve Wesnousky for all their support and invaluable mentoring; John Wakabayashi for advice, encouragement, and Bigfoot Ale; a very special thanks to Anna Henke who's beautiful artwork adorns the the guidebook cover and T-shirts; Doug Lafarge for advice on the guidebook and for handling the FOP hub; all the geoscience students and faculty at SFSU for support and encouragement; the folks who have helped to pull this year's trip off and don't even know it yet; and the way-too-many-to-mention-here who have helped out in so many ways over the years. But it's the enormous enthusiasm and commitment of all the Friends that really make these special gatherings possible, so thank you all for making this year's and every year's FOP happen.

References

Bell, J. W., 1984, Quaternary fault map of Nevada, Reno Sheet, Map 79: Nevada Bureau of Mines and Geology.

Caskey, S. J., Wesnousky, S. G., Zhang, P., and Slemmons, D. B., 1996, Surface faulting of the 1954 Fairview Peak (Ms7.2) and Dixie Valley (Ms6.9) earthquakes, central Nevada: Bulletin of the Seismological Society of America, v. 86, no. 3, p. 761-787.

Dohrenwend, J. C., Schell, B. A., Menges, C. M., Moring, B. C., and McKittrick, M. A., 1996, Reconnaissance photogeologic map of young (Quaternary and late Tertiary) faults in Nevada, Open File Report, OFR 96-2: Nevada Bureau of Mines and Geology, in cooperation with the U.S. Geological Survey, scale 1:1,000,000.

Doser, D., 1986, Earthquake processes in the Rainbow Mountain-Fairview Peak-Dixie Valley, Nevada region 1954-1959: Journal of Geophysical Research, v. 91, p. 12572-12586.

Morrison, R.B., 1964, Lake Lahontan: Geology of the southern Carson Desert, Nevada: U.S. Geological Survey Professional Paper 401, 156 p.

Morrison, R.B., 1991, Quaternary stratigraphic, hydrologic and climatic history of the Great Basin, with emphasis on Lakes Lahontan, Bonneville, and Tecopa, in Morrison, R.B., ed., Quaternary nonglacial geology: Conterminous U.S.: Boulder, Colo, Geological Society of America, The Geology of North America, v. K-2, p. 283-320.

Slemmons, D.B. (1957). Geological effects of the Dixie Valley-Fairview Peak, Nevada, earthquakes of December 16, 1954, Bull. Seism. Soc. Am. 47**,** 353-375.

Svarc, J.L., J.C. Savage, W.H. Prescott, and A.R. Ramelli, 2002, Strain accumulation and rotation in western Nevada, 1993-2000: Journal of Geophysical Research, v. 107, no. B5, 10.1029/2001JB000579.

Thatcher, W., G.R. Foulger, B.R. Julian, J. Svarc, E. Quilty, and G.W. Bawden, 1999, Present day deformation across the Basin and Range Province, western United States: Science, v. 283, p. 1714-1718.

Thompson, G.A., L.J. Meister, A.T. Herring, T.E. Smith, D.B. Burke, R.L. Kovach, R.O. Burford, I. A Salehi, and M.D. Wood, 1967, Geophysical study of Basin-Range structure, Dixie Valley region, Nevada: Part VI, Air Force Cambridge Research Labratories Report AFCRL-66-848, 72 p.

Thompson, G.A., and D.B. Burke, 1973, Rate and direction of spreading in Dixie Valley, Basin and Range province, Nevada, GSA Bull., 84, 627-632.

Wallace, R.E., Profiles and ages of young fault scarps, north-central Nevada, Geol. Soc. Am. Bull., 88, 1267-1281.

Wallace, R.E. (1984a). Patterns and timing of late Quaternary faulting in the Great Basin province and relation to some regional tectonic features, J. Geophys. Res. 89**,** 5763-5769.

Wallace, R.E. (1984b). Fault scarps formed during the earthquakes of October 2, 1915, in Pleasant Valley, Nevada, and some tectonic implications, U. S. Geol. Surv. Prof. Pap. 1274-A**,** 1-33.

Wallace, R.E., and Whitney, R.A. (1984). Late Quaternary history of the Stillwater seismic gap, Nevada, Bull. Seism. Soc. Am. 74**,** 301-314.

FOP Road Log

Fallon to Rainbow Mountain
(Directions to Thursday night's camp site)

Day 1
Rainbow Mountain to Terrace Creek

Day 2
Terrace Creek to Dixie Hot Springs

Day 3
Terrrace Creek to Dixie Comstock area

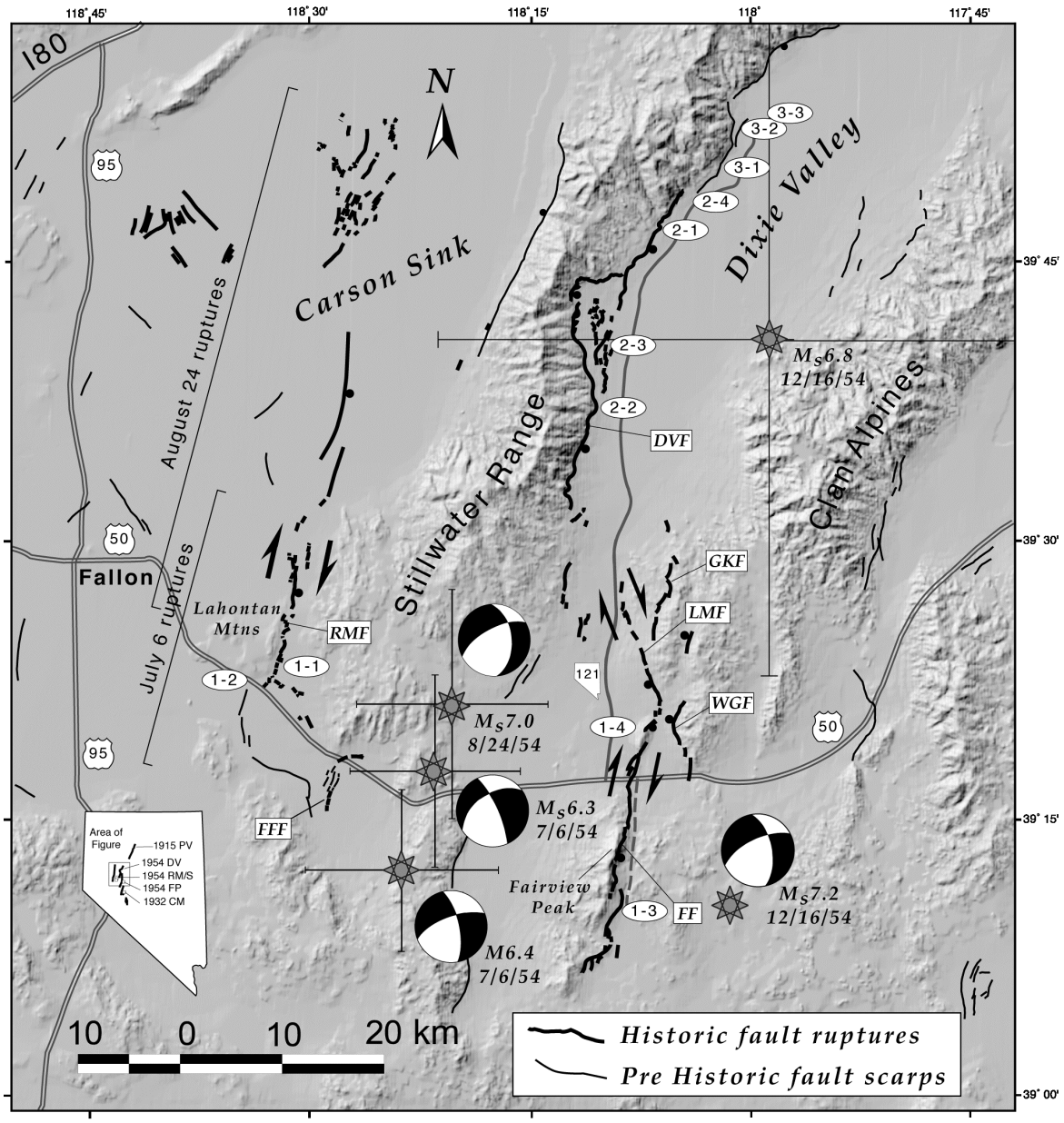

Figure 1 - Field trip route map showing the locations of field trip stops (labelled ovals 1-1 through 3-2), earthquake rupture zones (bold lines) of the July 6 and August 24 Rainbow Mountain-Stillwater and December 16, 1954 Fairview Peak and Dixie Valley earthquake sequence (Caskey et al.; 1996; in prep), and other late Quaternary faults (Bell, 1984; Dohrenwend et al., 1996). Ball on the down-thrown side of faults. Focal mechanisms and locations (stars with associated location uncertainty bars) are from Doser (1986). Inset map shows locations and generalized rupture zones associated with the the 1915 Pleasant Valley (PV), 1932 Cedar Mountain (CM), and 1954 Fairview Peak (FP), Dixie Valley (DV), and Rainbow Mountain-Stillwater (RM/S) earthquakes. Abbreviations: Fault names (boxes); DVF - Dixie Valley fault; FF - Fairview fault; FFF - Fourmile Flat fault; GKF - Gold King fault; LMF - Louderback Mountains fault; RMF -Rainbow Mountain fault; and WGF - West Gate fault.

Road Log

FALLON to RAINBOW MOUNTAIN
(Directions to Thursday night's pre-trip Gathering of Friends and camp site, September 19)

Approximate mileage	
0.0	**Reset odometer at intersection with U.S. Hwy 95 south (Taylor St.). Proceed east on U.S. Hwy 50.**
2	Fallon (Figure 1) is located in the southern Carson Desert, the type locale for the extensive stratigraphic studies of Lake Lahontan by Morrison (1964), which forms the basis for much of the chronostratigraphy in western Nevada. Lake Lahontan occupied more than 21,000 km^2 in the western Basin and Range, first during the mid-Pleistocene and then later during the late Wisconsin glacial period, principally between 13-30 ka. The pluvial sequence includes alternating intervals of deep-water lacustrine deposition with subaerial alluvial deposition beginning about 1 Ma. For the most recent detailed description of Lake Lahontan stratigraphy, the refer to Morrison (1991). The principal Lake Lahontan stratigraphic units in the Fallon region include the lacustrine Eetza Formation (130-300 ka), the subaerial Wyemaha Formation (30-130 ka), and the Sehoo Formation (13-30 ka). The Sehoo lake interval was followed by subaerial deposition of the Turupah Formation in the mid-Holocene, and the occupation of small lake phases in late Holocene time, represented by the Fallon Formation. The late Holocene lake phases will be the topic of discussion at Stop 1-2 of the field trip (see Adams, Appendix 1-2). Fallon lies within a large structural basin, the Carson Sink, that is likely a transtensional feature of the dextral Walker Lane belt (Stewart, 1988) which lies on the western margin of the sink. The basin contains hundreds of meters of lacustrine sediment, and during the 1954 Rainbow Mountain earthquakes, buildings and fields in Fallon were widely damaged largely due to amplified ground motion and liquefaction. Agriculture in the region is made possible in part by the U.S. Bureau of Reclamation's first ever project (Newlands Reclamation Project), which diverts irrigation water from the Truckee River.

8.2 The rounded hills at 9:00-11:00 are the Lahontan Mountains where Roger Morrison (1964) did much of his seminal work on pluvial Lake Lahontan stratigraphy; note the prominent shorelines etched into Miocene volcanic rocks.

Lazy B Ranch (on the left), an old brothel now closed for business.

10.3 Grimes Point archaeological area, one of the largest and most accessible petroglyph sites in northern Nevada, hosts more than 150 basalt boulders with over 1000 pieces of rock art. Most of the petroglyphs date between 5000 B.C. and 1500 A.D. and are attributed to the native American people of the Northern Paiutes (Cattail-eaters or "Toidikadi") who used abundant marsh resources to supply most of their material needs. The area also lies near the burial site of Spirit Cave Man, the oldest known mummified ancient American, dated at 9,400 yrs. B.P.. Spirit Cave Man, along with Kennewick Man (9,200 yrs. B.P.) found along the banks of the Columbia River in Washington, may provide clues to the earliest immigrants of the Western Hemisphere.

At 1:30 Mt. Grant (elev. 3426 m (11,239 ft)) of the Wassuk Range (near the south end of Walker Lake) is visible on the skyline on a clear day. The peak is about 100 km due south.

Note the prominent tufa coated pluvial Lake Lahontan strandlines as the road bends slightly eastward.

14.4 Salt Wells brothel

14.9 **Turnoff to first night's camp and Stop 1-1**; turn left and downhill onto dirt road and proceed through the open gate; road turns to the right (east). Thursday night's camp site is about 5 miles from the turnoff. After 1 mile, road swings to the north just beyond the corral.

Trenches with orange fencing on the left (west) are the focus of **Stop**
17.1 **1-1**, the first stop on Friday morning. Continue north to camp site.

Rainbow Mountain at 10:00, and the southern part of the Stillwater
18.9 Range to the east are composed of interbedded Miocene basalt and lacustrine deposits. Bright white units are diatomite.

20.4 **Turn right onto dirt road leading out to the small playa**

20.6 **Enter playa. Gathering of the Friends, pre-trip registration, and camp site for the first night. Camp anywhere on the playa.**

DAY 1: (Friday, September 20)

RAINBOW MOUNTAIN TO TERRACE CREEK

Approximate mileage	
0.0	**(Leave camp at 7:30 AM). Reset odometer at left (south) turn onto the dirt road we came in on. Proceed south ~3 mi to Stop 1-1.** Small 1954 fault ruptures with vertical offsets of about 30 cm cross the main dirt road several meters north of the playa road-main road intersection. Details of ground ruptures formed during 1954 Rainbow Mountain-Stillwater earthquake sequence in this area are shown in Appendix 1-1A, Figure 2b.
0.5	Rainbow Mountain summit at 2:00.
1.3	Lahontan Summit (~1290 m) marks a local divide between the Carson Sink to the north and Salt Wells Basin to the south (Figure 2). Prominent Lake Lahontan beach ridges (elevation ~1270 m) on the north and south sides of the summit represent the recessional dendritic (S_2) shoreline, one of three principal Lahontan shorelines defined by Morrison (1991). The S_2 dendritic shoreline is radiocarbon dated (from tufa) at ~11 ka (Broeker and Kaufman, 1965). Morrison's S_1 shoreline represents the lake highstand (~1332 m), extensively dated at ~13 ka (Broeker and Kaufman, 1965; Benson and Thompson, 1987; Adams and Wesnousky, 1998). New age data presented at Stop 1-1 indicate that Morrison's S_3 shoreline (~1228 m) is less than 8-10 ka and may be as young as ~6.3 ka.

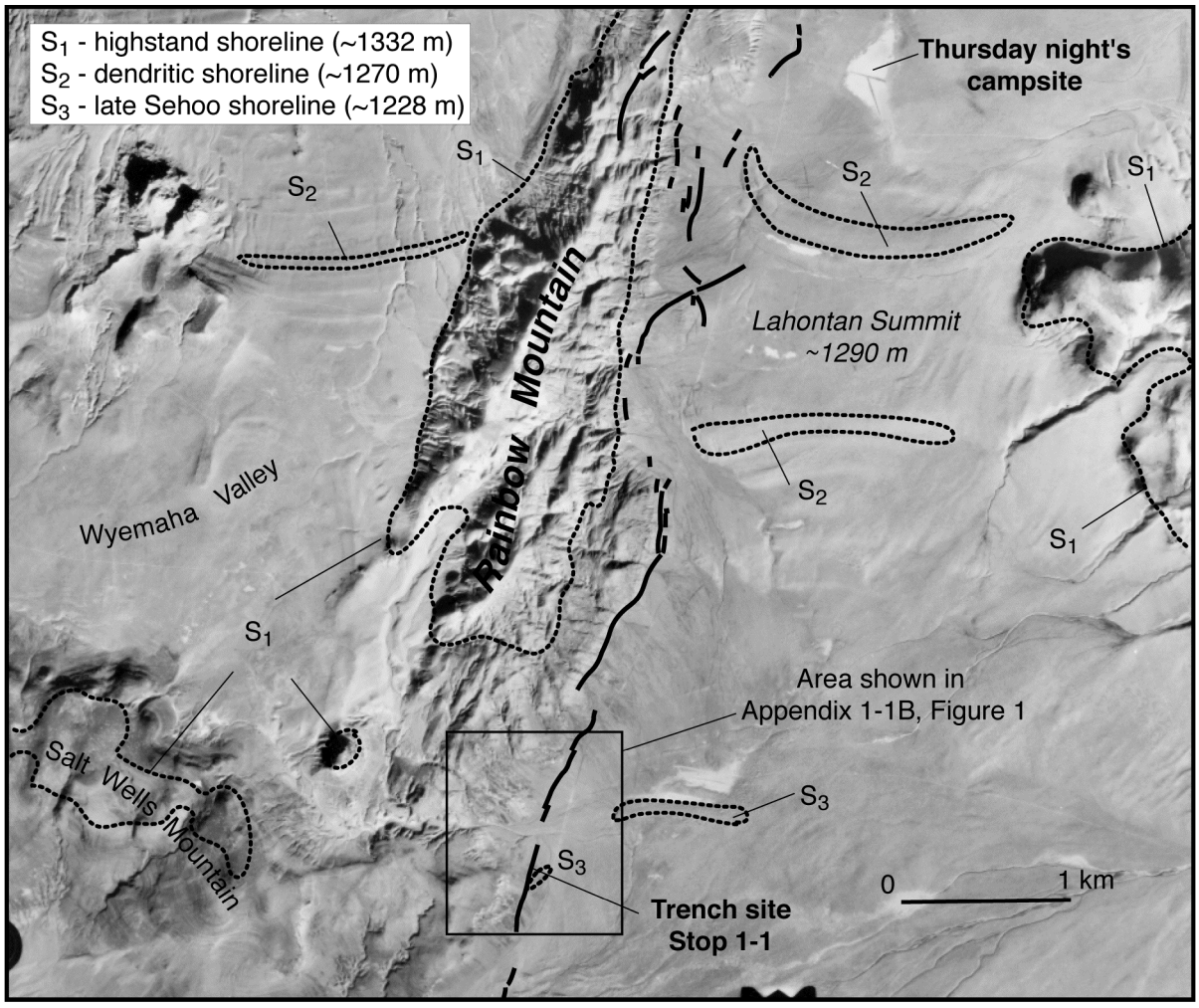

Figure 2 - Low-sun-angle aerial photo of the Rainbow Mountain area between Thursday night's camp site and Stop 1-1. Photo shows July 6 - August 23, 1954 fault ruptures (solid bold lines) and locations of the principal pluvial Lake Lahontan shorelines defined by Morrison (1991). The S_1 highstand shoreline (~1332 m), is extensively dated at ~13 ka (Broeker and Kaufman, 1965; Benson and Thompson, 1987; Adams and Wesnousky, 1998). The S_2 dendritic shoreline (~1270 m) is radiocarbon dated (from tufa) at ~11 ka (Broeker and Kaufman, 1965). New age data presented at Stop 1-1 indicate that Morrison's S_3 shoreline (~1228 m) is younger than 8-10 ka.

3.2 **Pull over to right side of the road and park. Walk west up to the two trenches across the Rainbow Mountain fault.**

Stop 1-1. (8:00-10:00) Caskey, Ramelli, and Adams. See Appendices 1-1A, -1B, and -1C.

Field trip overview, the July 6-August 23, 1954 earthquake rupture sequence; paleoseismicity and latest Pleistocene and Holocene(?) pluvial Lake Lahontan shoreline fluctuations along the Rainbow Mountain fault; shoreline processes.

After stop continue forward on dirt road back to US 50.

5.4 **Return to US 50 intersection**

0.0 **Reset odometer**. **Turn right (northwest) onto US 50.**

3.6 **Turn left (south) onto gravel road (before you get to Macari Road). Road swings back around to the southeast.**

4.0 **At intersection with dirt road near the beach barrier, make a hard left and park on the right side of the road. The front of the caravan should make the turn and proceed forward toward US 50 before parking.**

Stop 1-2. (10:30-11:45) Adams. See Appendix 1-2

Age and paleoclimatic significance of late Holocene Lakes in the Carson Sink.

After stop continue forward to US 50.

4.2 **Turn right and proceed east on US 50. The lunch stop is a 1 hour drive from Stop 1-2. The views from the lunch stop are worth the wait.**

8.2 Entering Eightmile Flat (western portion of Salt Wells Basin). The floor of this valley consists mainly of middle Sehoo clay deposits. Channel cuts into these deposits commonly reveal one to three tephra layers, each about 2 mm-thick, derived from Mono Craters (Sarna-Wojcicki, personal communication).

9.5 South end of the Stillwater Range at 11:00.

13.1 Thick, middle Sehoo-aged beach bar complex at 10:00 (see notes shown on Appendix 1-1A, Figure 2c)

14.9 Crossing the Fourmile Flat fault and entering Fourmile Flat. Highway damage was reported here as well as a large cloud of dust following the second July 6, 1954 earthquake (Tocher, 1956). Small (15-cm-high) 1954 fault ruptures were also mapped locally along the fault and these likely represent minor, primary surface ruptures associated with the second event of the July-August sequence (Caskey et al., in prep.). Paleoscarps offset the playa surface by as much as 2 m (Appendix 1-1A, Figure 2c), and likely formed subsequent to late Holocene lakes that occupied this portion of the basin.

15.5 Huck Salt Mine at 2:00 and Sand Mountain at 10:00.

Huck Salt mines the pure salt crust that precipitates annually from the evaporation of winter runoff and recharge that ponds in the Fourmile Flat depression. Salt has been harvested from the playa since the 1860's when it was hauled to the mining towns of Virginia City and Austin.

Sand Mountain is about 180 m in height. The quartz sands have an original Sierran provenance (Nick Lancaster, Desert Research Institute, personal communication) and are derived mostly from deflated pluvial lake sediments reworked by prevailing southwesterly winds. The quartz sands have been introduced to the Carson Desert by way of the Carson River and at times the diverted Walker River, but also by eolian processes evidenced by large active sand dunes that occupy the crest of the Blow Sand Mountains ~ 15 km to the south.

16.6 Prominent Lahontan shorelines etched into gently west-tilted Miocene basalt at 11:00. The high shoreline at ~1332 m (4370 ft) is clearly visible.

18.6 Turnoff to Sand Mountain and the loneliest phone

18.7 Sand Springs Range at 12:00 consists primarily of Mesozoic metasedimentary and granitic intrusive rocks.

On October 26, 1963 the U.S. Atomic Energy Commission and Department of Defense detonated a 12 kiloton, underground nuclear device in the granitic rock of range. The purpose was to direct a nuclear explosion from a recently seismically active area to gain information useful for discriminating between seismically recorded earthquakes and nuclear tests in the Soviet Union and elsewhere. The

blast registered a magnitude of 4.5-5.0.

20.6 Approximate crossing of the high shoreline elevation (~1332 m) of Lake Lahontan.

20.8 Exposed on the left (north) are Triassic and Jurassic metasedimentary rocks and Cretaceous felsic dikes and sills.

22.1 Sand Springs Pass (elevation 1415 m (4644 ft)). The ~13 ka high Lahontan shoreline at 1332 m came to within about 80 m of spilling over Sand Springs Pass. Evidence recorded elsewhere in the Great Basin indicates that earlier Pleistocene lakes in the Lahontan basin reached elevations of up to 1400 m and perhaps then, could have spilled eastward into Fairview and Dixie valleys (Reheis, Appendix 1-4). At Stop 1-4 we will discuss possible evidence for such an overflow.

23.3 Leaving the Sand Spring Range and entering Fairview Valley. Panorama includes the Stillwater Range at 9:00, Dixie Valley depression at 10:30, Clan Alpine Mountains at 10:30-12:00, Desatoya Mountains on the skyline at 12:00, and Fairview Peak at 1:30 beyond Labou Flat.

24.0 Sand Springs fault; immediately to the right of the road are small (~1-m-high) Holocene paleoscarps preserved along the fault trace. Although the Sand Springs fault did not rupture in 1954, it is one of most active faults in the area, showing evidence for 3 surface rupturing earthquakes in the last ~13 ka, and a slip rate of 0.6 mm/yr over this time interval (Bell et al., in review).

24.5 Turnoff to NV Route 839 to Rawhide and the Scheelite Mine

27.3 Entering Labou Flat. This basin was host to latest Pleistocene pluvial Lake Labou that reached a highstand elevation of 1264 m (4180 ft) and then overflowed northward into pluvial Lake Dixie which filled to an elevation of about 1097 m (3600 ft) (Mifflin and Wheat, 1979).

29.5 Fairview Site (point of interest sign). The boomtown of Fairview prospered around 1905-1907 from rich silver discoveries. At its peak, the town had a population of 2,000 with hotels banks, saloons, and a newpaper. The town and nearby mines were active until about 1917. Since then, all buildings, including a large mill, have been removed or destroyed. All that remains is a concrete bank vault left behind on the alluvial fan (visible at 2:00).

32.3 Intersection with NV Route 121 (Dixie Valley Rd.)

33.4 Drumm Summit, 1402 m (4600 ft.)

33.8 **"Fairview Peak Earthquake Faults" sign. Turnoff (south) on gravel road toward Stop 1-3.** This is a good road, but it gets a little bumpy on the steeper part of the ascent.

34.2 Road crosses northeast-trending 1954 ruptures along the Fairview fault. Prominent Fairview Peak escarpment at 12:00. 1954 fault scarps are visible along much of the range front on the way to Stop 1-3. A brush fire in this area in 1999 has provided a smooth grassy landscape and a great perspective for viewing the scarps and geomorphology.

39.2 Turnoff to "main site" referred to in Appendix 1-3B. This is the epicentral area for the December 16, 1954 Fairview Peak earthquake (Doser, 1986) and the area of maximum right-lateral and vertical offsets along the fault (Slemmons, 1957; Caskey et al., 1996).

Deeply dissected Qfi fan deposits (Bell, Appendix 1-3B). A road cut in this area exposes a tephra interbedded within the Qfi gravel several meters below the upper surface (marked by orange flagging at mile 37.5). The tephra correlates with the 35.4 ka Wilson Creek Ash Bed 19 (Sarna-Wojcicki, personal communication).

39.6 **LUNCH STOP (1:00-2:00). There are several options for lunch parking areas: 1) As the main road approaches the summit, you can pull over to the right and park for lunch. There are great views from here and interesting exposures to check out. 2) Closer to the summit, there is a side road off to the left (east) that offers a nice view and gets you off the main road. 3) It's also a very short drive up to the "main site" (see last mile mark) which is a classic location to view 1954 fault ruptures. However, parking would get rather crowded at the main site if everyone chose this option for lunch.**

NOTE: the mileage on the road log following the lunch stop assumes the option of parking on the side of the main road for lunch, so if you have lunch at the main site adjust your mileage accordingly.

This is not an official trip stop. Nothing will be presented to the group at this location. However, this a great place to mill around and observe roadcut exposures of soil developed on Qfi fan surfaces

(Bell, Appendix 1-3C, Figure 2), and a buried Qfo(?) soil. It's also a great place to view some of the largest 1954 offsets on the Fairview fault, either from the road (at a distance) or up close at the "main site".

The M_s7.2 Fairview Peak earthquake initiated in this area and propagated bilaterally 35 km to the north and 35 km to the south, ultimately producing surface rupture on five different faults (Caskey et al., Appendix 1-3A, Figure 1). Looking north, down into Stingaree Valley from the summit area, you are viewing Chalk Mountain (middle ground), the Louderback Mountains (skyline at 12:00), and the Clan Alpine Mountains (skyline at 12:30). Right-oblique ruptures along the east-dipping Fairview fault broke to the northeast end of Chalk Mountain. Subsequent ruptures during the northward propagating earthquake broke along three west-dipping faults; the West Gate fault which bounds the west side of the Clan Alpines, the Louderback Mountains fault which strikes northwest from the north end of Chalk Mountain for a distance of ~14 km, and the Gold King fault which lies within the Louderback Mountains. The fifth fault that ruptured during the earthquake is the Phillips Wash fault located in Gabbs Valley, 30 km to the south. After a 4 minute and 20 second time delay, the M_s6.8 Dixie Valley earthquake occurred, producing surface ruptures along a 46-km-long section of the east-dipping Dixie Valley fault which bounds the east side of the Stillwater Range.

After lunch continue south on the main road and proceed ~2 mi to Stop 1-3.

40.4 Beautiful right-oblique fault offsets visible at 3:00 where the fault breaks across ephemeral stream channels and rounded ridge crests. Lateral offsets in this area reached up to 2.5 m (Caskey et al., 1996).

420 **Pull over to right side of the road and park. Walk west up to the large fault scarp.**

Stop 1-3. (2:30-4:00) Caskey and Bell. See Appendices 1-3A, -3B, and -3C.

Overview of the December 16, 1954 Fairview Peak-Dixie Valley earthquake sequence; overview of Quaternary chronostratigraphy in the Fairview Peak-Dixie Valley-Stillwater seismic gap area; paleoseismicity along the Fairview fault.

After stop, turn vehicles around and return to US 50.

49.0 Chalk Mountain at 12:00 consists primarily of Mesozoic

metasedimentary carbonate rocks (white) and Tertiary intrusive rocks (salmon rocks visible(?) at the north end of the range). The dark brown rocks lower down on the west side of the mountain are Cretaceous granitic rocks with a dark desert varnish.

49.8 **Return to US 50, turn left (west).**

51.3 **Turn right (north) onto NV 121 (Dixie Valley Road)**

52.7 Low ridge about 1 mile east consists mostly of Miocene gypsiferous lacustrine deposits, dated by correlation of two tephra layers (Reheis et al., in press) exposed on the east flank (not visible). Moderately dipping (20-25º) carbonate-cemented gravel beds crop out upslope in uncertain stratigraphic relation to the lacustrine deposits (probably unconformable). The gravel beds grade upward from coarse angular fan gravel to moderately sorted and bedded pebble gravel and then to well rounded granule to pebble gravel with abundant discoidal clasts. The moderate dips and well-bedded upper layers suggest shoreface deposition, and may indicate overflow from Lake Lahontan at 1400 m (Stop 1-2 in Reheis and Morrison, 1997).

55.2 Road bends slightly west

56.0 Graded gravel road on the west turns west to access radar station atop ridge west of Dixie Valley Road.

56.3 **Pull over to right side of Dixie Valley road and park.**

Stop 1-4. (4:30-5:45) Reheis. See Appendix 1-4.

General overview of large pre-late Pleistocene pluvial lakes in Nevada and possible evidence for overflow of a larger Lake Lahontan into Fairview-Dixie Valleys.

After stop, continue north ~30 mi on Dixie Valley road to Terrace Creek and camp.

57.2 1954 fault ruptures are visible at 2:30 in late afternoon sun along Louderback Mountains range front (~5 km to the northeast)

60.6 Oligocene felsic dike swarm (white bands) visible at Pirouette Mountain (2:00) and in the Louderback Mountains at 3:00. A similar dike swarm exists directly west across the valley in the Stillwater Range (visible at mile 59.7). The alignment of this apparently correlative dike swarm suggests there is no significant long-term

lateral offset across Dixie Valley (Christopher Henry, Nevada Bureau of Mines and Geology, personal communication), despite the relatively large component of right-lateral displacement documented along portions of the 1954 rupture zone, including the Louderback Mountains fault.

62.7 Step-over region between the north end of the Fairview Peak earthquake ruptures (Gold King and Louderback Mountains faults) to the east and the south end of Dixie Valley ruptures to the west. The rupture zones overlap along-strike by about 7 km.

The felsic dike swarms in the Stillwater Range referred to at mile 57.7 are visible at 9:00.

65.8 Job Peak at 10:30, highest point in the Stillwater Range at 2680 m (8790 ft); Mt. Augusta at 2:30, highest point in the Clan Alpine Mountains at 3040 m (9999 ft).

68.4 1954 Dixie Valley fault ruptures clearly visible at the range front for most of the next 40 km to the north.

Coyote Canyon at 9:00; the maximum vertical offset along the 1954 Dixie Valley fault ruptures (2.8 m) was measured about 2 km north of the canyon.

72.9 Road crosses latest Pleistocene pluvial Lake Dixie beach ridge at 1094 m (3590 ft). The beach ridge lies along the south shore of the lake and formed near the lake highstand at ~13 ka. The presence of metamorphic clasts in the deposit indicates that the beach gravel was longshore-transported from at least as far north as the IXL Canyon fan (~10 km).

75.6 Fault scarps along the piedmont fault zone are clearly visible for about the next 10 km to the north. Large ~10-m-high compound paleoscarps (i.e., multiple event scarps) offset the older (Qfo) fans, whereas smaller ~2-m-high paleoscarps are locally visible on inset Holocene fan surfaces between the larger compound scarps. Only small vertical offsets of about 20-30 cm occurred along the piedmont fault zone in 1954 (Caskey et al, 1996; Appendix 1-3A, Figure 2b).

77.9 Dixie Settlement Road turnoff to the east . This is the road that leads to the swimming hole (see Road Log Addendum). Continue north.

78.1 Pavement and NV 121 ends. Continue north.

83.4 **Turnoff to Terrace Creek (informal name for this unnamed drainage) and camping area for both Friday and Saturday night. There is a very large, sparsely vegetated, bouldery fan surface to camp on. CAMP ANYWHERE EXCEPT AT THE FAN HEAD where there are delicate 1954 scarps we would like to keep preserved. Be aware that the group fire and business meeting site (Saturday night) will be up toward (but not at) the fan head, so you might wish to set your camp a bit lower on the fan for obvious reasons. There are also good camping places off the road up past the fan head, but the road is washed out about a kilometer past the fan head.**

Note that the alluvial fans on the piedmont and the terraces near the fan head will be topics for discussion for the first stop on day two (Stop 2-1), so check out the more distal perspectives of the geomorphology (and the huge fault scarp north of the draingage) as you head up the fan.

DAY 2: (Saturday, September 21)

TERRACE CREEK TO DIXIE HOT SPRINGS

Approximate mileage	
	(Gather up near the fan head at Terrace Creek (8:00 AM).
	Stop 2-1. (8:00-10:00) Caskey and others. See Appendix 2-1.
	Geomorphology, chronostratigraphy, and active faulting at Terrace Creek; natric soil development
	After stop, pullout of camp, and return in vehicles to Dixie Valley road.
0.0	**Reset odometer at Terrace Creek road – Dixie Valley road intersection. Turn right (south) and proceed ~10 mi to Stop 2-2.**
6.8	Gravel quarry at 9:00 in pluvial Lake Dixie beach deposits. At about 2:00, a large piedmont paleoscarp shows small 1954 breaks near its base (thin, crisp, highly reflective line in morning sunlight).
7.4	Pavement starts.
11.3	**As road approaches the crest of the large alluvial fan look for right turn onto jeep trail. Turn right (west) and proceed ~1 mi to Stop 2-2. Only high-clearance vehicles should make the drive up to Little Box Canyon. Although this jeep trail is rugged in a couple of places, 4-wheel-drive is not necessary. Stop 2-2 also serves as the LUNCH STOP, so if you need to ride up in another vehicle, make sure to bring what you need for lunch.**
12.2	**Jeep trail forks; veer right toward Little Box Canyon.**
12.4	**Make a hard left (south) turn. The front of the caravan should proceed all the way down to the jeep trail fork at mile 11.6. Drive forward and park ~bumper to bumper to make sure we can fit the entire caravan on the loop. Walk up to the overlook toward Little Box Canyon from the graben south of the creek.**
	Stop 2-2. (10:30-1:30) Caskey. See Appendix 2-2.

Geological and geophysical evidence for low-dip on the Dixie Valley fault; fault trace graben development; Little Box to Big Box Canyon round-trip traverse; lunch.

After presentation and discussion at Little Box site, everyone is on their own to have lunch, make the round-trip traverse along the fault to Big Box Canyon, explore the magnificent box canyons, or whatever in whatever order.

After stop, return to vehicles at announced time (hopefully 1:30 if we are on schedule) and return down fan to Dixie Valley road.

13.5 **Return to Dixie Valley road. Turn left (north) and proceed about 3.5 mi to Stop 2-3.**

14.8 Cattle Rd intersection. The seismic reflection line and gravity survey mentioned at Stop 2-2 were run from just north of the (recently burned) spring area at the range front, down across the highway and along Cattle Rd.

17.4 **At intersection with Settlement Road, turn left onto dirt road which immediately forks. Veer right toward gravel quarry. Proceed toward the back of quarry road loop and park off to the right.**

Stop 2-3 (2:00-3:30) Bell. See Appendix 2-3.

Structural-chronostratigraphic relations of the Dixie Valley fault in The Bend; pluvial Lake Dixie beach bar complex.

After stop return to Dixie Valley road.

18.3 **Turn left (north) on Dixie Valley road. Pavement ends. Continue north for ~9 mi to Stop 2-4.**

21.7 Out of view ~100 m west of the road is an impressive 1954 lateral-spread zone characterized by graben, fissures, and sinkholes. These features resulted from liquefaction of water saturated sediments likely within 10 m of the ground surface during the Dixie Valley earthquake. They are worth checking out on the way out on Sunday. A good pullover spot is marked with bright orange flagging on the west side of the road. As impressive as these features are, they are dwarfed in comparison to the magnitude of the lateral spreads formed during a ~M_w7.3 earthquake that ruptured through this area ~2.0-3.4 ka as we'll see at Stop 2-4.

23.9 Road crosses large 3-m-high lateral-spread scarps formed ~2.0-3.4 ka. Much smaller-scale 1954 lateral-spreads formed locally along the base of these paleo-liquefaction features and actually damaged and closed the road ~0.5 mi to the north.

25.6 Terrace Creek turnoff. Continue north for ~3 mi to Stop 2-4.

27.8 Enter area of intensive, large-magnitude lateral-spreading. Look for a cleaned-off exposure of a ~10-cm-thick Mazama ash bed immediately left (west) of the road. The ash lies in deposits interpreted to be marginal lacustrine. A thin 1-2-m-thick mantle of Qfm alluvial fan gravel overlies the lacustrine section at this location.

28.6 **Pull over to the right and park. Walk west up past the large mounds of gravel and up to the large escarpment.**

Stop 2-4. (4:00-5:00) Caskey. See Appendix 2-4.

Large-scale lateral-spread paleoscarps and mid-Holocene lacustrine deposits at Humboldt Salt Marsh; Stillwater seismic gap.

After stop, turn vehicles around and proceed back to Terrace Creek for dinner and festivities.

The business meeting will commence at the group fire pit at 8:00-8:30 or thereabouts.

NOTE: If the weather is warm and you want to rinse some dust off there is a great swimming hole about 13 mi from camp in Dixie Settlement. See Road Log Addendum at the end of the main log for directions.

DAY 3: (Sunday, September 22)

TERRACE CREEK TO DIXIE COMSTOCK AREA

Approximate mileage

(Depart camp at 8:30 AM).

NOTE: Stops 3-1 to 3-3 are all less than ~8 mi north of Terrace Creek. So you have the option of breaking down your camp on the way back from these stops.

0.0 **Reset odometer at Terrace Creek road – Dixie Valley road intersection. Turn left (north). Proceed north ~6 mi to Stop 3-1.**

6.2 **Pull over to right side of road and park. Walk west up to sparsely vegetated fan surface.**

Stop 3-1. (9:00-10:30) Caskey and Ramelli. See Appendix 3-1.

Tectonic and isostatic deformation of latest Pleistocene Lake Dixie shorelines

After stop, continue north on the Dixie Valley road ~2.2 mi to Stop 3-2.

8.2 **Pull over to right side of road and park. Walk west to the large lateral –spread graben and trench.**

Stop 3-2 and 3-3 (10:45-12:00) Caskey. See Appendix 3-2

Timing of the most recent surface faulting in the Stillwater seismic gap based on trench data across a lateral –spread graben.

A very short hike to Stop 3-3 at the playa margin is accessed from a large pullout 0.3 mi farther north off Dixie Valley road. Features of interest at Stop 3-3 will be described at the trench site. Participants can then drive to the pullout access for Stop 3-3 and wander out to the playa margin on their own. It's worth the short hike!

8.5 **Proceed north on Dixie Valley road 0.3 mi from the trench site to**

a large pullout at the loud pressurized well head and holding pond. Park anywhere. Stop 3-3 is located along the playa margin a couple 100 m east of the parking area. Walk down to the playa from the south side of the holding pond. There's a trail at least part of the way down.

Stop 3-3 (12:00 to ??) Caskey. See Appendix 3-2

Lateral-spread-induced(?) contractional deformation of playa-margin lacustrine deposits

THIS IS THE LAST STOP OF THE FOP! Safe and Happy Trails!!! See ya next year!

References

Adams, K.D. and S.G. Wesnousky, 1998, Shoreline processes and the age of the Lake Lahontan highstand in the Jessup embayment, GSA Bulletin, 110, no. 6, p. 1318-1332.

Bell, J.W., S.J. Caskey, A.R. Ramelli, L. Guerrieri, and A.M. Sarna Wojcicki, (in review to Geology), Patterns and rates of faulting in the central Nevada seismic belt.

Benson, L.V. and R.A. Thompson, 1987, Lake-level variation in the Lahontan basin for the past 50,000 years: Quaternary Research, v. 28, p. 69-85.

Broecker, W.S. and A. Kaufman, 1965, Radiocarbon chronology of Lake Lahontan and Lake Bonneville II, Great Basin: Geological Society of America Bulletin, v. 76, p. 537-566.

Caskey, S.J., S.G. Wesnousky, Zhang, P., and D.B. Slemmons, 1996, Surface faulting of the 1954 Fairview Peak (Ms7.2) and Dixie Valley (Ms6.8) earthquakes, central Nevada: Seismological Society of America Bulletin, v. 86, p. 761-787.

Caskey, S.J., J.W. Bell, Wesnousky, and A.R. Ramelli, in preparation, Historical surface faulting and paleoseismicity in the area of the 1954 Rainbow Mountain-Stillwater earthquake sequence, central Nevada.

Mifflin, M.D., and M.M. Wheat, 1979, Pluvial lakes and estimated pluvial climates of Nevada. Nevada Bureau of Mines and Geology Bulletin 94, 57 p.

Morrison, R.B., 1964, Lake Lahontan: Geology of the southern Carson Desert, Nevada: U.S. Geological Survey Professional Paper 401, 156 p.

Morrison, R.B., 1991, Quaternary stratigraphic, hydrologic and climatic history of the Great Basin, with emphasis on Lakes Lahontan, Bonneville, and Tecopa, in Morrison, R.B., ed., Quaternary nonglacial geology: Conterminous U.S.: Boulder, Colo, Geological Society of America, The Geology of North America, v. K-2, p. 283-320.

Reheis, M.C., and R.B. Morrison, 1997, High, old pluvial lakes of western Nevada, *in* Link, P. K., and Kowallis, B. J., eds., Proterozoic to recent stratigraphy, tectonics, and volcanology, Utah, Nevada, southern Idaho and central Mexico: Brigham Young University Geology Studies, Provo, v. 42, pt. 1, pp. 459-492.

Slemmons, D.B., 1957, Geological effects of the Dixie Valley-Fairview Peak, Nevada, earthquakes of December 16, 1954: Seismological Society of America Bulletin, v. 47, no. 4, p. 353-375.

Stewart, J. H., 1988, Tectonics of the Walker Lane belt, western Great Basin: Mesozoic and Cenozoic deformation in a zone of shear, *in* "Metamorphism and Crustal Evolution of the Western United States," W. G. Ernst (Editor), Prentice Hall, Englewood Cliffs, New Jersey, pp. 683-713.

Road Log Addendum

Directions to the swimmimg hole at Dixie Settlement

Approximate mileage

The swimming hole is out in Dixie Settlement . Proceed to the Dixie Valley road – Dixie Settlement Rd. intersection, located just south of where NV 121 ends and the Dixie Valley road turns to gravel. At the time of making the road log, the Dixie Settlement Rd. sign was down.

0.0 **Reset odometer at the Dixie Valley road – Dixie Settlement Rd. intersection. Turn east onto Dixie Settlement Rd.**

The ditch off the south side of the road for the next few 100 meters exposes thick beds of Mazama ash in silty fluvial deposits.

3.3 Turn left (north).

4.8 Turn right (east) (i.e., just stay on main road)

6.3 Turn left (north) into parking area at swimming hole.

This pond is fed by an artesian well. In many places in the valley, artesian water is tapped from only about 10-20 m depth.

APPENDIX 1-1A

Overview of the 1954 Rainbow Mountain - Stillwater Earthquake Sequence

John Caskey, John W. Bell, Steven G. Wesnousky, and Alan R. Ramelli

The 1954 Rainbow Mountain-Stillwater earthquake sequence consisted of three moderate to large earthquakes that occurred within the Basin and Range province, approximately 20 km east of Fallon, Nevada (Figure 1). The initial 6 July, M_s6.3 Rainbow Mountain earthquake was followed ~11 hours later by a large M6.4 aftershock(?), herein referred to as the Fourmile Flat earthquake, and then 49 days later by the 24 August, M_s7.0 Stillwater earthquake (Figure 1). The three earthquakes combined to produce a discontinuous, north-trending zone of surface ruptures 70-km-long and up to 12-km-wide. The most prominent ruptures occurred along the Rainbow Mountain fault which bounds the eastern escarpment of Rainbow Mountain, a moderately west-tilted block of Tertiary volcanic and sedimentary rocks (Stewart and Carlson, 1978).

Tocher (1956) originally reported on the general geological characteristics of the 1954 Rainbow Mountain-Stillwater earthquake sequence. Steinbrugge and Moran (1956) reported on damage caused in the Fallon area during the earthquake sequence. Tocher's field study was initiated during the interval between the 6 July and 24 August events, so he was largely able to discriminate between the 6 July and 24 August rupture traces which partially overlap along the Rainbow Mountain fault (Figure 1). Tocher (1956) published 1:76,000-scale fault rupture maps that showed only about a 20-km-long portion of the rupture zone and included about a dozen measurements of surface offset. Slemmons (1957) later published a 1:250,000 scale compilation of the entire July-December 1954 rupture zones which included additional rupture traces mapped by Tocher that were not shown on Tocher's (1956) original maps. Slemmon's compilation extended the mapped zone of the July-August rupture zone approximately 40 km northward into the Carson Sink. Bell's (1984) 1:250,000-scale fault compilation extended the zone of ruptures approximately 17 km farther north into Carson Sink (Figure 1). None of these investigations entailed a comprehensive study of the distribution, amount, and style of surface offsets for the July-August earthquake sequence. For these reasons, we recently conducted a detailed field survey of the 6 July and 24 August 1954 earthquake rupture zones to document the full extent and style of surface offsets, as well as the paleoseismic histories of the faults that were reactivated during the earthquake sequence (Caskey et al., in preparation).

Details of the 6 July–24 August earthquake ruptures were mapped in the field on low-sun-angle aerial photographs taken in 1968, 1979, and 1990 at scales of 1:10,000 to 1:40,000. Conventional Army Map Service (AMS) photographs flown in 1957 (Nevada Bureau of Mines and Geology photo collection) were used to map details of surface ruptures in the northern part of the Carson Sink that are no longer preserved. Field observations compiled on 1:24,000 scale base maps were then reduced to the 1:50,000 scale annotated maps included in this overview (Figures 2a-c). Because there are no significant field observations for the concealed ruptures north of Stillwater Reservoir (Figure 2a), a 1:50,000 scale map is not provided for this area.

Over 50 field measurements of surface offsets constrain the distribution of slip along the discontinuous and distributed rupture zone that formed during the earthquake sequence (Figure 3). Vertical offsets reach a maximum of ~0.8 m with the average vertical offset being ~0.2 m. In contrast to original reports, we see evidence for a right-lateral component of slip along

portions of the rupture zone (Figures 2 and 3) including offset stream channels (0.5-1.0 m), left-stepping *en echelon* scarps, and a well-preserved, 100 m-long mole track on the playa surface in Carson Sink. The right-slip component is consistent with focal plane solutions for the events (Doser, 1986; Figure 1) and recent geodetic results (Hodgkinson et al., 1996).

Surface ruptures along the previously unmapped Fourmile Flat fault are subparallel to the Rainbow Mountain fault. The two faults are separated by 10 km left step across Eightmile Flat (Figure 1). Event locations and anecdotal information (Tocher, 1956; see road log at Fourmile Flat) indicate that the Fourmile Flat ruptures represent minor, primary surface rupture associated with the large July 6 aftershock, triggered ~11 hrs after the initial July 6 Rainbow Mountain event.

Finally, there is a mismatch between the north-northeast striking surface ruptures, and the north-northwest fault strikes delineated by focal mechanisms. This relationship is also true for the1954 Fairview Peak and aspects of the1932 Cedar Mountain earthquakes (Bell et al., 1999). It is possible that fault surfaces in the region, particularly those within the transition between the northwest-trending Walker Lane belt to the west and the northeast-trending structural grain of the central Great Basin, may rotate and fan upward from focal depths in the fashion of Riedel shears above lateral slip faults (Figure 4).

References

Bell, J.W., 1984, Quaternary fault map of Nevada, Reno Sheet, Nevada Bureau of Mines and Geology Map 79, Reno.

Bell, J.W., C.M. de Polo, A.R. Ramelli, A.M. Sarna-Wojcicki, and C.E. Meyer, 1999, Surface faulting and paleoseismicity of the 1932 Cedar Mountain earthquake area, west-central Nevada, and implications for modern tectonics of the Walker Lane, GSA Bulletin, 111, no.6, pp. 791-807.

Caskey, S.J., J.W. Bell, A.R. Ramelli, and S.G. Wesnousky, Historic surface faulting and paleoseismicity in the area of the 1954 Rainbow Mountain-Stillwater earthquake sequence, central Nevada (in preparation).

Dohrenwend, J.C., B.A. Schell, C.M. Menges, B.C. Moring, and M.A. McKittrick, 1996, Reconnaissance photogeologic map of young (Quaternary and late Tertiary) faults in Nevada, Open File Report, OFR 96-2: Nevada Bureau of Mines and Geology, in cooperation with the U.S. Geological Survey, scale 1:1,000,000.

Doser, D., 1986, Earthquake processes in the Rainbow Mountain-Fairview Peak-Dixie Valley, Nevada region 1954-1959, J. Geophys. Res. 91**,** 12572-12586.

Hodgkinson, K.M., R.S. Stein, and G. Marshal, 1996, Geometry of the 1954 Fairview Peak-Dixie Valley earthquake sequence from a joint inversion of leveling and triangulation data: Journ. Geophys. Res. 101(B11): 25,437-25,457.

Naylor, M.A., G. Mandl, and C.H.K. Sijpesteijn, 1986, Fault geometries in basement-induced wrench faulting under different initial stress states: Journal of Structural Geology, 8, 737-752.

Slemmons, D.B., 1957, Geological effects of the Dixie Valley-Fairview Peak, Nevada, earthquakes of December 16, 1954, Bull. Seism. Soc. Am. 47**,** 353-375.

Steinbrugge, K.V. and D.F. Moran, 1956, Damage caused by the earthquakes of July 6 and August 23, 1954: Bull. Seism. Soc. Am. 46, no. 1 p. 16-33.

Stewart, J.H., and Carlson, J.E., 1978, Geologic Map of Nevada, U.S. Geol. Surv. in cooperation with Nevada Bureau of Mines and Geology.
Tocher, D., 1956, Movement on the Rainbow Mountain fault: Bull. Seism. Soc. Am. 46, no. 1, p.10-14.

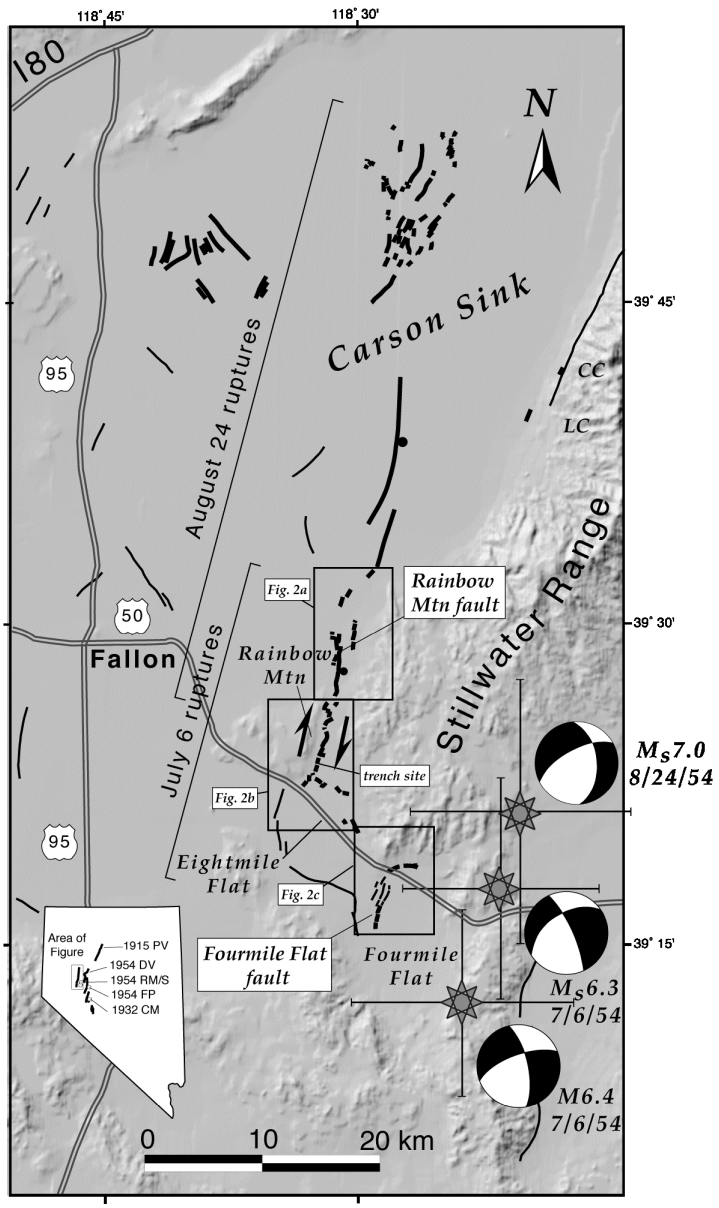

Figure 1 - Rupture zones (bold lines) of the July 6-August 24, 1954 earthquake sequence. Bar and ball on the downthrown side of faults. Focal mechanisms and locations (stars with associated location uncertainty bars) are from Doser (1986). Pre-historic faults (thin lines) from Bell (1984) and Dohrenwend et al. (1996). Inset map shows locations and generalized rupture zones associated with the the 1915 Pleasant Valley (PV), 1932 Cedar Mountain (CM), and 1954 Fairview Peak (FP), Dixie Valley (DV), and Rainbow Mountain-Stillwater (RM/S) earthquakes. Abbreviations for place names along the west sided of the Stillwater Range: CC - Cox Canyon; LC - Lambing Canyon. Small boxes denote locations of figures in text.

Figure 2

MAP OF FAULT SCARPS FORMED DURING THE JULY 6 AND AUGUST 23, 1954 RAINBOW MOUNTAIN AND STILLWATER EARTHQUAKE SEQUENCE, CENTRAL NEVADA

by

S. John Caskey, John W. Bell, Steven G. Wesnousky, and Alan R. Ramelli

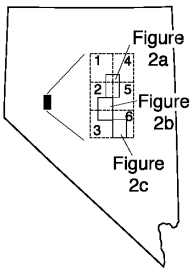

MAP AREAS FOR FIGURES 2a,b, AND c SHOWN WITH RESPECT TO 1:24,000 SCALE 7.5 MINUTE QUADRANGLES 1-6: 1-STILLWATER; 2-LAHONTAN MTS.; 3-BUNEJUG MTS.; 4-FOXTAIL LAKE; 5-DIAMOND CANYON; 6-FOURMILE FLAT

MAP EXPLANATION

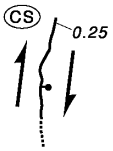

Fault scarp formed in 1954

Bar and ball on downthrown side. Arrows indicate areas with field evidence of right lateral motion. Numbers indicate measurements sites of vertical separation of the ground surface in meters. Dotted lines indicate surface breaks that are visible on aerial photos but not in tthe field. "CS" indicates sections of the fault exibiting a compound scarp with 1954 offset.

Pre-1954 fault scarp formed on latest Pleistocene to late Holocene surfaces

Bar and ball on downthrown side. Numbers indicate measurement sites of vertical separation of the ground surface. Dashed lines indicate inferred fault traces.

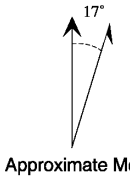

Approximate Mean Declination

Scale

1 0 1 2 Miles

1 0 1 2 Kilometers

CONTOUR INTERVAL 10 METERS - *(for Bunejug Mts. and Lahontan Mts. quadrangles)*
CONTOUR INTERVAL 2 METERS - *(for Stillwater quadrangle)*
CONTOUR INTERVAL 20 FEET- *(for Foxtail Lake and Fourmile Flat quadrangles)*
CONTOUR INTERVAL 40 FEET - *(for Diamond Canyon quadrangle)*

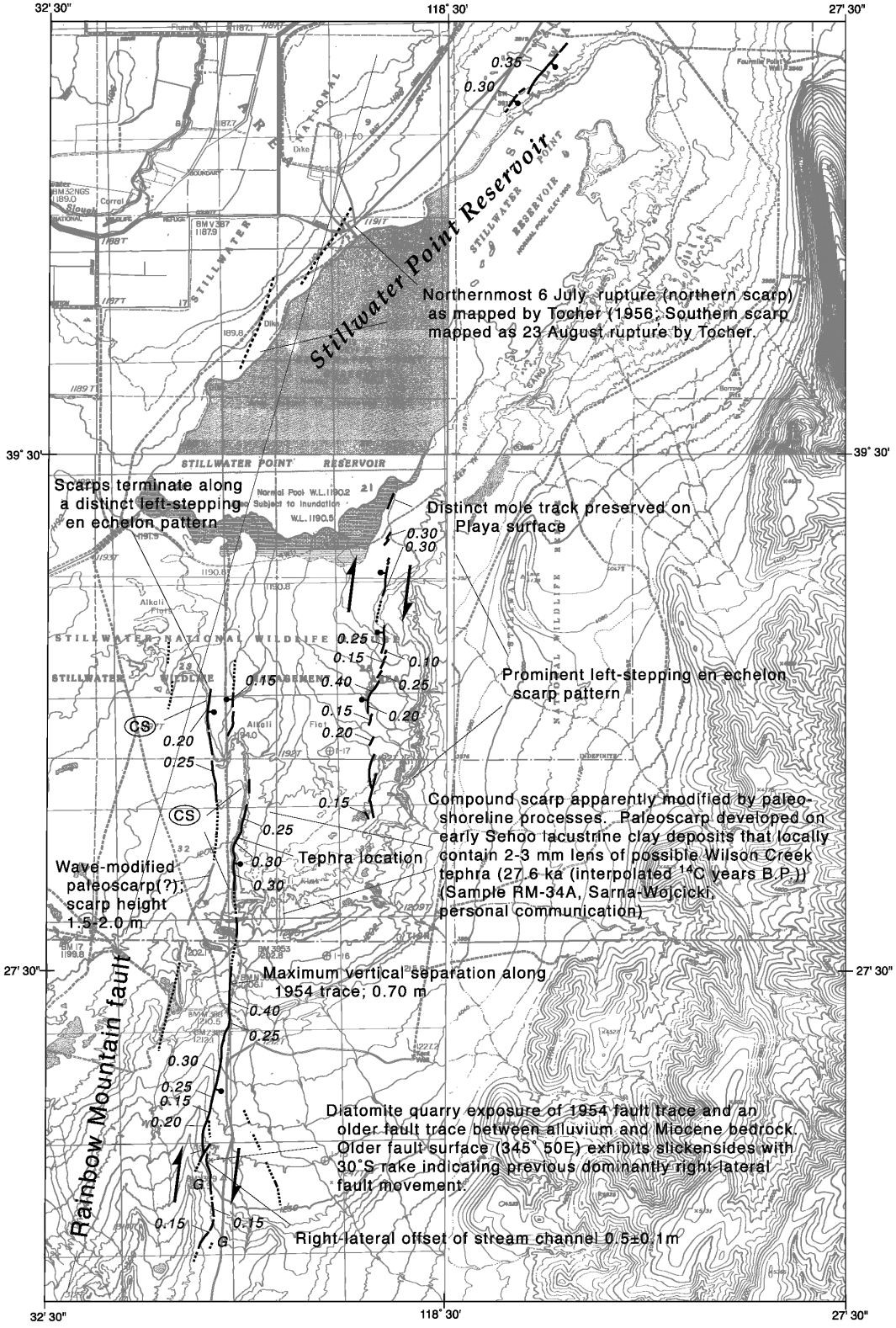

Figure 2a - Map of fault scarps formed during the July 6 and August 23, 1954 Rainbow Mountain-Stillwater earthquake sequence. See Figure 1 for location.

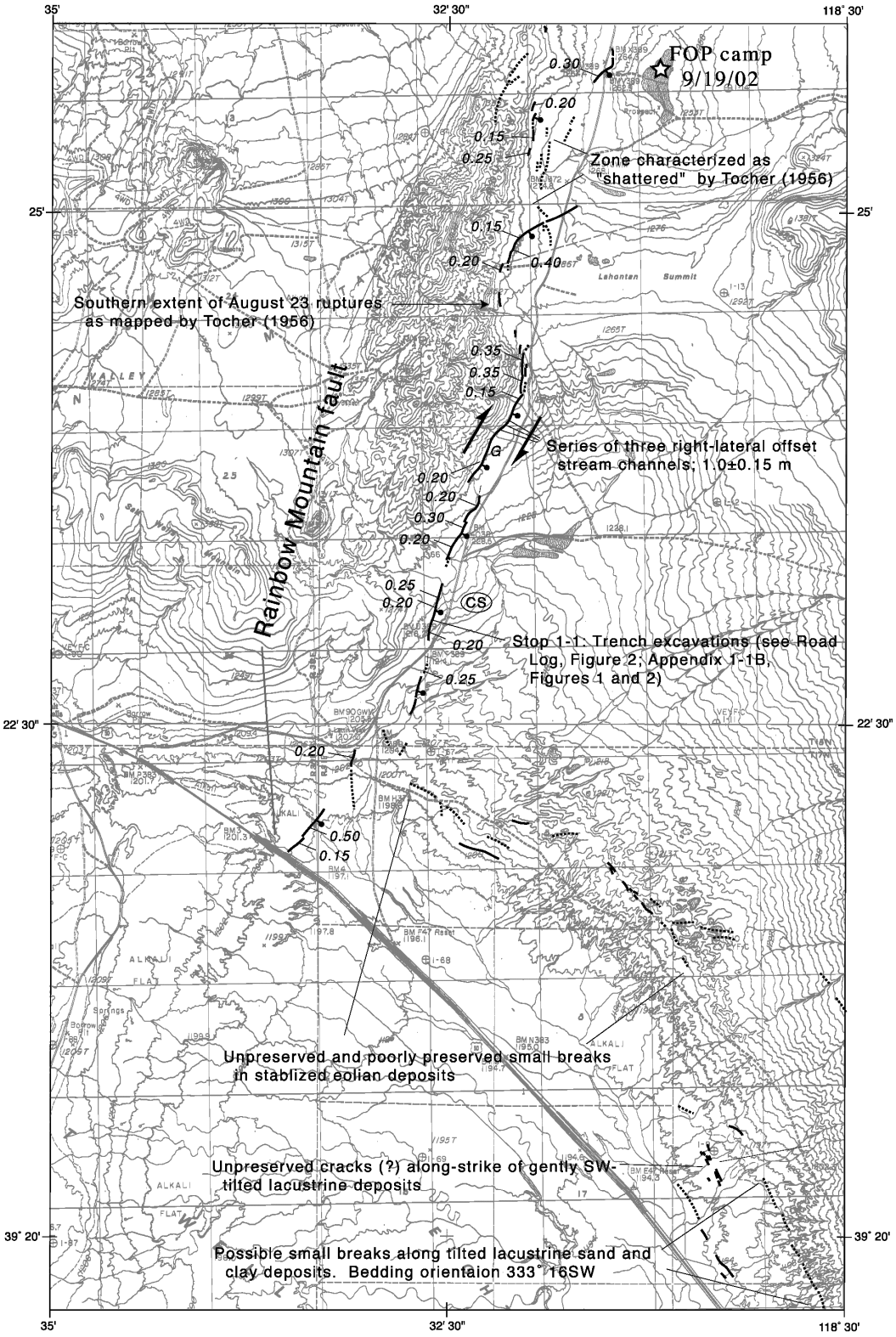

Figure 2b - Map of fault scarps formed during the July 6 and August 23, 1954 Rainbow Mountain-Stillwater earthquake sequence. See Figure 1 for location.

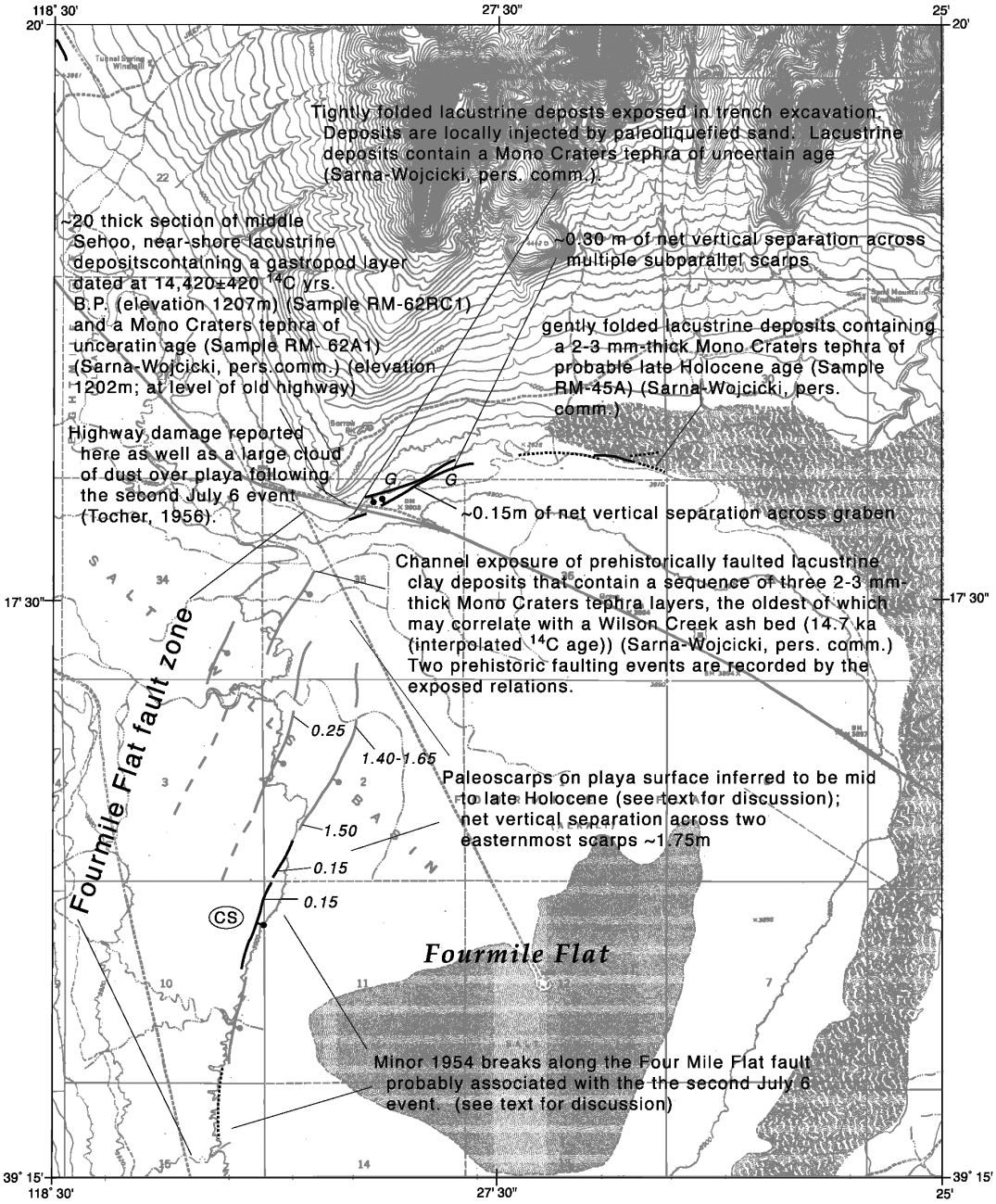

Figure 2c - Map of fault scarps formed during the July 6 Fourmile Flat earthquake. See Figure 1 for location.

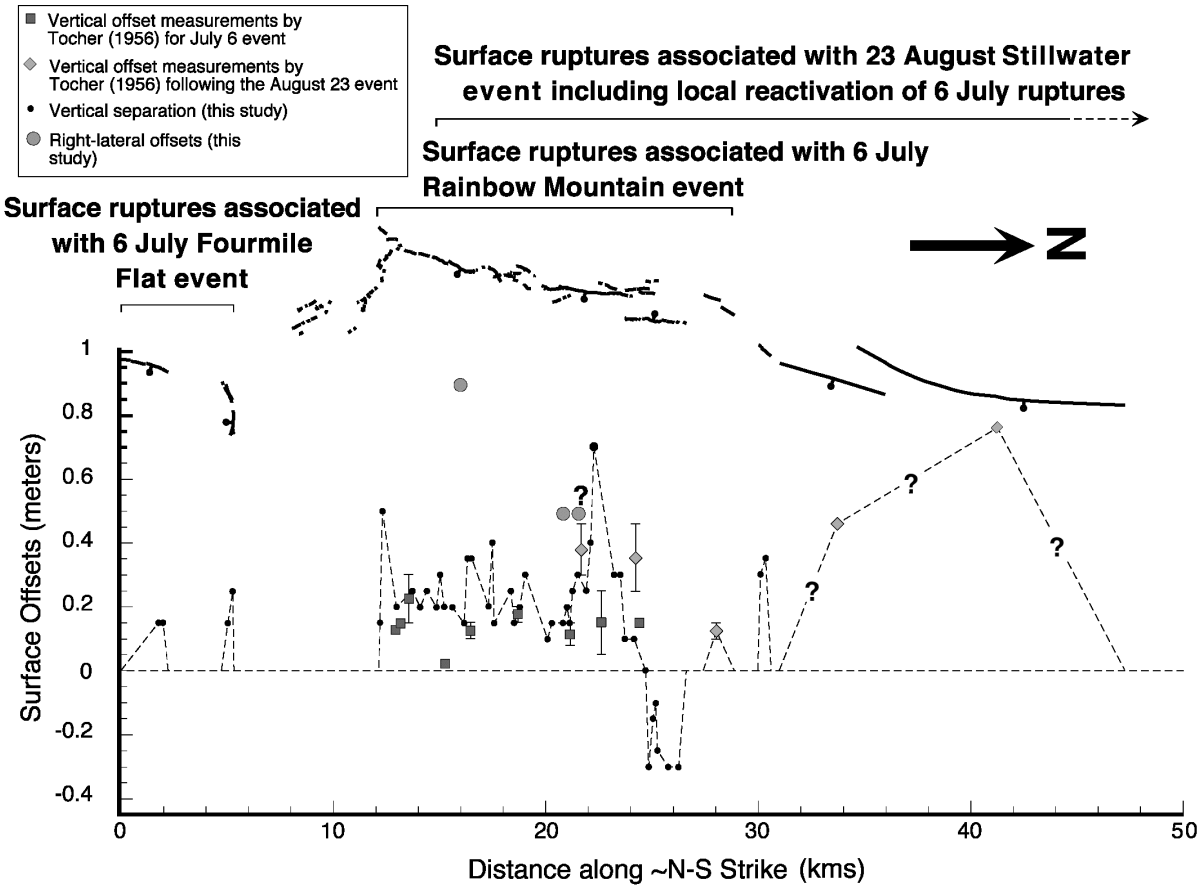

Figure 3 - Slip distribution for the Rainbow Mountain-Stillwater earthquake sequence. Squares - Vertical offset measurements made by Tocher (1956) for the July 6 event; Diamonds - vertical offset measurements made by Tocher (1956) following the August 23 event; Black dots - measurements of vertical separation across fault scarps (this study); and Large circles - measure ments of right-lateral offset stream channels (this study). Error bars on Tocher's measurements represent the range of offsets reported at specific locations. Note that the right-lateral offset measurement at the 15 km mark represents several consistent mea surements on a series of three stream channels at that location (see Figures 2a-c). The 1954 rupture trace is shown above and regis-tered to the slip distribution plot for reference. No displacement data is available for the ruptures that broke in the northern portion of the Carson Sink (Figure 1), so these ruptures are omitted for simplicity.

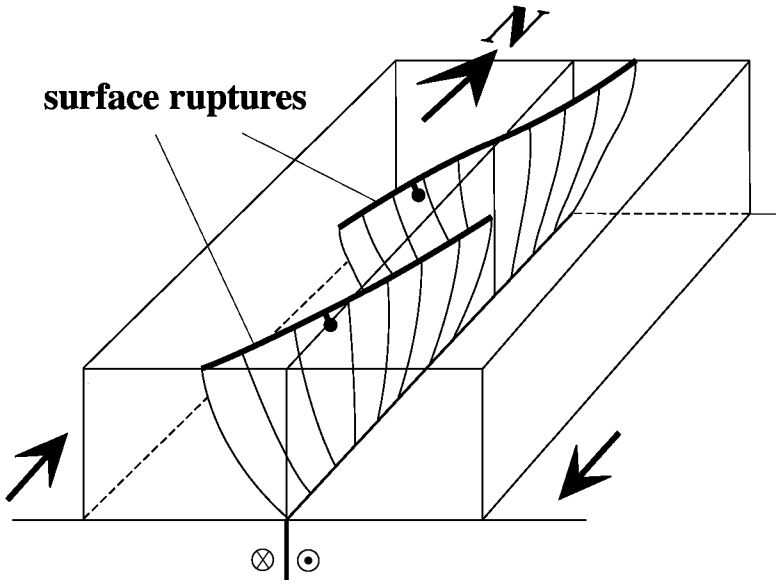

Figure 4 - Possible 3-dimensional model for ruptures of the 1954 earthquake sequence. The north-northeast-striking fault ruptures along the 1954 Rainbow Mountain-Stillwater-Fairview Peak earthquaksequence are all oblique to the north-northwest striking nodal planesfor the events (Doser, 1986). The observations suggest that the faultrupturesmay rotate clockwise and fan upward from fault ruptures at depth in the fashion of Riedel shears. Figure modified from Naylor et al.(1986).

APPENDIX 1-1B

Paleoseismicity and Lake Lahontan Shoreline Fluctuations along the Rainbow Mountain Fault

Alan R. Ramelli, John Caskey, and John W. Bell

Two trenches across the 1954 Rainbow Mountain fault rupture expose offset lacustrine and subaerial deposits that record fluctuating levels during the most recent major lacustral cycle of Lake Lahontan. The Sehoo lake cycle, as termed by Morrison (1964), began at 25-30 ka with the rise of the early-Sehoo lake (Morrison, 1991). The early-Sehoo lake had receded nearly completely by about 15 ka and then rose rapidly to a highstand elevation of ~1332 m during mid-Sehoo time at ~13 ka (Broecker and Kaufman, 1965; Benson and Thompson, 1987; Morrison, 1991; Adams and Wesnousky, 1998). Following the mid-Sehoo highstand, the lake receded rapidly to near desiccation level, and then fluctuated during smaller Holocene lacustral phases in late Sehoo and Fallon time.

The Rainbow Mountain trenches are located within an area of erosional shorelines and constructional beach bars at an elevation of 1228 m (Figure 1). Located well below the 1332-m mid-Sehoo highstand, these well-preserved shoreline features record recession of the lake after 13 ka. The principal post-highstand shorelines defined by Morrison (1991) include the recessional S_2 (dendritic) shoreline at 1290 m and a late Sehoo S_3 shoreline at approximately 1228 m (Morrison, 1964; see Road Log, Figure 2). The S_2 shoreline has been radiocarbon dated at about 11 ka (Broecker and Kaufman, 1965) and the S_3 shoreline was estimated to be 8-9 ka by Morrison (1991).

Low-sun-angle aerial photography (Figure 1) and field investigations reveal important cross-cutting relations between the fault scarp and shorelines at this site. An older, higher set of recessional strandlines are cut both by a paleoscarp and by the 1954 rupture, whereas a younger, lower constructional S_3 beach gravel bar truncates the paleoscarp and is offset only by the 1954 rupture. The cross-cutting relations therefore record an earthquake that postdates the S_2 stand and predates the S_3 gravel bar.

North trench

The North trench was excavated across the preserved paleoscarp, exposing a sequence of lacustrine and subaerial deposits exhibiting evidence for two pre-1954 faulting events (Figure 2a).

North trench stratigraphy

The footwall of the fault is composed primarily of tuffaceous sandstone and mudstone of the Tertiary Truckee Formation (Morrison, 1964), which at this location has been extensively eroded by shoreline processes and is overlain by a thin mantle of late Pleistocene and Holocene deposits.

The lowest unit in the hanging wall (Qf_1) is a poorly sorted, angular pebble sand consisting of locally derived clasts. The poorly sorted, angular clasts and a buried soil with a paleoroot zone in the top of Qf_1 indicate this unit was deposited in a subaerial, alluvial-fan environment. The paleoroot horizon yielded a radiocarbon age of 17.8 ka (Table 1; sample RM-

8), indicating Qf_1 represents a subaerial period predating the mid-Sehoo lake phase. The presence of Stage II+ pedogenic carbonate suggests the Qf_1 deposits may be older than the 17.8 ka soil age, which we interpret to approximate the timing of subaerial exposure.

Qf_1 is disconformably overlain by a sequence of mid-Sehoo beach deposits (Qsg_{1a-c}). The lowest unit of the sequence ($Qsg_{1a)}$ consists of interbedded lacustrine beach sand and gravel; sand grades laterally (to the east) into horizontally bedded, sandy, rounded, pebble beach gravel. Units Qsg_{1b} and Qsg_{1c} consist of sandy pebble to cobble beach gravel, similar to Qsg_{1a}, but contain inclined layering and clast imbrications characteristic of deposition along a beach barrier. Qsg_{1b} contains locally prominent eastward- (lakeward-) inclined clast imbrications representing beach barrier frontsets, whereas Qsg_{1c} contains prominent, westward- (landward-) inclined imbrications and layering characteristic of prograding beach-bar foresets. Calcareous tufa collected from Qsg_{1c} gravel yielded a radiocarbon age of 30.1 ka (Table 1; sample RM-1), which is anomalously old based on multiple underlying radiocarbon ages, a relation we attribute to contamination by older, inherited carbonate.

Lower and upper beach gravels (Qsg_{1b-c} and Qsg_2) are separated by Qsc, a distinctive red-brown, 15-cm-thick clayey mud layer. Qsc likely represents offshore deposition during the period the site was submerged by the mid-Sehoo lake. Organic material in Qsc yielded a radiocarbon age of 11.8 ka (Table 1; sample RM-2).

Qsc is overlain by beach gravel foresets of unit Qsg_2 likely deposited during the recessional phase that followed the S_2 stand. A 1-m-thick colluvial wedge (Qc_2), which is likely associated with the 1-m-high paleoscarp, in turn overlies unit Qsg_2.

Subaerial deposits ($Qf_{2/3}$) occur on the footwall where they overlie Qsc and a thin layer of Qsg_{1b} sand and gravel. The footwall surface is characterized by a moderately developed soil containing 10-cm-thick Av, 20-cm-thick Bw, and 35-cm-thick stage I-II Bk horizons. The hanging wall is also capped by a thin veneer of $Qf_{2/3}$ gravel that thickens to about 0.7 m near the scarp and may, in part, grade into the uppermost Qc_2 wedge deposits. A near-surface charcoal sample from $Qf_{2/3}$ yielded a radiocarbon age of 1.7 ka (Table 1; sample RM-4).

Adjacent to the fault zone, $Qf_{2/3}$ is overlain by a thin colluvial-wedge deposit (Qc_3) associated with the 1954 rupture.

North trench structural relations

The North trench exposes evidence of the three most recent earthquake ruptures, including the 1954 event. The small fault scarp and offset exposed in the trench indicate the 1954 earthquake produced only about 0.3 m of vertical offset at this location.

Qsc (i.e., the reddish mud layer described above) is offset vertically by about 1.3 m (the combined offset of the 1954 event and the penultimate, or second most recent event). Subtracting the 1954 offset indicates the penultimate event caused about 1 m of vertical offset. This estimate is supported by the 1-m-thick colluvial wedge (Qc_2), because the thickness of colluvial wedges must be less than or equal to the associated vertical offset.

Qf_1 and Qsg_1 are offset in an apparent reverse sense across a steeply west-dipping fault strand located less than a meter east of the main fault zone. This apparent reverse fault is stratigraphically truncated by Qsc, and therefore records the oldest event exposed in the trench (i.e., the triultimate, or third most recent event). The apparent reverse offset suggests this event involved a strike-slip component of fault movement. Qsc forms a marker bed that can be traced across the fault zone and within the footwall block at the western end of the trench. The profile

geometry of Qsc suggests it may have been deposited over a preexisting fault scarp formed as a result of the triultimate event.

Table 1 - Radiocarbon Age Data for the Rainbow Mountain Area

GX#	Field sample number	Age (non-calibrated ^{14}C ages (years B.P.))	Material sampled
27178	RM-1	30,140±1090	tufa
27179-AMS	RM-2	11,810±50	bulk sample
27180-AMS	RM-4	1730±40	detrital charcoal
27181-AMS	RM-6	8060±70	detrital charcoal
27182-AMS	RM-7	14,550±60	bulk sample from buried root zone
27252-AMS	RM-8	17,790±70	bulk sample from buried root zone
27682-AMS	RM11	6340±40	bulk sample from organic rich sediment
28206	RM12	17,980±270	ostracods
28207	RM-13	18,200±200	ostracods
81208-AMS	RM-14	9950±60	detrital charcoal
24186	RM-62	14,420±420	gastropods

All GX#'s refer to Geochron Laboratories sample numbers except for sample RM-14, which is a Lawrence Livermore National Laboratory sample number. AMS refers to samples analyzed by accelerator mass spectrometry.

South trench

The South trench (Figure 2b) is located slightly lower than the North trench and crosses the 1954 rupture where the late Sehoo lake phase associated with the S_3 shoreline largely eroded the paleoscarp visible at the North trench. The South trench exposed relations similar to the North trench, with the addition of deposits associated with the S_3 gravel bar. The South trench also similarly records evidence for two pre-1954 earthquakes.

South trench stratigraphy

Similar to the North trench, the footwall of the South trench is composed primarily of the Tertiary Truckee Formation (Morrison, 1964) which is overlain by a thin mantle of Holocene alluvium ($Qf_{2/3}$).

The lowermost unit in the hanging wall of the South trench correlates to the mid-Sehoo subaerial deposit (Qf_1) exposed in the North trench. Here, Qf_1 includes a lower section of angular, poorly sorted, alluvial gravel and an upper section of silt containing a soil and paleoroot horizon. The paleoroot horizon yielded a radiocarbon age of 14.5 ka (Table 1; sample RM-7), similar to the 17.8 ka age from the North trench. Qf_1 is disconformably overlain by $Qsg_{1/2}$ which consists of a thin deposit of undifferentiated mid-Sehoo beach gravel. Correlation of $Qsg_{1/2}$ to

Qsg_1 or Qsg_2 in the North trench is uncertain because $Qsg_{1/2}$ pinches out east of the fault zone and it is unclear whether $Qsg_{1/2}$ pre- or post-dates movement on the fault.

Qf_1 and $Qsg_{1/2}$ are disconformably overlain by a 10-cm-thick layer of predominantly poorly sorted, angular Qf_2 alluvial-fan gravels and reworked rounded beach cobbles. Organic sediment from Qf_2 yielded a radiocarbon age of 8.1 ka (Table 1; sample RM-6). Qf_{2a} consists of subaerial(?) sand composed of abundant ~1 mm diameter ostracod shells. Detrital charcoal from the base of Qf_{2a} yielded a radiocarbon age of 9.9 ka (Table 1; sample RM-14).

Qf_{2a} is overlain by as much as one meter of late Sehoo beach-barrier gravel (Qsg_3) and sand (Qss_3) that represent the S_3 shoreline identified elsewhere by Morrison (1964). Qsg_3 consists of pebble-cobble gravel with locally prominent eastward-inclined clast imbrications in the eastern part of the trench and prominent westward-inclined imbrications and layering in the western part, representing beach-barrier frontsets and foresets, respectively. The S_3 beach barrier is geomorphically well preserved (Figure 1) and clearly truncates the paleoscarp present at the North trench.

S_3 shoreline gravel is also present about 600 m northeast of the trench sites (Figure 1). A channel-cut at this location exposes beach gravel overlying an organic-rich sandy mud that yielded a radiocarbon age of 6.3 ka (Table 1; sample RM-11). An ostracod-rich sand that is similar to unit Qf_{2a} in the South trench lies below the 6.3-ka mud horizon. Shells from the sand in the channel-cut and from the South trench yielded nearly identical radiocarbon ages of 17.9 and 18.2 ka, respectively (Table 1; samples RM-12, RM-13). Because these ages are older than multiple ages from stratigraphically lower or equivalent units, we believe the ostracod shells were reworked from older lacustrine deposits and likely emplaced by eolian processes during the subaerial period preceding the late-Sehoo lacustral phase.

South trench structural relations

Similar to the North trench, the South trench exposes evidence of three fault events. In the South trench, Qsg_3 gravel is offset only by the 1954 break that splays upward from the main east-dipping fault. Qsg_3 clearly post-dates older west-dipping and subvertical strands of the fault zone related to earlier events. The 1954 vertical offset is similar to that at the North trench (about 0.3 m).

Qf_2 is displaced by a subvertical fault trace that exhibits a few centimeters of sandy fissure fill and at least 15 cm of vertical separation of the top of Qf_1. This fault trace is in turn truncated by Qf_{2a} and therefore records the penultimate event. If Qf_2 correlates to $Qf_{2/3}$ gravel capping the footwall, then the gravel unit is vertically offset by about 1.5 m, similar to the 1.3 m offset seen in the North trench. The radiocarbon ages from Qf_2 and Qf_{2a} (8.1-9.9 ka) approximate the age of the penultimate event because these two units appear to bracket movement on the subvertical fault.

Similar to the North trench, an easternmost fault strand dips west and displaces Qf_1 in an apparent reverse sense. Within the fault zone, the upper silty alluvium and paleoroot horizon of Qf_1 are missing, suggesting the silt unit was relatively uplifted and eroded prior to deposition of Qf_2. Because they have similar relations, we interpret the older, apparent reverse faults in both trenches to represent the same (triultimate) faulting event.

The lower part of the main east-dipping fault zone is filled by a 20-cm-thick, well-sorted, medium-grained sand that appears emplaced by injection related to liquefaction, indicating that either the lake level or groundwater were close to the trench elevation during at least one of the

paleo-events. The lack of shear fabric in the sand suggests that it was injected during the more recent, penultimate event.

Summary of lacustral and subaerial deposition

- The oldest Quaternary unit exposed in the trenches (alluvial-fan gravel Qf_1) was deposited subaerially during the desiccation phase separating the early- and mid-Sehoo lake phases (Figure 3; Morrison, 1991); radiocarbon ages of 17.8 and 14.5 ka from Qf_1 estimate the age of the desiccation phase.

- The lowermost beach sand and gravel (Qsg_{1a} in the North trench) represents the onset of the transgressive mid-Sehoo lacustral phase (after 14.5 ka).

- The rising lake went through at least minor fluctuations, producing the succession of Qsg_{1a-c} beach sand and gravel.

- Following deposition of the Qsg_{1c} gravel-bar deposits, the lake then rose to the maximum mid-Sehoo highstand at an elevation of 1332 m (~13 ka) (Figure 3).

- During the period the trench site was submerged, the offshore mud (Qsc) was deposited (~11.8 ka).

- During the post-S_2 recessional phase, the lake level dropped rapidly below the trench site to near desiccation level (Morrison, 1991), and subaerial alluvial-fan gravel and eolian sand (Qf_2 and Qf_{2a} in South trench) were deposited (9.9-8.1 ka).

- During late-Sehoo time, the lake rose during the last major lacustral (S_3) phase to the elevation of the South trench (1228 m); our radiocarbon ages suggest that this phase took place after 8-10 ka, and possibly after 6.3 ka. This latter age suggests a significantly younger age for the S_3 stand than Morrison's (1991) estimate of 8-9 ka, although this would place the S_3 stand within the early part of the Altithermal, a period generally accepted to be drier than normal.

- Finally, the lake again receded to near desiccation level, and late Holocene Qf_3 alluvial-fan gravel was deposited at the site.

Event timing and slip rate estimates for the Rainbow Mountain fault

Based on structural-stratigraphic relations, two pre-1954 faulting events are recognized in both trenches (Figure 2). The older of the two events (i.e., triultimate event) offsets Qf_1 and lower Qsg_1 deposits, but does not offset Qsc. The event age is constrained between 11.8 and 14.5-17.8 ka. In the South trench, the penultimate event displaces Qsc lake mud, Qsg_2 gravel, and Qf_2 deposits, but it does not displace overlying Qsg_3. The age of the penultimate event is constrained between 6.3 ka and 8.1-9.9 ka.

The cumulative vertical separation during the three events is estimated from 3.1 m of apparent vertical offset of the bottom of Qsg_1 deposits in the South trench. Approximately 0.3 m

of the 3.1 m net vertical offset is accounted for by the 1954 event. The geometry of the Qsc mud layer suggests that it was draped over a preexisting scarp formed by the triultimate event. Net vertical separation of Qsc across the two main fault traces in the North trench is estimated to be 1.3 m. Subtracting the 0.3 m of 1954 vertical offset provides an estimate of the vertical separation during the penultimate event (1.0 m). Hence, the triultimate and penultimate events show about 1.8 m and 1.0 m of apparent vertical offset, respectively. The apparent vertical offset of ~3.1 m averaged over the past 14.5-17.8 ka suggests a vertical slip rate of 0.17-0.21 mm/yr.

A component of lateral slip during the triultimate event is suggested by the apparent reverse offsets. A quarry across the fault ~13 km north of the trench sites revealed slickensides with a rake angle of 30˚S on a pre-1954, north-striking strand of the fault. A slip azimuth of 325˚ determined from the fault measurements is very similar to those determined instrumentally for the Rainbow Mountain and Stillwater events (326˚ and 340˚, respectively; Doser, 1986). Inferring a similar net slip azimuth (325˚) at the trench sites, where the fault strikes 015˚and dips 65˚E, suggests a right-oblique slip rate of 0.20-0.25 mm/yr. Alternatively, inferring that a 30˚S rake angle (rather than a 325˚ slip azimuth) characterizes the direction of net fault slip suggests a significantly larger right-oblique slip rate of 0.37-0.46 mm/yr.

References

Adams, K.A. and S.G. Wesnousky, 1998, Shoreline processes and the age of the Lake Lahontan highstand in the Jessup embayment, GSA Bulletin, 110, no. 6, p. 1318-1332.

Benson, L.V. and Thompson, R.A., 1987, Lake-level variation in the Lahontan basin for the past 50,000 years: Quaternary Research, v. 28, p. 69-85.

Broecker, W.S. and Kaufman, A., 1965, Radiocarbon chronology of Lake Lahontan and Lake Bonneville II, Great Basin: Geological Society of America Bulletin, v. 76, p. 537-566.

Doser, D., 1986, Earthquake processes in the Rainbow Mountain-Fairview Peak-Dixie Valley, Nevada region 1954-1959: Journal of Geophysical Research, v. 91, p. 12572-12586.

Morrison, R.B., 1964, Lake Lahontan: Geology of the southern Carson Desert, Nevada: U.S. Geological Survey Professional Paper 401, 156 p.

Morrison, R.B., 1991, Quaternary stratigraphic, hydrologic and climatic history of the Great Basin, with emphasis on Lakes Lahontan, Bonneville, and Tecopa, in Morrison, R.B., ed., Quaternary nonglacial geology: Conterminous U.S.: Boulder, Colo, Geological Society of America, The Geology of North America, v. K-2, p. 283-320.

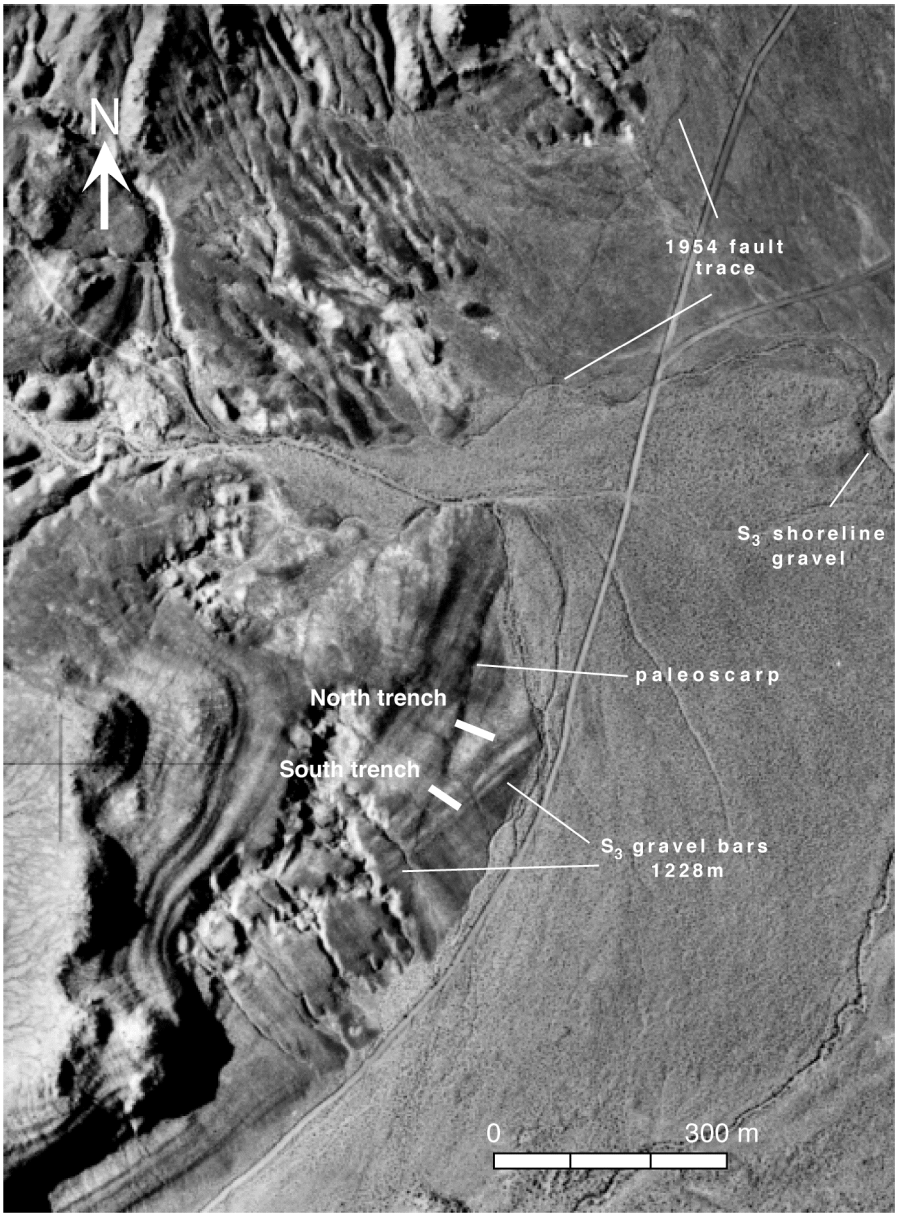

Figure 1 - Low-sun-angle aerial photograph in the area of Stop 1-1 showing trench locations across the 1954 rupture trace and cross-cutting relationships between the Rainbow Mountain fault and recessional Lake Lahontan shorelines. A set of older, higher strandlines is cut both by a paleoscarp and by the 1954 rupture at the North trench, whereas younger S_3 beach ridges truncate the paleoscarp and are offset only by the 1954 rupture near the South trench. The cross-cutting relations therefore record an earthquake that predates the S_3 gravel bar and postdates recessional shorelines above 1228 m, including the S_2 dendritic shoreline at ~1270 m (see Road Log, Figure 2).

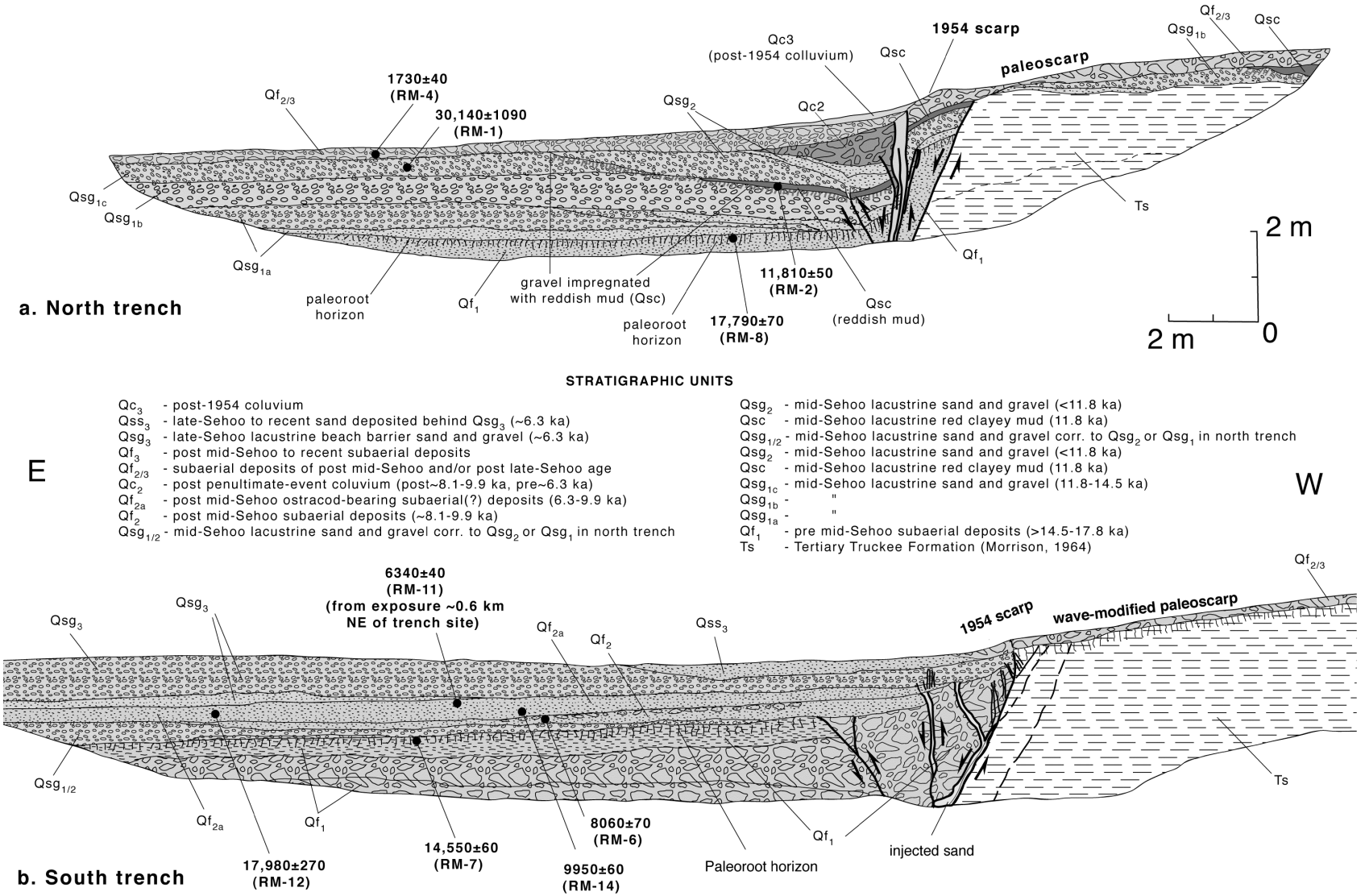

Figure 2 - Simplified logs for Rainbow Mountain trenches: a) North trench and b) South trench. See Figure 1 for trench locations and text for discussion of the stratigraphic and structural relations.

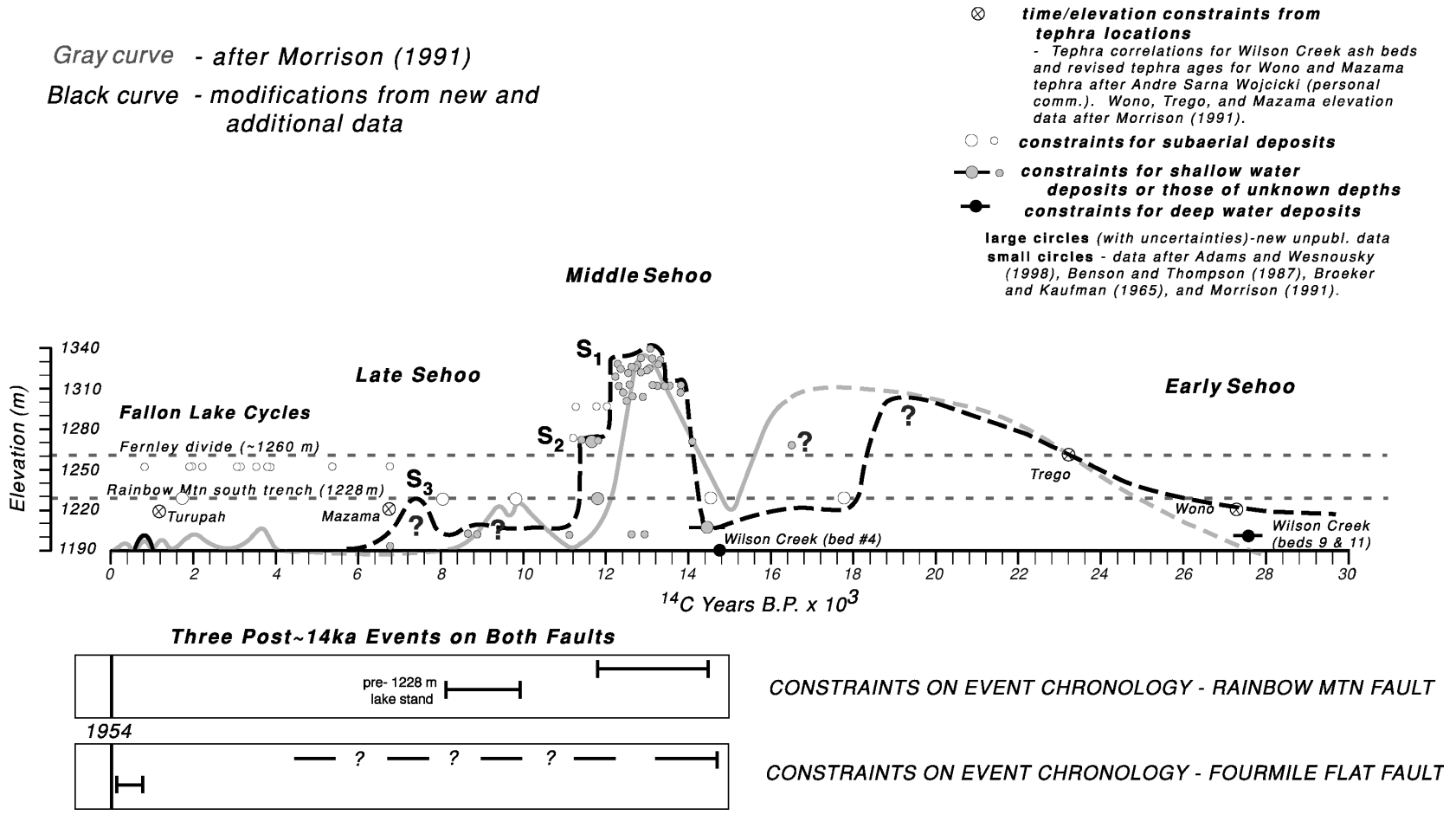

Figure 3 - Preliminary modified Lake Lahontan elevation fluctuation curve for the Carson Desert region and earthquake chronolology for the Rainbow Mountain and Fourmile Flat faults. The modified (black) lake curve reflects new constraints (large gray and white circles) acquired from the Rainbow Mountain and Fourmile flat area (Caskey et al., in prep), a Fallon lake at 1204 m (Adams, Appendix 1-2), and unpublished observations at the Wono ash constraint (Adams, personal communication). The Fernley divide (~1260 m) represents the elevation at which the Carson Desert and western subbasins were connected. Most of the data above this elevation comes from the western subbasins (e.g., Benson and Thompson, 1987). The S_1, S_2, and S_3 shoreline elevations (1332 m, 1270 m, and 1228 m) correspond to the three principal Lake Lahontan shorelines defined by Morrison (1991)(see Road Log, Figure 2).

APPENDIX 1-1C

Paleowind Estimates From Beach Clasts on Pluvial Lake Shorelines

Kenneth D. Adams

Introduction

Wind, by its very nature, is ephemeral and often leaves little or no trace of its passing. Yet, winds are a major component of a region's climate, along with temperature and precipitation. Although exceptionally strong winds can entrain particles of up to several millimeters in diameter (Sakamoto-Arnold, 1981), most winds are only capable of moving very fine to coarse sand (Pye & Tsoar, 1990; Ritter *et al*., 1995). The limiting factor in the ability of wind to transport coarser sediment is the low viscosity of air. Wind blowing over water, however, effectively transfers energy to the formation of waves, that when reaching the shore can entrain gravel, cobbles, and sometimes boulders.

The primary objective of this paper is to present a methodology using ancient beach deposits to estimate the paleowind conditions that formed them. Because the methodology developed herein is widely applicable to any number of former and present lake basins, this research represents the first step toward quantifying past wind conditions for multiple locations and different time intervals. Wind is an important climatic parameter that provides information about atmospheric pressure gradients, the trajectory of storms, and the general vigor of atmospheric circulation (Thompson et al., 1993). Paleowind conditions are also an important component delineated by global circulation models (Kutzbach et al., 1998; Thompson et al., 1993). Therefore, a general technique to "ground truth" the wind predictions in these models is important in assessing their reliability for reconstructing past climatic conditions and predicting future climatic scenarios.

Methodology

The lack of field studies and flume experiments documenting threshold transport conditions for gravel, cobbles, and boulders under oscillatory waves has led to the adaptation of flow competence evaluations from fluvial settings that deal solely with unidirectional flow (e.g. Komar, 1988, 1996). This adaptation requires the assumption of solitary wave theory where nearshore waves behave as solitary masses of water propagating shoreward at some average velocity, dictated by their height and the depth of water (Komar, 1998).

The basic procedure to estimate the strength of winds from the maximum size of beach clasts is to: 1) calculate the critical shear stress necessary to move the particle of interest (threshold condition); 2) convert the critical shear stress to a velocity profile that estimates the average velocity at the center of the grain of interest; 3) convert the mean velocity of the water mass at the particle level to breaking wave height; 4) transform the breaking wave height to the energy equivalent deepwater wave height; 5) calculate the wind stress factor from the deepwater wave height; and 6) calculate the wind speed from the wind stress factor. The assumptions for this sequence of transformations will be discussed below.

In a deposit of mixed sizes, the critical shear stress necessary to entrain a particle of a certain diameter on a plane bed is given by the following equation:

$$\tau_c = 0.045(\rho_s - \rho)gD_B^{0.6}D_m^{0.4} \qquad \text{Eq. 1}$$

where t_c = critical shear stress, 0.045 = Shield's parameter, ρ_s = density of the sediment grains, ρ = density of water, g = acceleration due to gravity (981 cm/sec^2), D_B = median diameter of bed material (b-axis, cm), and D_m = maximum particle size (b-axis; cm) (Komar, 1996). For deposits of mixed sizes, the critical shear stress necessary to move a particle of interest is, in part, dependent on the median diameter of the bed material because the height at which the particle projects into the flow above the average bed roughness controls the amount of flow stress to which the particle is subjected. The different particle sizes also affects the pivoting angle of D_m as it moves over a bed of size D_B.

To adjust the critical shear stress (t_c) to account for the upward slope of the beach and the grain pivot angle, Evans & Hardisty (1989) have derived the following equation:

$$\tau_{cB} = \tau_c\left(\frac{\tan\varphi + \tan B}{\tan\varphi}\right)\cos B \qquad \text{Eq. 2}$$

where τ_{cB} = adjusted threshold shear stress, B = beach slope (degrees), and φ = grain pivot angle. The grain pivot angle (φ) accounts for the mechanical movement of one grain over another and depends on the ratio of the size of pivoting grains to those of the bed (Komar & Li, 1986; Li & Komar, 1986):

$$\varphi = 31.9\left(\frac{D_m}{D_B}\right)^{-0.36} \qquad \text{Eq. 3}$$

where D_m = maximum particle size and D_B = median diameter of bed material. For this application, ellipsoidal particles are assumed to pivot through the saddles formed by the underlying grains.

Equations 1, 2, and 3 provide the relationships to evaluate the critical shear stress necessary to move a particle of given dimensions across a sloping bed of particles of some other dimensions. To convert this critical shear stress to a velocity profile where the velocity can be evaluated at the center of the particle of interest, the following equation applies:

$$u(z) = 5.75U_{*t}\log(30z/k_s) \qquad \text{Eq. 4}$$

where u(z) is the mean particle level velocity at the height z above the bed (taken to be 0.5 b-axis diameter), $U_{*t} = \sqrt{\tau_{cb}/\rho}$ is the shear velocity (cm/s), and $k_s = \zeta D_{50}$ is the equivalent sand roughness (Komar, 1976; Komar & Li, 1988). The factor k_s is not a measure of the physical roughness height, but a measure of the effects on flow of the roughness elements. Bayazit (1983) provides a review of experimentally derived k_s values, where it was found that z (bottom roughness coefficient) varies from 2 to 5 for gravel clasts. In this study, z is assumed to equal 3, as no studies are known to the author that experimentally derive z values for solitary waves moving over a gravel bed.

Equating the threshold velocity for a given grain size to the horizontal water velocity imparted by a shoaling wave allows the transformation of particle movement into wave characteristics. The maximum horizontal water velocity (U_{max}) beneath a wave is dependent on wave height and water depth, and is given by:

$$U_{\max} = \frac{H_b \sqrt{g h_b}}{2 h_b} \qquad \text{Eq. 4}$$

where H_b = height of the breaking wave, h_b = breaking water depth, and g = 981cm/sec^2 (CERC, 1984). In order to eliminate the specific dependence on water depth, the wave-breaking ratio (g) is used that places h_b into terms of H_b (Komar, 1998):

$$\gamma = \frac{H_b}{h_b} = 1.20 \xi_\infty^{0.27} \qquad \text{Eq. 5}$$

or rearranging,

$$h_b = \frac{H_b}{1.20 \xi_\infty^{0.27}} \qquad \text{Eq. 6}$$

where $\xi_\infty = \frac{S}{(H_\infty / L_\infty)^{0.5}}$, S is slope (tan$B$), and $\left(\frac{H_\infty}{L_\infty}\right)$ is the deepwater wave steepness. Because all large waves on lakes are locally generated storm waves, a maximum wave steepness of 1/7 = 0.142 is assumed, which is consistent with the observation of widespread whitecaps on lakes during windstorms, indicating that many of the waves are at or near breaking.

Rearranging Eq. 4 and substituting Eq. 6 for h_b, yields an equation that relates the water velocity beneath a solitary wave to the breaking wave height:

$$H_b = 0.001223 \left(\frac{1.667 U_{\max}}{\left(\frac{S}{0.3768} \right)^{0.27}} \right)^2 \left(\frac{S}{0.3768} \right)^{0.27} \qquad \text{Eq. 7}$$

The breaking wave height (H_b) is related to the deepwater wave height (H_∞) by the following equation from Komar (1998):

$$H_b = 0.39 g^{1/5} \left(T H_\infty^2 \right)^{2/5} \qquad \text{Eq. 8}$$

where T is the wave period in seconds. The functional form of this relationship is:

$$H_\infty = \left(\frac{1}{T}\right)^{0.5} \left(\frac{H_b}{0.39 g^{0.2}}\right)^{1.25} \quad \text{Eq. 9}$$

which provides the desired deepwater wave height from which wind velocity can be estimated. To use Eq. 9, the wave period must be estimated. For typical fetch lengths of 10 to 100 km, wave periods range from about 3 to 10 seconds (CERC, 1984). Once a wave period is selected for the initial calculation, it can be subsequently adjusted to better match the particular wave and fetch conditions in an iterative process.

A relatively simple method has been devised by the Coastal Engineering Research Center (CERC) for hindcasting waves, given that the waterbody is relatively simple and wave conditions are either fetch-limited or duration-limited (CERC, 1984). In fetch-limited conditions, winds have blown constantly enough for wave heights at the end of the fetch to have reached equilibrium with the winds. In the duration-limited case, wave heights are limited by the length of time that the winds have blown (CERC, 1984). By assuming fetch-limited conditions, the wind stress factor can be calculated:

$$U_A = \frac{H_\infty}{(5.112 \times 10^{-4}) F^{.0.5}} \quad \text{Eq. 10}$$

where U_A = wind stress factor (ms^{-1}), H_∞ = deep water wave height (m), and F = fetch (m) (CERC, 1984). In this procedure, it is assumed that the deepwater wave height calculated in Eq. 9 is the spectrally based significant wave height used in Eq. 10, which is equal to the average height of the highest one third of the waves (Komar, 1998). The wind stress factor (U_A) is related to the wind speed by:

$$U_A = 0.71 U^{1.23} \quad \text{Eq. 11}$$

where U is wind speed (ms^{-1}) at a height of 10 meters above the surface. This latter transformation accounts for the nonlinear relationship between wind stress and wind speed (CERC, 1984). Fetch for a particular shore location is estimated by constructing a series of nine radials at 3° intervals and extending these radials until they first intersect a far shoreline. The length of each radial is measured and then averaged to estimate the fetch (CERC, 1984).

The above methodology has been developed for deepwater wave conditions, but similar wave forecasting equations exist for waves generated in shallow water (CERC, 1984). The shallow water wave forecasting curves were developed to account for frictional losses to the lakebed, but otherwise are similar to the deepwater wave equations.

Validation

A field experiment was conducted at the Great Salt Lake of Utah to test the beach particle technique (BPT) using shorelines formed during the 1980's. After a series of wet winters, the Great Salt Lake reached its historic highstand of 1283.8 meters in 1986 and again in 1987 (Atwood, 1994). The Great Salt Lake only occupied this level for approximately two years, but during this brief period, prominent gravel ridges and coarse beach deposits were formed around

the north, west, and south sides of Antelope Island. The 1986-87 deposits are composed of coarse gravel, cobbles, and boulders that extend up to 2 meters above the still water level of 1283.8 m (Atwood, 1994).

Comparison of wind estimates using the BPT to the instrumental wind record at nearby Salt Lake City Airport indicates that they match fairly well. Estimates from the BPT range from about 6.5 to 17.4 ms^{-1}, whereas significant wind events ($\geq$ 9 ms^{-1}, $\geq$ 3 hours) observed at the Airport during 1986-87 range from 9 to 13.5 ms^{-1}. Seven of the fifteen BPT wind estimates are in the range of 6 to 9 ms^{-1}, below what has been defined as a significant wind event, but strong enough to generate waves capable of moving clasts ranging from 10 to 15 cm. For more details, see Adams (2002).

Wind Conditions Forming the Rainbow Mountain Shoreline at 1228 m

Data collection for the BPT is simple. Required information includes rock type (density), particle size measurements (b-axis), beach slope, and fetch. As an example, the constructional beach ridge at the south trench at STOP 1 (Z11 0367117 4360360) is primarily composed of basalt clasts (2.9 gm/cm^3) with the b-axes of the larger clasts ranging in size from 10 to 22 cm. A maximum b-axis particle size of 18 cm and a median B-axis size of 10 cm were selected to represent this deposit. The slope of the beach is approximately 4° and the fetch is about 17 km from the south-southeast.

Using the BPT (Eqs. 1 - 11), estimated breaking wave heights (H_b) of about 1.95 m were necessary to move the clasts found on this beach. This breaker height corresponds to a deepwater wave height (H_∞) of about 1.9 m. Given the 17 km fetch, wave period (T) was about 5 seconds. Assuming fetch-limited conditions, a deepwater wave height of about 1.9 m corresponds to a paleowind estimate of about 20 ms^{-1} (45 mph) from the south.

Comparing this paleowind estimate to an instrumental wind record from Fallon Naval Air Station (FNAS) (Fig. 1) suggests that winds may have been stronger when the 1228 m shoreline was occupied, at least for a brief time. Hourly wind observations from FNAS for the period January 1992 to December 1999 were distilled to produce a record of significant wind events for the period (Fig. 2). In this study, a significant wind event is defined as $\geq$ 9 ms^{-1} and $\geq$ 3 hours in duration. This eight year instrumental record may be comparable to the duration of the 1228 m still stand, but probably does not capture the full variability of wind events that have occurred in the historic record. Approximately 203 significant wind events were defined from the 1992-99 data with predominant directions ranging from northwest to south-southeast and average speeds from 9 to 15.5 ms^{-1} (Fig. 2). The paleowind estimate of about 20 ms^{-1} for the Rainbow Mountain 1228 m shoreline is significantly higher than the instrumental winds. Further analyses comparing pluvial lake beaches to the instrumental wind record are found in Adams (2002).

The BPT provides a new paleoclimatic tool to estimate past wind conditions in lake basins around the world, covering the time period from at least the Pleistocene to the present. Delineating past wind conditions should provide estimates of the vigor of atmospheric circulation and may prove valuable for validating global circulation models that predict wind strength at specific places and time periods as part of their output (e.g. Kutzbach (1998)). The BPT should also be applicable to modern lakes where instrumental wind records do not exist and possibly to the more ancient rock record to provide a glimpse of wind conditions in the deep geologic past.

Acknowledgements

I thank Kelly Redmond, Jim Ashby, and Greg McCurdy of the Western Regional Climate Center for supplying historical wind data from the Salt Lake City Airport and from Fallon Naval Air Station. Many helpful discussions concerning this data are also appreciated. This research was funded by the NSF-EPSCoR Interdisciplinary Science of Nevada's Unique Environments Program.

References

Adams, K.D., 2002, Estimating paleowind strength from beach deposits: Sedimentology, in press.

Atwood, G., 1994, Geomorphology applied to flooding problems of closed-basin lakes...specifically Great Salt Lake, Utah: Geomorphology, v. 10, p. 197-219.

Bayazit, M., 1983, Flow structure and sediment transport mechanics in steep channels, *in* Mutlu Sumer, B., and Muller, A., eds., Euromech 156, Mechanics of sediment transport: Rotterdam, A.A. Balkema, p. 197-206.

CERC, 1984, Shore Protection Manual: Washington, D.C., U.S. Army Corps of Engineers, U.S. Govt. Printing Office, 607 p.

Chorley, R. J., Schumm, S. A., and Sugden, D. E., 1984, Geomorphology: New York, NY, Methuen and Co., 605 p.

Evans, A. W., and Hardisty, J., 1989, An experimental investigation of the effect of bedslope and grain pivot angle on the threshold of marine gravel transport: Marine Geology, v. 89, p. 163-167.

Komar, P. D., 1976, Boundary layer flow under steady unidirectional currents, *in* Stanley, D. J., and Swift, D. J. P., eds., Marine sediment transport and environmental management: New York, Wiley Interscience, p. 91-106.

Komar, P. D., 1996, Entrainment of sediments from deposits of mixed grain sizes and densities, *in* Carling, P. A., and Dawson, M. R., eds., Advances in Fluvial Dynamics and Stratigraphy: New York, NY, John Wiley and Sons, p. 127-181.

Komar, P. D., 1998, Beach processes and sedimentation: Upper Saddle River, NJ, Prentice Hall, 543 p.

Komar, P. D., and Li, Z., 1986, Pivoting analyses of the selective entrainment of sediments by shape and size with application to gravel threshold: Sedimentology, v. 33, p. 425-426.

Komar, P. D., and Li, Z., 1988, Applications of grain-pivoting and sliding analyses to selective entrainment of gravel and to flow-competence evaluations: Sedimentology, v. 35, p. 681-695.

Kutzbach, J., Gallimore, R., Harrison, S., Behling, P., Selin, R., and Laarif, F., 1998, Climate and biome simulations for the past 21,000 years: Quaternary Science Reviews, v. 17, no. 6-7, p. 473-506.

Li, Z., and Komar, P. D., 1986, Laboratory measurements of pivoting angles for application to selective entrainment of gravel in a current: Sedimentology, v. 33, p. 413-423.

Ritter, D. F., Kochel, R. C., and Miller, J. R., 1995, Process geomorphology: Dubuque, IA, Wm. C. Brown Publishers, 546 p.

Sakamoto-Arnold, C. M., 1981, Eolian features produced by the December 1977 windstorm in southern San Juaquin Valley, California: Journal of Geology, v. 89, p. 129-137.

Thompson, R. S., Whitlock, C., Bartlein, P. J., Harrison, S. P., and Spaulding, W. G., 1993, Climatic changes in the Western United States since 18,000 yr B.P, *in* Wright, H. E., Jr., Kutzbach, J. E., Webb, T., III, Ruddiman, W. F., Street, P. F. A., and Bartlein, P. J., eds., Global climates since the last glacial maximum.: Minneapolis, MN, United States, University of Minnesota Press, p. 468-513.

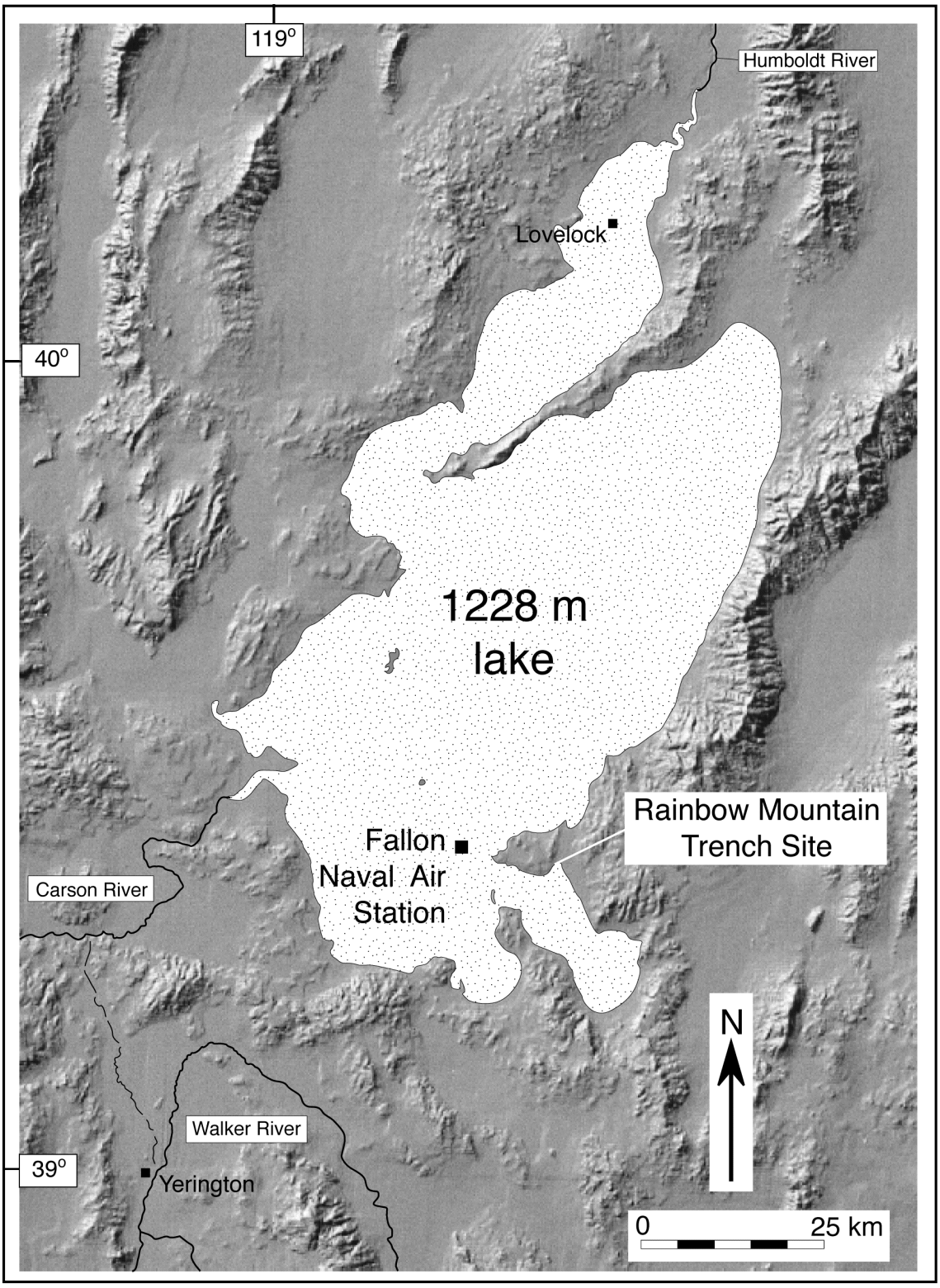

Figure 1. Map showing the approximate outline of the 1228 m lake stand represented by the beach ridge at the Rainbow Mountain trench site (south trench). Also shown is the location of the instrumental wind record from Fallon Naval Air Station.

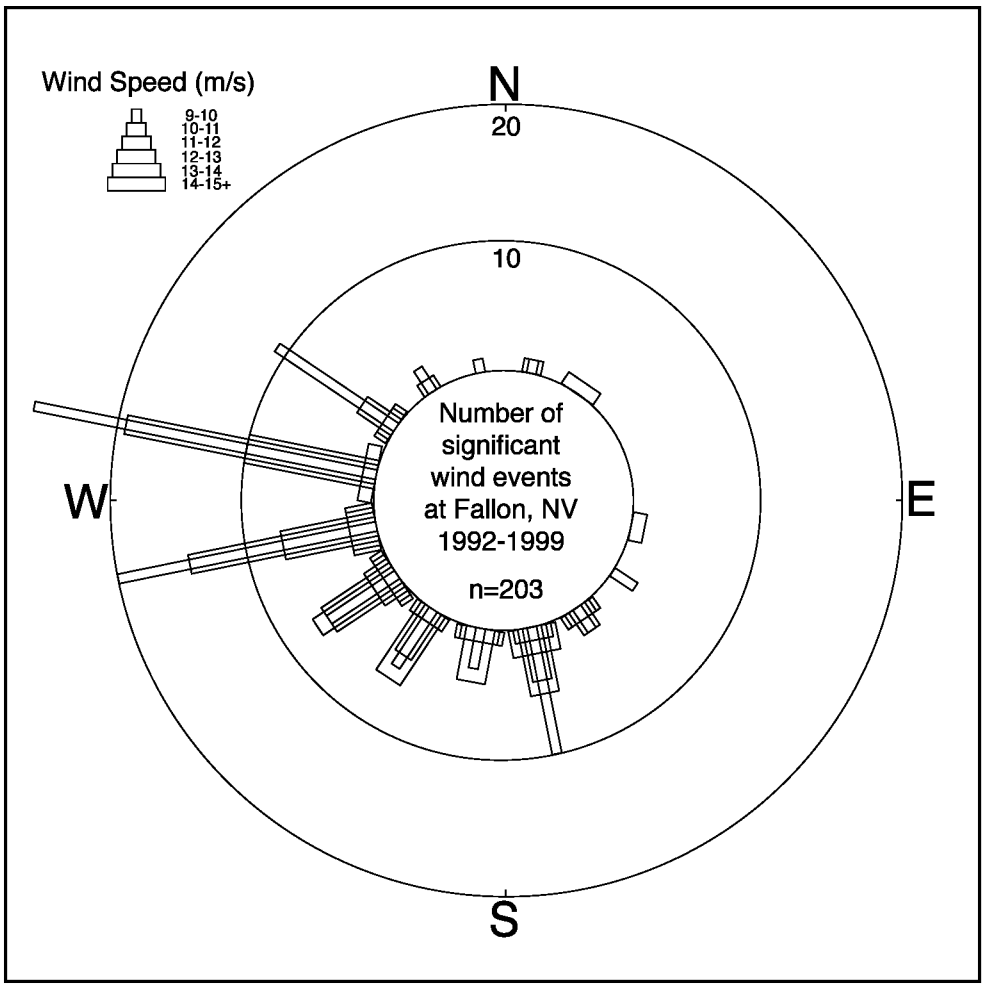

Figure 2. Wind rose of significant wind events recorded at Fallon Naval Air Station from 1992-1999. For this study, a significant wind event is defined as one that has average speeds greater than or equal to 9 ms^{-1} and durations greater than or equal to 3 hours.

APPENDIX 1-2

Late Holocene Lakes in the Carson Sink: Age and Paleoclimatic Significance

Kenneth D. Adams

Introduction

The late Holocene record of multi-decadal to multi-centennial droughts in the western Great Basin is becoming increasingly well established (e.g. Benson et al. (2002), Stine (1994)). Evidence for extended periods of drier than historic average conditions is derived from tree ring studies (Graumlich, 1993), rooted tree stumps now submerged beneath lakes and streams (Stine, 1994), and lacustrine oxygen isotope variations (Benson et al., 2002). These records suggest that long duration, severe droughts are possible in the current climatic regime and that, if they were to occur today, such droughts could severely impact the continued vitality of communities in the region.

The flipside of this climatic coin is that in the recent past there were also multiple periods when climate was effectively wetter than the historic average (e.g. Grayson (1993), Leavitt (1994), Stine (1990)). The causes for these changes are not exactly known, but they may have to do with large-scale changes in atmospheric circulation patterns and their effects on the hydrologic cycle (Cayan et al., 1999; Redmond and Koch, 1991). Because different researchers have used different proxy records from different parts of the Great Basin, it is also not clear if these climatic fluctuations affected the entire region in a synchronous manner.

This paper focuses on the late Holocene lake-level history of the Carson Sink, where lakes repeatedly expanded to sizes much larger than their historic counterparts. Whether this was due to climatic changes or was in part due to the diversion of the Walker River into and then away from the Carson Sink is not yet known. Documentation of lake-level fluctuations in the Carson Sink is part of a broader effort to delineate the post-highstand (post 13 ka) behavior of the Walker River and its effects on the paleohydrologic histories of both Walker Lake and the Carson Sink. This information is important in understanding the paleoclimate of the region and its relevance to the modern climatic regime. The results of this study are also being used to evaluate the effects of paleoenvironmental fluctuations on early inhabitants of the region and to improve existing isostatic rebound models for the Lahontan Basin.

The Fallon Lakes

Roger Morrison (1964) was the first to define a series of shallow lakes in the Carson Desert below an elevation of about 1204 m. He identified five distinct lake stands that he named Fallon lakes 1 through 5 (oldest to youngest) and grouped them in the Fallon formation (renamed Fallon Alloformation (Morrison, 1991)) that also included interbedded subaerial sediments. The Fallon lake stands are expressed as a series of roughly concentric shore features and deposits that rim the Carson Desert between about 1204 m and 1186 m. At lower elevations, there were at least two separate water bodies that included the large playa of the Carson Sink to the north and Carson Lake to the southeast (Fig. 1). Because each of the lakes was relatively shallow and lasted just a brief time, shore features are discontinuous and not very conspicuous. However,

mappable deposits and shore features marking the former margins of the Fallon lakes are locally preserved (Morrison, 1964).

Morrison (1964; 1991) correlated the first (~1204 m) and second (~1198 m) Fallon lakes with the "32-inch midden" and the "Top midden", respectively, from nearby Hidden Cave. Davis (1982; 1983) proposed two alternate radiocarbon chronologies for the sediments in Hidden Cave, the first of which places the "32-inch midden" and the "Top midden" at about 3.8 ka and 1.9 ka, respectively. The second hypothesis suggests that both midden layers were deposited in a 200-year period beginning about 3.8 ka. For a discussion of this chronology and its archaeological implications see Rhode et al. (2000).

In constructing the tephrochronology of the Lahontan Basin Davis (1978) noted that at the Marcari Road site (JOD40; Davis, 1978) near Salt Wells, the Turupah Flat Bed was exposed at the base of a dune that later had several shore features cut into its southwest surface. These relationships suggested to Davis (1978) that a lake had reached 1204 m (Fallon 1 level) in the Carson Sink at some time after 2 ka. Broecker and Kaufman (1965) reported a radiocarbon age of 1000 $\pm$ 100 yr B.P. from *Anodonta* shells associated with charcoal in a midden on the 1204 m shoreline, which is consistent with Davis' (1978) interpretation that this feature postdates 2 ka.

Currey (1988) was the first to suggest that the Fallon 1 lake shoreline (~1204 m) may date from the latest Pleistocene and correlated it to the Gilbert shoreline in the Bonneville Basin. Following Bonneville tradition, Currey (1988) proposed renaming the Fallon 1 lake shoreline the Russell shoreline in honor of Israel Russell, the first person to comprehend the history of the Lahontan Basin (e.g. Russell, (1885)). This reinterpretation was based on three radiocarbon dates thought to relate to the 1204 m lake stand that range from about 11.3 ka to 10.3 ka (Benson et al., 1992; Currey, 1988; Currey, 1990). The oldest of these dates (11,300 $\pm$ 130 yr B.P.) is from a marl deposit (deep water lacustrine sediment) at an elevation of about 1198 m in the Stillwater Slough area. A second date of 11,100 $\pm$ 110 yr B.P. was generated from dense nodules of tufa exposed on the surface of a paleodelta of the Carson River on the east side of Upsal Hogback. A third date of 10,380 $\pm$ 80 was derived from *Anodonta* shells from a 0.5 m thick shore zone sand on the north side of Humboldt Bar at 1198 m (Benson et al., 1992). These dates strongly suggest that one or more lakes existed around the 1200 m level during the latest Pleistocene. What remains to be discerned is whether this was the last time that lakes reached this elevation in the Carson Sink.

Field Sites

This section describes the stratigraphic and geomorphic settings and ages of two sites that strongly suggest that at least two late Holocene lakes reached elevations of 1198 m and 1204 m, respectively, within the Carson Sink.

Salt Wells Beach Barrier (STOP 2)

A well-defined beach barrier, herein referred to as the Salt Wells beach barrier (SWBB), is located on the south end of the Lahontan Mountains, about 2 km southeast of the Grimes Point Archaeological Area, and fringes the north edge of Turupah Flat (Fig. 2). The barrier, mapped as a Fallon 1 shoreline and defined as the Fallon type locality by Morrison (1964), is composed primarily of sand and prescribes a sinuous path about 2 km long (Fig. 2). At its eastern end, the

ridge is free standing and is surrounded by a relatively flat playa. The slightly irregular crest is at about 1204 m, but varies because of eolian erosion and deposition.

Davis (1978) found the Turupah Flat bed at two sites (JOD37 and JOD40) in this area, one to the west of the SWBB and one to the east (Fig. 2). The Turupah Flat bed has since been determined to consist of a series of at least three relatively indistinguishable tephra layers from the Mono Craters area and dating from about 0.6-2 ka (Davis, 1978; Miller, 1985; Sarna-Wojcicki et al., 1991; Sieh and Bursik, 1986; Wood, 1977). The presence of this tephra within the SWBB provides a limiting age for the deposits of < 2 ka.

The tephra exposed at Stop 2 can be traced almost continuously from the Marcari Road site (JOD40) to the eastern tip of the SWBB, a distance of almost two kilometers (Fig. 2). Along its length, the tephra crops out in a consistent manner with respect to attitude, elevation, and relation to overlying and underlying units. The tephra forms a distinct graded layer about 5 cm thick and is encased by conformable sand beds, with minor silty interbeds, that dip to the north. The layer has a smooth, abrupt lower contact and grades upward into parallel, interbedded laminae of fine sand and tephra particles over 5 cm. Below the tephra layer, the sand beds gradually become siltier. Along most of its length the tephra crops out about 2-3 m above the playa surface and is distinguished by its slightly resistant character with respect to surrounding beds. At the eastern tip of the ridge, the tephra gently descends toward and apparently intersects the playa surface. Tephra beds cropping out in ridge-like features south of the SWBB are very similar with respect to thickness, stratigraphic position, elevation, and the fact that they dip away from the playa or former lakebed (Fig. 2).

Fine detrital charcoal ($\leq$ 1-2 mm) was collected from a single thin layer about 5 cm below the tephra at Stop 2. There was no obvious bioturbation in the immediate vicinity of the sample and the charcoal appeared to lie on a depositional surface between thin sand beds. Its AMS radiocarbon age of 812 $\pm$ 72 yr B.P. (~730 cal yr B.P.) agrees with the limiting age provided by the overlying tephra layer. Thus, the Salt Wells beach barrier was being formed about 730 years ago (AD 1222) when a lake stood at about 1204 m in the Carson Sink.

The field relations and morphology of the Salt Wells beach barrier raise an obvious question as to whether its genesis has been misinterpreted. Could this feature actually be a sand dune and have nothing to do with late Holocene lake levels? The ridge is primarily composed of fine to medium sand, is located in an area of active dunes, and has obvious eolian features associated with it, all of which point to eolian processes involved in its formation.

One of the strongest arguments against an entirely eolian interpretation for the SWBB is its morphology and the outcrop pattern of the tephra, both of which express the sedimentary architecture of the ridge. The nearly continuous and consistent outcrop pattern of the tephra in the SWBB indicates that it was deposited at a common elevation over a distance of almost 2 km on a northward sloping (~10° to 25°) depositional surface (Fig. 2). If this feature were a sand dune, it would have had an active slip face approximating these dimensions at the time of tephra deposition. Although there are many obvious dunes in the area, they are generally barchan dunes or crescentic ridges of much smaller proportions and restricted slip faces. The general orientation of these smaller features is about N45W, which is approximately perpendicular to the prevailing southwest winds in the area. Barchans and crescentic ridges typically form at right angles to a narrow range of effective wind directions (Lancaster, 1995). In contrast, the trend of the SWBB ranges from N45W at its western end, to approximately E-W in its central part, and about N48W at its eastern end. In terms of dune morphology, the planform of the SWBB best approximates a

single, sinuous crescentic ridge. These types of dunes consist of a series of connected crescents that form the higher parts of the dune ridge with intervening lower, but more rapidly migrating, saddle areas (Lancaster, 1995). This variation in height should also be reflected in the sedimentary architecture of the ridge. The SWBB, however, is approximately horizontal along its crest and the architecture of this feature, as evidenced by the outcrop pattern of the tephra, indicates that it accreted vertically as a roughly horizontal unit along its length.

The most logical explanation for the field relations is that the tephra was deposited on the backside (landward side) of an active beach barrier from wave overwash processes. This process well explains the regular outcrop pattern of the tephra, which is now exposed on the lakeward side of the barrier because continued overwash probably eroded material from the front of the barrier and deposited it on the landward side causing the landward migration of the barrier crest (Adams and Wesnousky, 1998). Eolian erosion of the windward (south) side of the ridge appears to have played an important, but lesser role in exposing the tephra. A beach ridge genesis also explains the sinuous planform of the ridge where waves traveling from the southwest transported the sandy sediment to the east, causing the ridge to build into a spit at its eastern end. It is likely that the waves utilized preexisting dunes and other eolian deposits to form the beach ridge. Davis (1978) concluded that the 1204 m shoreline postdated the deposition of the tephra but based on field relations it appears that they are essentially coeval and date from about 730 cal yr B.P., the age of detrital charcoal from within the deposit.

Wildcat Scarp

The Wildcat scarp is an arcuate feature that wraps around the south and east sides of Carson Lake for a distance of about 19 km (Fig. 1). The escarpment is up to 10 m high in its central part but decreases to less than a meter at either end. Morrison (1964) presents evidence that the feature is tectonic in origin, but indicates that it has been modified by shore processes of the Fallon lakes. In 1980, John Bell (Nevada Bureau of Mines and Geology) excavated four trenches across the north-striking eastern part of the Wildcat scarp in an effort to reconstruct the faulting history of this feature. Two of these trenches (trenches 5 and 6) were excavated across a subsidiary escarpment located upslope and slightly to the east of the main scarp. In trench 5 (UTM Zone 11, 0358589 4354403), there was a single, small (1-2 cm) reverse offset of a tephra layer, but otherwise no other evidence of tectonic deformation. Instead, Bell found a wedge-shaped deposit of interbedded sand and silty clay/clayey silt that pinches out near the base of the scarp. A thin tephra unit is located within the wedge-shaped deposit and may be overlying a minor buried soil. Bell interpreted the minor scarp to be a wave-formed feature and the abutting sediments to be shore deposits from one of the Fallon lakes. These deposits overlie clay, which Bell interpreted to represent the Sehoo Alloformation. A gravel lag (?), shells, and an extensive grass mat were found at the contact between the underlying clay and the shore deposits. These relations were interpreted to represent the transgression of a lake over an area covered by grass. An AMS radiocarbon age of 1510 $\pm$ 40 yr B.P. (~1375 cal yr B.P.) on the grass dates this transgression that reached an elevation of at least 1198 m.

If this lake reached 1198 m about 1375 cal yr B.P., then it implies that the 1204 m lake transgressed over this site about 650 years later (~730 yr B.P.) and inundated it to a depth of about 6 m. Is there evidence for a second transgression in the wedge-shaped deposit that abuts the 1198 m scarp? Bell interpreted a probable paleosol immediately underlying the tephra in this section. The tephra and the sediments above the minor paleosol may represent the transgression

and regression of the 1204 m lake, but more work is required to confirm or refute this interpretation.

Discussion and Conclusions

The presence of large late Holocene lakes in the Carson Sink has long been postulated (e.g. Morrison, 1964), but their timing is not very well known. The new radiocarbon dates reported herein now provide strong evidence for the timing and extent of at least two of these lakes. Further, these dates refute the interpretation of Currey (1988; 1990) and Benson et al. (1992) that the 1204 m level was last reached in the latest Pleistocene. Instead, this shoreline was occupied about 730 years ago and represents a lake that covered about 3300 km^2 (Fig. 3). The rise of this lake was not an isolated event, as a lake rose to at least 1198 m (~2800 km^2) at about 1375 cal yr B.P.

Lakes of this size would clearly inundate most of the Carson Sink, including the Stillwater Marsh area where a fairly continuous late Holocene record of human occupation exists. Reconciling the geologic evidence for large, late Holocene lakes with the archaeological evidence from the floor of the Carson Sink is an area of active research, the results of which will be presented elsewhere. For more information see Rhode (2000) and Kelly (2001).

Comparing the Carson Sink lake level record to other paleohydrologic records in the region yields interesting results. In the Mono Lake basin, Stine (1990) reported a lowstand at about 730 cal yr B.P., but a moderate highstand at 1375 cal yr B.P. Conversely, in the Pyramid Lake basin Benson et al. (2002) reported a positive water balance at about 730 cal yr B.P. and negative or falling lake level at 1375 cal yr B.P. These interpretations, however, are based on oxygen isotope variations which do not provide information on the intensities of dry or wet periods because the variations can not be uniquely related to lake volume (Benson et al., 2002).

Stine (1994) reported the existence of relict tree stumps rooted in present-day lakes, marshes, and streams that suggest two extreme droughts in the Sierra Nevada lasting more than two centuries prior to AD ~1112 and for more than 140 years prior to AD ~1350. The timing of the 730 cal yr B.P. (AD ~1222) lake stand at 1204 m in the Carson Sink falls right between these two mega-drought periods. If all of these interpretations are correct, then they imply that recent climatic fluctuations in the Sierra Nevada and western Great Basin have been severe and long lasting, both on the wet and dry sides of the climatic continuum.

The surface area and volume of a 1204 m lake in the Carson Sink are about 3300 km^2 and 58 km^3, respectively (Fig. 3) (Benson and Mifflin, 1986). For an 1198 m lake, the numbers are a bit lower but still quite substantial (~2800 km^2 and 40 km^3, respectively). Considering that the historic average inflow into the Carson Sink each year from the Humboldt and Carson rivers is about 1.5 km^3/year (Benson and Paillet, 1989), each of the Fallon lakes must have been present for relatively long periods of time, at least decades. The historic average annual lake evaporation rate for the Fallon area is about 1.04 m/year, but ranged from 0.72 to 1.29 m/year during the period 1951-1992. If imposed on a 3000 km^2 lake, this rate would equate to approximately 3 km^3 of water evaporated per year. Thus, modern discharge rates for the Humboldt and Carson rivers must be increased by a factor of two simply to overcome the amount of water evaporated from the surface of a 1204 m lake.

One way to add substantial inflow into the Carson Sink, without a change in climate, is to divert the Walker River from Walker Lake to the Carson Sink via Adrian Valley (Figs. 1 and 3). When this happened, Walker Lake became shallow or desiccated to a playa and the Carson Sink

received a substantial new source of water (Benson and Thompson, 1987). The average historic (~32 years data) discharge of the Walker River is about 0.4 km^3 of water per year, or roughly 26% of the combined flow of the Carson and Humboldt rivers (Benson and Paillet, 1989). Work is currently in progress in the Walker Lake basin and along the Walker River paleochannel in an attempt to integrate the diversion history of the Walker River and the paleohydrologic histories of the Carson Sink and Walker Lake. For more information on existing data for the diversion of the Walker River and its influence on Walker Lake see Benson et al. (1991), Benson and Thompson (1987), Bradbury et al. (1989), King (1993), King, (1996), and Grayson (1993).

Acknowledgements

I would like to thank John Bell for supplying the grass radiocarbon sample from his trench 5 along the Wildcat scarp, a trench log of the exposure, and for interesting discussions concerning this sample. Helpful discussions with Nick Lancaster on dune morphology and sedimentology are also appreciated, but the author takes full responsibility for the interpretations presented herein. This research was funded by the National Science Foundation (EAR 0087840).

References

Adams, K. D., and Wesnousky, S. G., 1998, Shoreline processes and the age of the Lake Lahontan highstand in the Jessup embayment, Nevada: Geological Society of America Bulletin, v. 110, no. 10, p. 1318-1332.

Benson, L., Kashgarian, M., Rye, R., Lund, S., Paillet, F., Smoot, J., Kester, C., Mensing, S., Meko, D., and Lindstrom, S., 2002, Holocene multidecadal and multicentennial droughts affecting northern California and Nevada: Quaternary Sceince Reviews, v. 21, p. 659-682.

Benson, L. V., Currey, D. R., Lao, Y., and Hostetler, S. W., 1992, Lake-size variations in the Lahontan and Bonneville basins between 13,000 and 9000 (super 14) C yr B.P: Palaeogeography, Palaeoclimatology, Palaeoecology, v. 95, no. 1-2, p. 19-32.

Benson, L. V., Meyers, P. A., and Spencer, R. J., 1991, Change in the size of Walker Lake during the past 5000 years: Palaeogeography, Palaeoclimatology, Palaeoecology, v. 81, p. 189-214.

Benson, L. V., and Mifflin, M. D., 1986, Reconnaissance bathymetry of basins occupied by Pleistocene Lake Lahontan, Nevada and California: U.S. Geological Survey Water Resources Investigations Report 85-4262, p. 14.

Benson, L. V., and Paillet, F. L., 1989, The use of total lake-surface area as an indicator of climatic change: examples from the Lahontan Basin: Quaternary Research, v. 32, p. 262-275.

Benson, L. V., and Thompson, R. S., 1987, The physical record of lakes in the Great Basin, *in* Ruddiman, W. F., and Wright, H. E., Jr., eds., North America and adjacent oceans during the last deglaciation: Boulder, CO, United States, Geological Society of America, p. 241-260.

Bradbury, J. P., Forester, R. M., and Thompson, R. S., 1989, Late Quaternary paleolimnology of Walker Lake, Nevada: Journal of Paleolimnology, v. 1, p. 249-267.

Broecker, W. S., and Kaufman, A., 1965, Radiocarbon chronology of Lake Lahontan and Lake Bonneville; Part 2, Great Basin: Geological Society of America Bulletin, v. 76, no. 5, p. 537-566.

Cayan, D. R., Redmond, K. T., and Riddle, L. G., 1999, ENSO and hydrologic extremes in the western United States: Journal of Climate, v. 12, p. 2881-2893.

Currey, D. R., 1988, Isochronism of final Pleistocene shallow lakes in the Great Salt Lake and Carson Desert regions of the Great Basin: Program and Abstracts of the Tenth Biennial Meeting, American Quaternary Association, p. 117.

Currey, D. R., 1990, Quaternary palaeolakes in the evolution of semidesert basins, with special emphasis on Lake Bonneville and the Great Basin, U.S.A: Palaeogeography, Palaeoclimatology, Palaeoecology, v. 76, no. 3-4, p. 189-214.

Davis, J. O., 1978, Quaternary tephrochronology of the Lake Lahontan area, Nevada and California, University of Nevada, Nevada Archeological Survey Research Paper 7, 137 p.

Davis, J. O., 1982, Bits and pieces: the last 35,000 years in the Lahontan basin, *in* Madsen, D. B., and O'Connell, J. F., eds., Man and Environment in the Great Basin, Society of American Archeology Papers No. 2, p. 53-75.

Davis, J. O., 1983, Geology of Gatecliff shelter: sedimentary facies and Holocene climate, *in* Thomas, D. H., ed., The archaeology of Monitor Valley 2: Gatecliff shelter: New York, Anthropological Papers of the American Museum of Natural History, p. 64-87.

Graumlich, L. J., 1993, A 1000-year record of temperature and precipitation in the Sierra Nevada: Quaternary Research, v. 39, p. 249-255.

Grayson, D. K., 1993, The desert's past: a natural prehistory of the Great Basin: Washington, D.C., Smithsonian Institution Press, 356 p.

Kelly, R. L., 2001, Prehistory of the Carson Desert and Stillwater Mountains. Environment, mobility, and subsistence in a Great Basin wetland: Salt Lake City, University of Utah Anthropological Papers Number 123, 325 p.

King, G. Q., 1993, Late Quaternary history of the lower Walker River and its implications for the Lahontan paleolake system: Physical Geography, v. 14, no. 1, p. 81-96.

King, G. Q., 1996, Geomorphology of a dry valley: Adrian Pass, Lahontan basin, Nevada: Association of Pacific Coasts Geographers Yearbook, v. 58, p. 89-114.

Lancaster, N., 1995, Geomorphology of desert dunes: New York, Routledge, 290 p.

Leavitt, S. W., 1994, Major wet interval in White Mountains Medieval Warm Period evidenced in $d^{13}C$ of Bristlecone Pine tree rings: Climatic Change, v. 26, p. 299-307.

Miller, C. D., 1985, Holocene eruptions at the Inyo volcanic Chain: Implications for possible eruptions in Long Valley Caldera: Geology, v. 13, p. 14-17.

Morrison, R. B., 1964, Lake Lahontan: Geology of the southern Carson Desert, U.S. Geological Survey Professional Paper 401, 156 p.

Morrison, R. B., 1991, Quaternary geology of the southern Basin and Range Province, *in* Morrison, R. B., ed., Quaternary nonglacial geology; conterminous U.S.: Boulder, CO, United States, Geol. Soc. Am., p. 353-371.

Morrison, R. B., 1991, Quaternary stratigraphic, hydrologic, and climatic history of the Great Basin, with emphasis on Lake Lahontan, Bonneville, and Tecopa, *in* Morrison, R. B., ed., Quaternary nonglacial geology; conterminous U.S.: Boulder, CO, United States, Geological Society of America, p. 283-320.

Redmond, K. T., and Koch, R. W., 1991, Surface climate and streamflow variability in the western United States and their relationship to large-scale circulation indices: Water Resources Research, v. 29, no. 9, p. 2381-2399.

Rhode, D., Adams, K. D., and Elston, R. G., 2000, Geoarchaeology and Holocene landscape history of the Carson Desert, western Nevada, *in* Lageson, D. R., Peters, S. G., and Lahren, M. M., eds., Great Basin and Sierra Nevada: Boulder, Geological Society of America Field Guide 2, p. 45-74.

Russell, I. C., 1885, Geological history of Lake Lahontan, a Quaternary lake in northwestern Nevada, U.S. Geological Survey Monograph 11, 288 p.

Sarna-Wojcicki, A. M., Lajoie, K. R., Meyer, C. E., Adam, D. P., and Rieck, H. J., 1991, Tephrochronologic correlation of upper Neogene sediments along the Pacific margin, conterminous United States, *in* Morrison, R. B., ed., Quaternary nonglacial geology; Conterminous U.S.: Boulder, CO, Geological Society of America, p. 117-140.

Sieh, K., and Bursik, M., 1986, Most recent eruption of the Mono Craters, eastern central California: Journal of Geophysical Research, v. 91, no. B12, p. 12,539-12,571.

Stine, S., 1990, Late Holocene fluctuations of Mono Lake, California: Palaeogeography, Palaeoclimatology, Palaeoecology, v. 78, p. 333-381.

Stine, S., 1994, Extreme and persistent drought in California and Patogonia during mediaeval time: Nature, v. 369, p. 546-549.

Stine, S. W., 1994, Droughts and deluges in late Holocene California: the record from lake fluctuations and drowned stumps, EOS Transactions, American Geophysical Union, p. 370.

Wood, S. H., 1977, Distribution, correlation, and radiocarbon dating of late Holocene tephra, Mono and Inyo craters, eastern California: Geological Society of America Bulletin, v. 88, no. 1, p. 89-95.

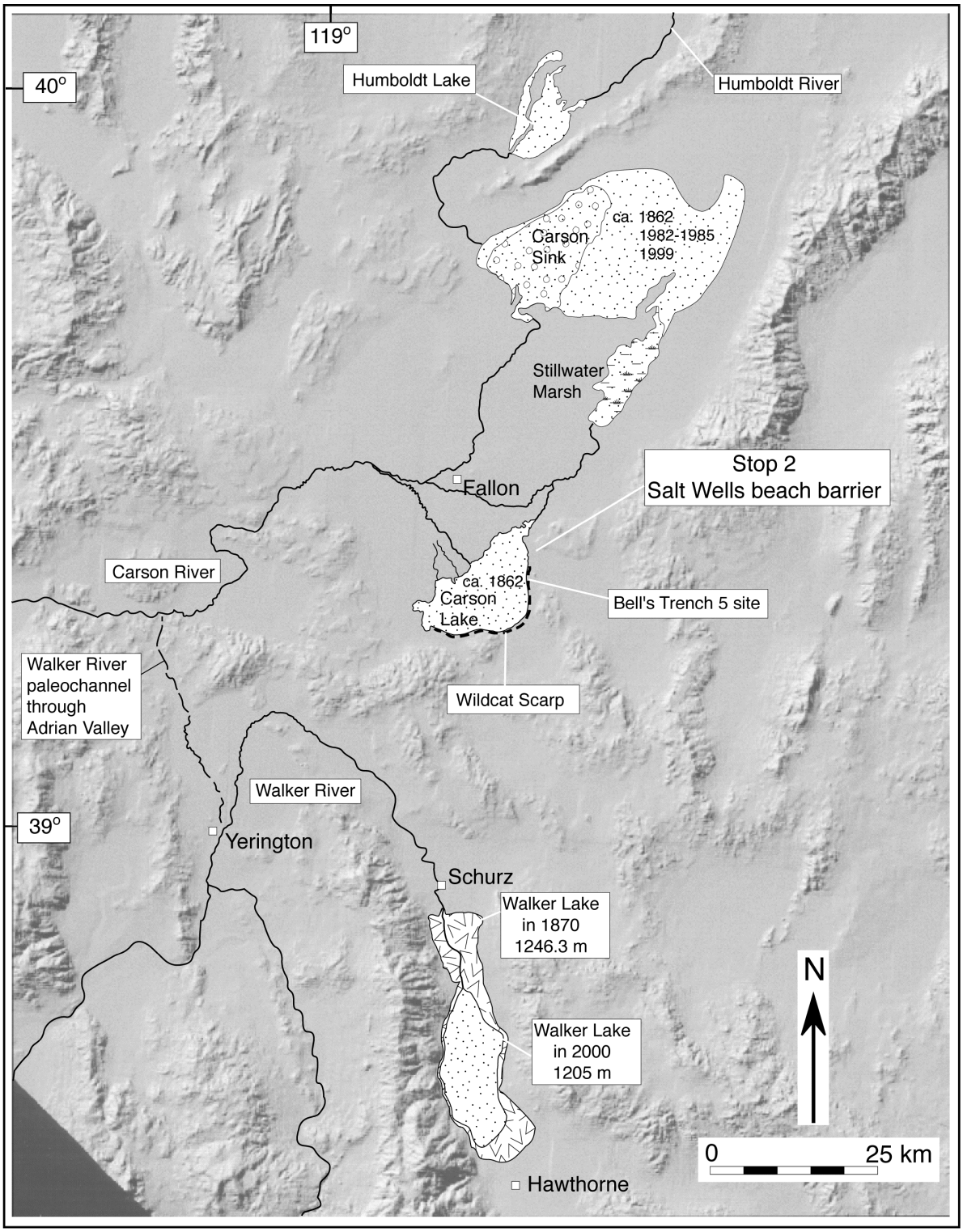

Figure 1 . Map of the Carson Sink and Walker Lake areas with relevant hydrographic features as they have appeared during historic times. Also shown are localities mentioned in the text. In average years, the Carson Sink is a playa and Carson Lake is shallow and marshy. The Walker River presently flows to Walker Lake but, in the past, has been diverted to become a tributary to the Carson River, thus providing a significant new source of water to the Carson Sink.

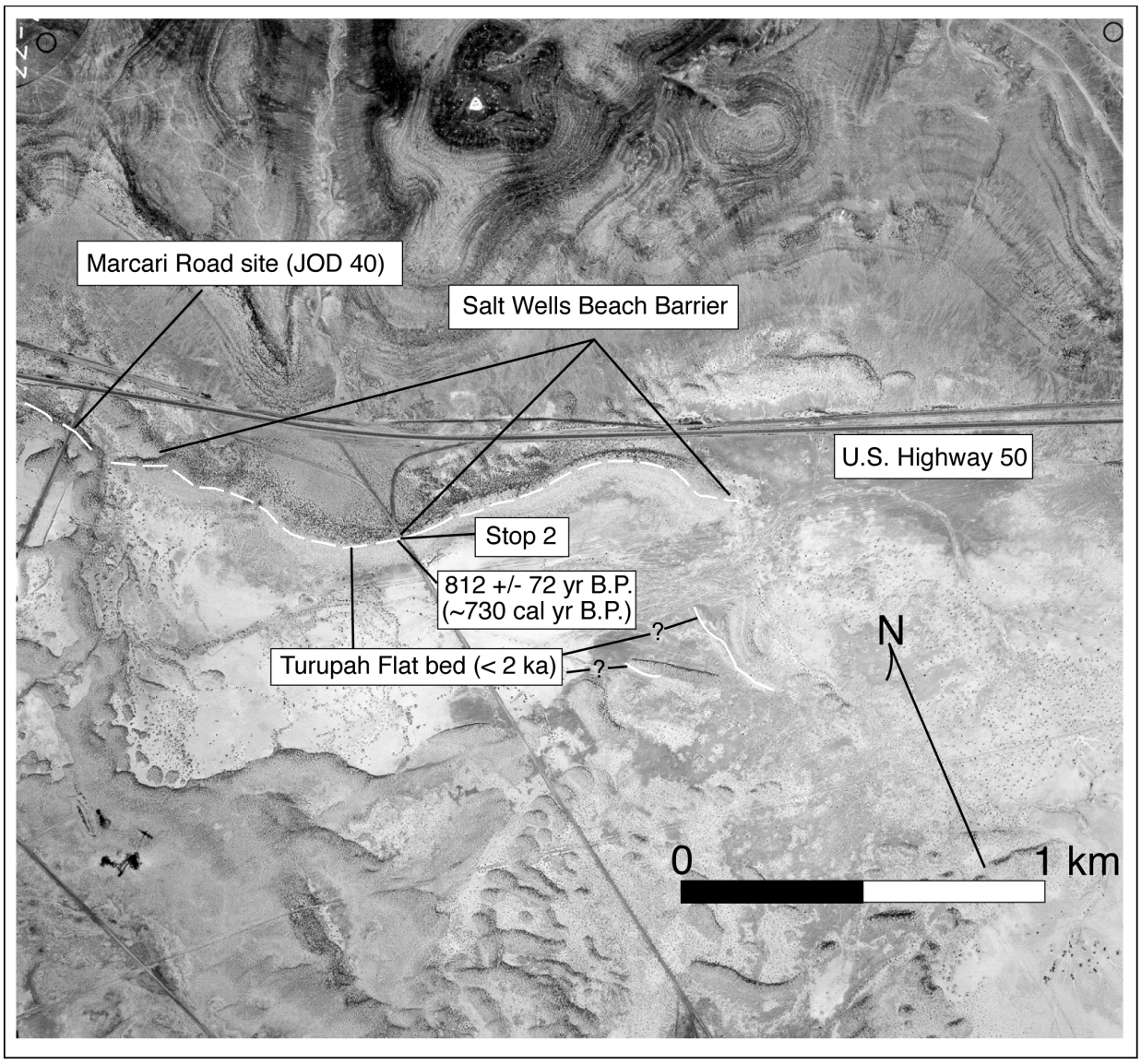

Figure 2. Vertical aerial photograph of the Salt Wells beach barrier and vicinity. The Turupah Flat bed outcrops in a very consistent manner suggesting that it was deposited by overwash processes on the backsides of beach barriers when water filled the Carson Sink to 1204 m. The radiocarbon age of detrital charcoal from within the Salt Wells beach barrier indicates that it was deposited about 730 cal yr B.P.

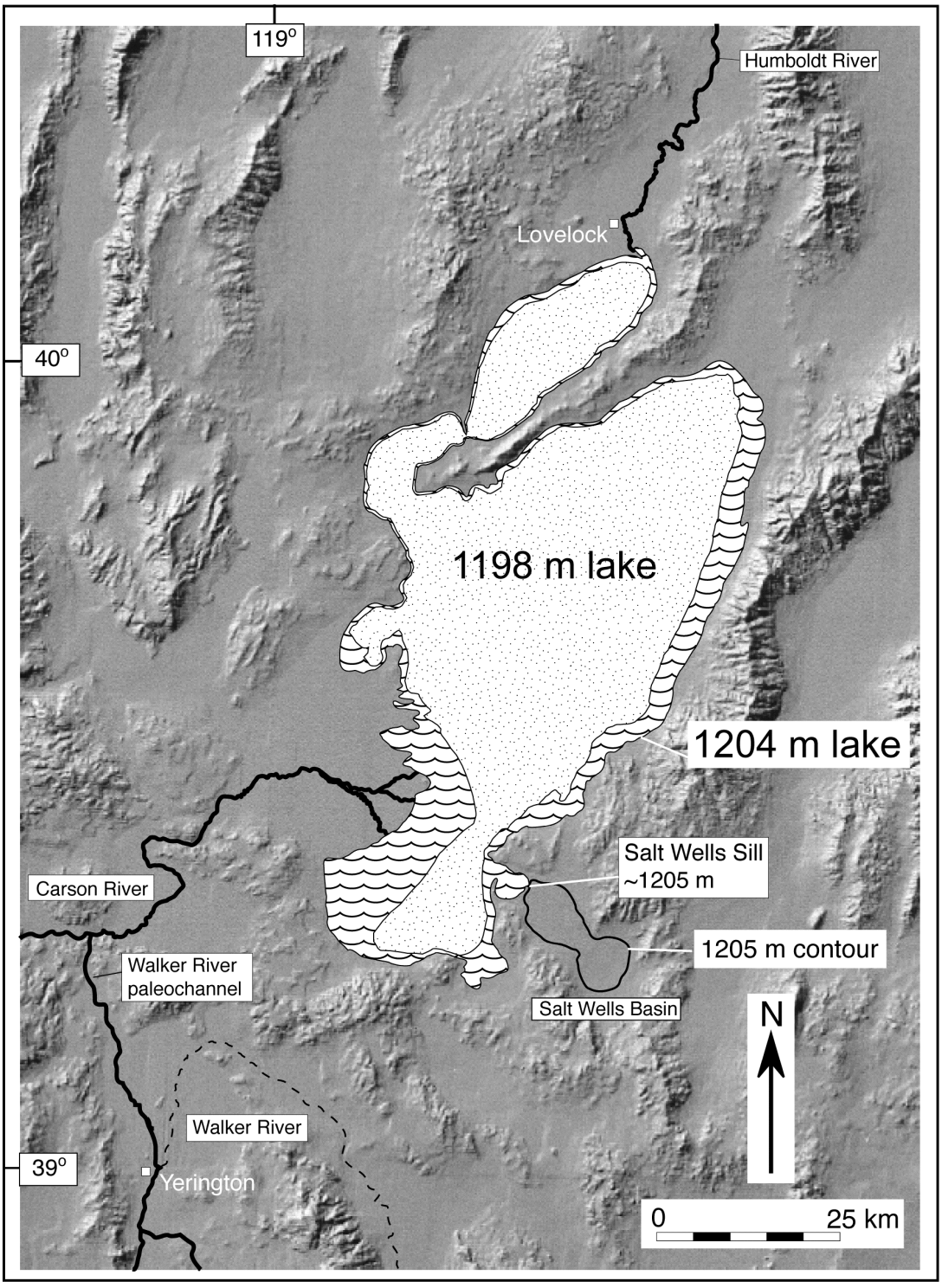

Figure 3. Map showing the approximate outlines of the 1198 m and 1204 m lakes in the Carson Sink. On this map, the Walker River is shown as a tributary to the Carson River, but the exact times of Walker River diversions to the Carson Sink are not yet known. Also shown is the 1205 m contour in the Salt Wells Basin. Spill to this basin probably acted as a control on the 1204 m lake.

APPENDIX 1-3A

Overview of the 1954 Fairview Peak-Dixie Valley Rupture Sequence

John Caskey, Steven G. Wesnousky, and D. Burton Slemmons

(The following summary is modified from Caskey et al. (2000))

The 16 December 1954 M_s7.2 Fairview Peak earthquake was followed 4 min and 20 sec later by the M_s6.8 Dixie Valley earthquake. Surface ruptures were distributed among six different faults that define a complex zone of normal and normal right-oblique surface ruptures 100 km long and over 15 km wide (Figure 1) (Slemmons, 1957; Caskey et al., 1996) The sequence progressed from south to north and initiated on the east-dipping Fairview fault. Surface ruptures on the Fairview fault extend for a distance of 32 km and exhibit primarily right-oblique displacements. A maximum right-lateral offset and vertical separation of 3.4 and 3.8 m, respectively, were measured near the epicentral region for the earthquake, just south of Fairview Peak (Figures 1 and 2). The subsequent Dixie Valley earthquake produced a 46-km-long zone of ruptures along the east-dipping Dixie Valley fault, which bounds the eastern escarpment of the Stillwater Range. In contrast to the Fairview fault, the Dixie Valley fault ruptures produced only dip-slip offsets. Maximum vertical separations of ~2.8 m were measured along two distinct reaches of the fault, one just north of Coyote Canyon, near the south end of the main rupture trace, and the other near IXL Canyon (Figures 1 and 2). Because the Dixie Valley event occurred only 4 minutes after the Fairview Peak earthquake, details of the Dixie Valley waveforms are obscured by those of the preceding event. Hence, efforts to locate the Dixie Valley epicenter have been problematic (Doser, 1986) (Figure 1) and first motion data are not available to constrain a focal mechanism for the event.

The west dipping West Gate, Louderback Mountains, and Gold King faults also ruptured during the sequence, although these fault ruptures are of relatively short length (10, 14, and 8.5 km, respectively). The West Gate and Louderback Mountains ruptures produced maximum right-oblique-slip offsets of 1.4 and 1.8 m, respectively. The Gold King fault ruptures showed only dip-slip offsets averaging about 0.5 m. The Gold King fault also produced minor surface ruptures during the 1903 Wonder earthquake (Slemmons et al., 1959). Although, there were no eyewitness reports to confirm whether the west-dipping faults ruptured with the first or second earthquake, it is generally assumed that the Fairview fault and faults along the eastern side of Dixie Valley ruptured with the initial Fairview Peak event. This interpretation is consistent with the balance of moment release calculated from geologic data for the two events (Caskey et al., 1996). The three west-dipping faults form a complex structural linkage within a 15 km left-step between the east-dipping Fairview and Dixie Valley faults (Figure 3). The west-dipping faults appear to have played an important role in the transfer of stress and subsequent triggering of the Dixie Valley earthquake (Caskey and Wesnousky, 1997). Finally, in the northern part of Gabbs Valley, minor ruptures broke along a 6 km-long portion of the Phillips Wash fault (southeast of the area shown in Figure 1) during the 1954 sequence. Curiously, the Phillips Wash ruptures trend subparallel to the Fairview fault, yet they produced left-oblique displacements.

During the summers of 1992 and 1993, the entire rupture zone was traversed and mapped on sets of ~1:12,000 scale, low-sun-angle aerial photos taken in 1968 and 1970. A total of about 600 measurements of vertical separation and lateral offset were made at intervals averaging about 300 m along-strike for each fault trace (e.g., Figure 2). These field measurements together with details of the rupture geometry provided the basis for the stress models of the rupture sequence.

References

Bell, J.W., 1984, Quaternary fault map of Nevada, Reno Sheet, Map 79: Nevada Bureau of Mines and Geology.

Caskey, S.J., J.W. Bell, D.B. Slemmons, and A.R. Ramelli, 2000, Historical surface faulting and paleoseismology of the central Nevada seismic belt, *in* Great Basin and Sierra Nevada, *Geol. Soc. Am. Field Guide 2*, Lageson, D.R., editor, pp.23-44.

Caskey, S.J., S.G. Wesnousky, P. Zhang, and D.B. Slemmons, 1996, Surface faulting of the 1954 Fairview Peak (Ms7.2) and Dixie Valley (Ms6.9) earthquakes, central Nevada: Bulletin of the Seismological Society of America, v. 86, no. 3, p. 761-787.

Caskey, S.J., and S.G. Wesnousky, 1997, Static stress changes and earthquake triggering during the 1954 Fairview Peak and Dixie Valley earthquakes, central Nevada: Bulletin of the Seismological Society of America, v. 87, no. 3, p. 521-527.

Caskey, S.J., J.W. Bell, A.R. Ramelli, and S.G. Wesnousky, Historic surface faulting and paleoseismicity in the area of the 1954 Rainbow Mountain-Stillwater earthquake sequence, central Nevada (in preparation).

Dohrenwend, J.C., B.A. Schell, C.M. Menges, B.C. Moring, and M.A. McKittrick, 1996, Reconnaissance photogeologic map of young (Quaternary and late Tertiary) faults in Nevada, Open File Report, OFR 96-2: Nevada Bureau of Mines and Geology, in cooperation with the U.S. Geological Survey, scale 1:1,000,000.

Doser, D., 1986, Earthquake processes in the Rainbow Mountain-Fairview Peak-Dixie Valley, Nevada region 1954-1959: Journal of Geophysical Research, v. 91, p. 12572-12586.

Slemmons, D.B., 1957, Geological effects of the Dixie Valley-Fairview Peak, Nevada, earthquakes of December 16, 1954: Bulletin of the Seismological Society of America, v. 47, no. 4, p. 353-375.

Slemmons, D.B., K.V. Steinbrugge, D. Tocher, G.B. Oakeshott, and V.P. Gianella, 1959, Wonder, Nevada, earthquakes of 1903: Bulletin of the Seismological Society of America, v. 49, no. 3, p. 251-265.

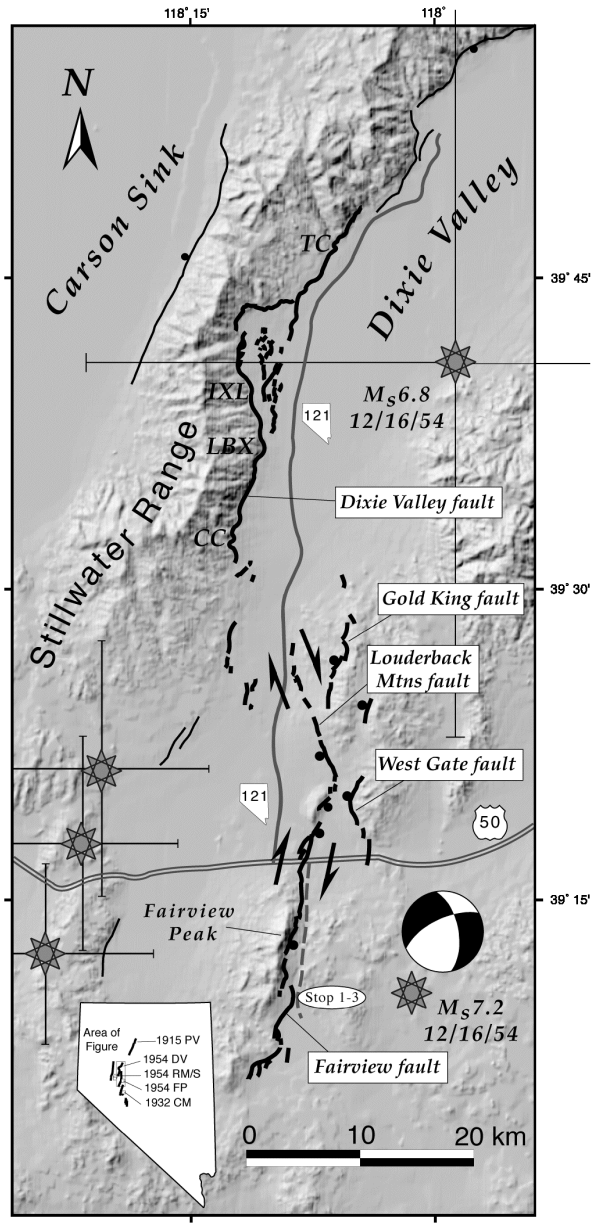

Figure 1 - Rupture zones (bold lines) of the December 16, 1954 Fairview Peak-Dixie Valley earthquake sequence and location of Stop 1-3. Bar and ball on the downthrown side of faults. Focal mechanism for the Fairview Peak event and locations (stars with associated location uncertainty bars) are from Doser (1986). Also shown are the epicenters for the July 6-August 23, 1954 sequence. All of the main December 16 rupture zones are represented except for the left-normal-oblique ruptures on the Phillips Wash fault south of the figure in Gabbs Valley. Pre-historic faults (thin lines) from Bell (1984) and Dohrenwend et al. (1996). Inset map shows locations and generalized rupture zones associated with the the 1915 Pleasant Valley (PV), 1932 Cedar Mountain (CM), and 1954 Fairview Peak (FP), Dixie Valley (DV), and Rainbow Mountain-Stillwater (RM/S) earthquakes. Abbreviations for place names along the Dixie Valley fault CC - Coyote Canyon; IXL - IXL Canyon; LBX - Little Box Canyon; TC - Terrace Creek.

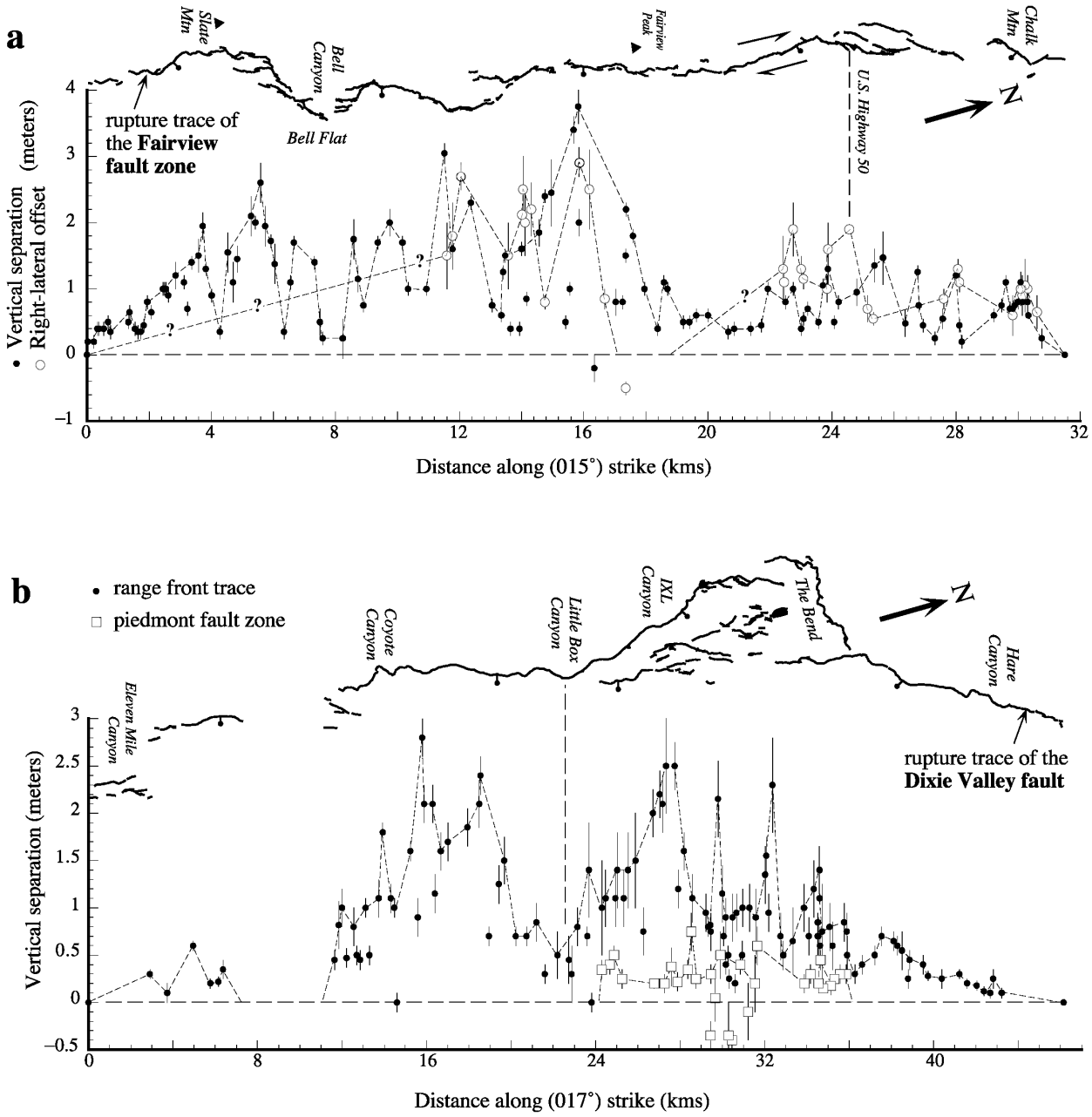

Figure 2 - Measurements of vertical separation (solid dots and open squares) and lateral offsets (open circles) versus distance along a line of average strike for the December 16, 1954 earthquake ruptures along (a) the Fairview fault, and (b) the Dixie Valley fault. The mapped rupture traces are registered with the horizontal axis for both plots; ball and stick shown on the down-thrown side of the faults. Negative values indicate either net down-to-the west vertical separations or in the one case in (a) localized left-lateral offset. Measurement error bars are shown as thin vertical lines through data points. After Caskey et al. 1996.

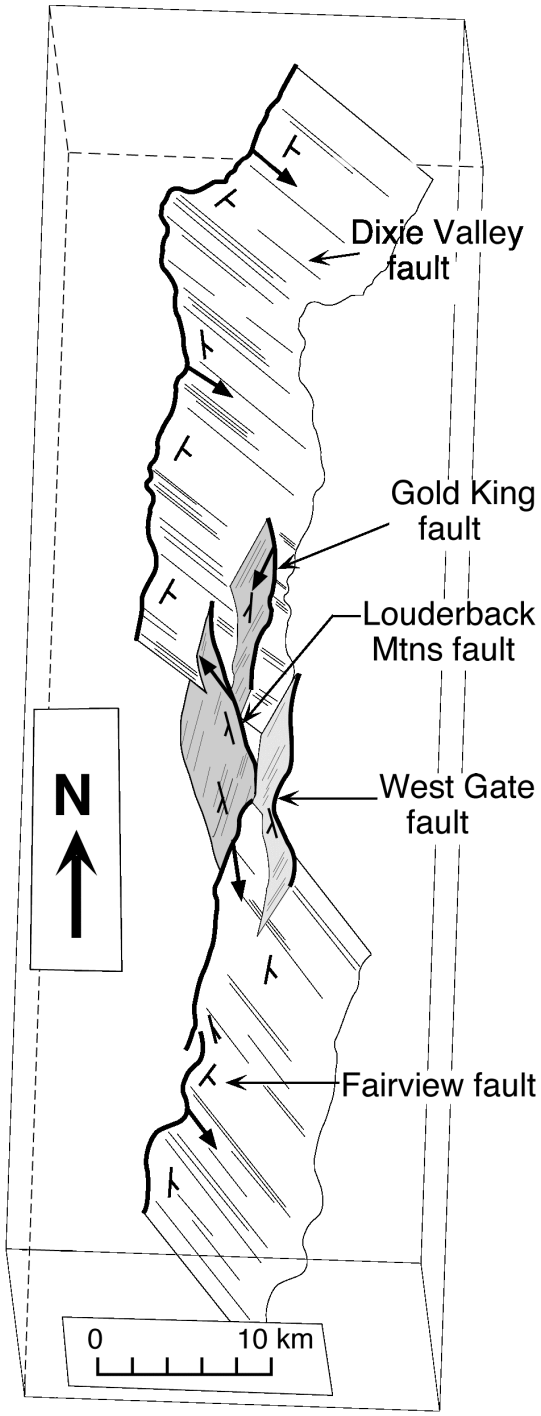

Figure 3 – Schematic block diagram of the geometry of the December 16, 1954 fault rupture system (with the exception of the Phillips Wash fault trace). Bold lines represent surface rupture traces. Bold arrows indicate the general direction of motion of hanging-wall blocks. Strike and dip symbols are shown for reference. West-dipping faults are gray (modified after Caskey et al., 1996).

APPENDIX 1-3B

Overview of Quaternary Chronostratigraphy in the Fairview Peak-Dixie Valley-Stillwater Seismic Gap Area

John W. Bell

A series of late Quaternary chronostratigraphic units was differentiated by Bell and Katzer (1987, 1990) in the Dixie Valley rupture area, and they provide the stratigraphic framework for interpreting and comparing the paleoseismic histories of the several fault zones in the region between Fairview Peak on the south and the Stillwater seismic gap on the north. Eight principal stratigraphic units are defined, ranging in age from mid-Pleistocene (100-200 ka) to modern (Figure 1). A sequence of alluvial fan-piedmont deposits are distinguished based on soil-geomorphic characteristics, the presence of chemically distinct volcanic tephra, and stratigraphic position relative to latest Pleistocene lake deposits.

Old alluvial-fan deposits (Qfo) occur as dissected fan-piedmont remnants preserved along range fronts and locally on high, perched piedmont slopes. The deposits typically exhibit strongly developed argillic Bt horzions overlying stage IV+ (Bqkm) carbonate horizons. These well-developed durargids and paleargids generally correspond to the Cocoon geosol of Morrison (1964, 1991), estimated by Morrison and Davis (1984) to be of oxygen-isotope stage 7 age or older (≥200 ka).

Intermediate-age fan deposits (Qfi) are late Pleistocene in age based on their stratigraphic position below the pluvial Lake Dixie deposits. The fan deposits contain well-developed argillic Bt horizons and stage II-III Bk carbonate horizons, confirming that the unit predates the 12-13 ka highstand of Lake Lahonton according to the soil morphology studies of Nettleton et al. (1975). Along the road leading to Bell Flat at the lunch stop (see Road Log, Figure 1), Qfi deposits contain the 35.4 ka Wilson Creek tephra bed 19 (A. Sarna-Wojcicki, 1998 data), and in the 1932 Cedar Mountain region, equivalent alluvial-fan deposits (Qf2b) contain a similar-age (32-36 ka) Wilson Creek tephra bed (Bell et al., 1999).

Lacustrine units Qbfo, Qbg, and Qbfy are associated with a Pleistocene pluvial lake that occupied central and northern Dixie Valley. Although the Dixie Valley-Fairview Peak area was not hydrologically connected to the Lake Lahontan drainage system, the area was occupied by a contemporaneous pluvial lake, Lake Dixie, providing a comparable regional late Pleistocene stratigraphic datum for this basin. In central Dixie Valley, Thompson and Burke (1973) radiocarbon-dated two samples of calcareous tufa from shoreline beach gravel deposits (Qbg) of Lake Dixie (elevation 1085-1090 m) and obtained ages of 11.6 and 11.7 ^{14}C ka. Our recent studies have provided additional tufa ages on the highest shorelines ranging between 10.4-13.1 ka. The old basin fill deposits (Qbfo) mapped by Bell and Katzer (1987) were inferred to be older lacustrine deposits, and the young basin fill deposits (Qbfy) were determined to be partly contemporaneous with, and partly younger than, Qbg. The upper Qbfy deposits contain Mazama ash (6.85 ka) and are likely associated with shallow lake and subaerial deposition.

The mottled alluvial fan deposits (Qfm) derive their name from the distinctive speckled or mottled appearance of the fan surfaces on aerial photography, produced by localized bioturbation of the well-developed desert pavement. The Qfm fan deposits occur extensively across the alluvial piedmonts, burying and beveling Qbg and older deposits. Although the oldest

Qfm deposits appear correlative with the highest Qbg deposits, they are mostly younger than the shoreline gravels, and upper Qfm deposits overlie Mazama ash; the unit thus contains several subunits ranging in age from mid-Holocene to latest Pleistocene (6.85-11.7 ka). A buried Av horizon exposed in a fault trench at La Plata Canyon in southern Dixie Valley was ^{14}C dated at 13.3 ka. Soils in Qfm deposits typically exhibit cambic Bw and stage I-II carbonate Bk horizons, although locally the B horizons are incipient to weak argillic (Btj) horizons owing to the strong influx of Na-rich dust from the valley floor or to high clay content of altered volcanic parent material.

The young alluvial fan deposits (Qfy) are as areally extensive as the Qfm deposits, covering large portions of the alluvial piedmonts. They consist of numerous, coalescing debris- and flood-flow deposits ranging in age from mid- to late Holocene. Soils in Qfy typically contain weak cambic Bw and Stage I carbonate Bk horizon. The upper Qfy deposits in Dixie Valley contain the Turupah Flat tephra, a 1.5 ka volcanic ash derived from the Mono Craters which is ubiquitously found in most drainages in the Dixie Valley-Fairview Peak area. Several other tephra chemically indistinguishable from the Turupah Flat bed occur in the region based on tephrochronologic stusied in the Cedar Mountin area (Bell et al., 1999). In Bell Flat at the southern end of the Fairview Peak rupture zone, a similar tephra in Qfy lies on charcoal ^{14}C dated at 515±215 yrs BP (J. Bell, unpub. data) and is likely one of these several similar tephras.

References

Bell, J.W., and Katzer, T., 1987, Surficial geology, hydrology, and late Quaternary tectonics of the IXL Canyon area, Nevada: Nevada Bureau of Mines and Geology Bulletin 102, 52.

Bell, J.W., and Katzer, T. 1990, Timing of late Quaternary faulting in the 1954 Dixie Valley earthquake area, central Nevada: Geology, v. 18, p. 622-625.

Bell, J.W., dePolo, C.M., Ramelli, A.R., Sarna-Wojcicki, A.M., and Meyer, C.E., 1999, Surface faulting and paleoseismic history of the 1932 Cedar Mountain earthquake area, west-central Nevada, and implications for modern tectonics of the Walker Lane: Geological Society of America Bulletin, v. 111, no. 6, p. 791-807.

Morrison, R.B., 1964, Lake Lahontan: Geology of the southern Carson Desert, Nevada: U.S. Geological Survey Professional Paper 401, 156 p.

Morrison, R.B., 1991, Quaternary stratigraphic, hydrologic, and climatic history of the Great Basin, with emphasis on Lakes Lahontan, Bonneville, and Tecopa, *in* Morrison, R.B., ed., Quaternary nonglacial geology: conterminous U.S.: Geological Society of America, The Geology of North America, Volume K-2, p. 283-320.

Morrison, R.B., and Davis, J.O., 1984, Quaternary stratigraphy and archeology of the Lake Lahontan area: a reassessment, *in* Lintz, J., ed., Western Geological Excursions(geological Society of America Annual Meeting Guidebook): Reno, Nevada, Mackay School of Mines, p. 252-281.

Thompson, G.A., and Burke, D.B., 1973, Rate and direction of spreading in Dixie Valley, Basin and Range province, Nevada: Geological Society of America Bulletin, v. 84, p. 627-632.

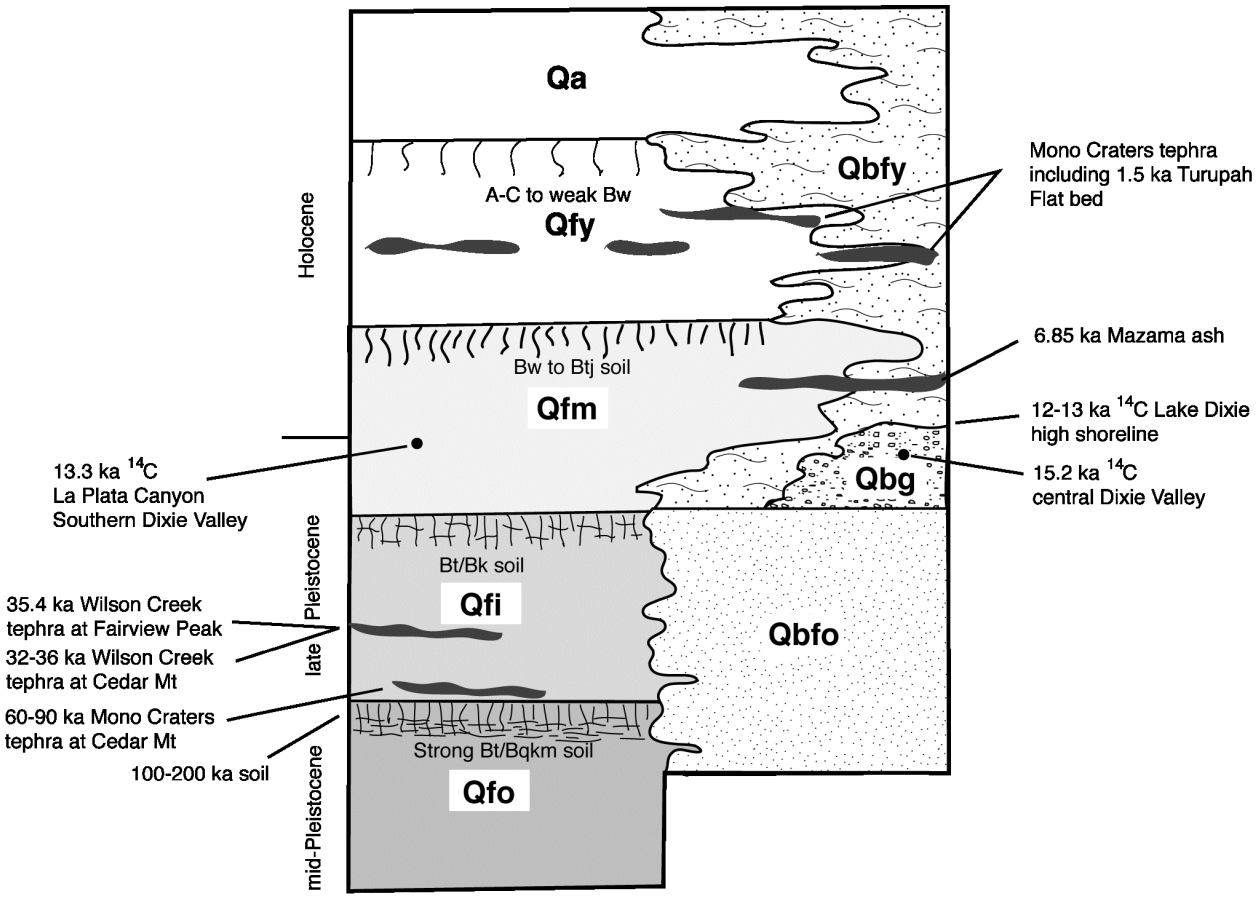

Figure 1 - Quaternary chronostratigraphy for the Dixie Valley-Fairview Peak region (after Bell and Katzer, 1990)

APPENDIX 1-3C

Paleoseismicity along the Fairview Fault

John W. Bell, John Caskey, and Alan R. Ramelli

Structural-chronostratigraphic relations at the main site

The portion of the 1954 Fairview Peak rupture, informally known as the main site, is on the northern segment of the Fairview fault and is located 4 km to the north (Figures 1 and 2). South of the main site, the fault rupture steps left into Bell Flat. The main site exhibits some of the largest displacements associated with the earthquake and provides key paleoseismic data bearing on the long-term slip history of the fault. Based on measurements made shortly after the earthquake, Slemmons (1957) described offsets at the main site ranging up to 2.1 m vertical, 3.4 m right-lateral, and 4.1 m net slip. Recent mapping by Caskey et al. (1996) documented numerous other sites exhibiting similar components of right-lateral offset. These offsets together with the development of graben in the steeply sloping offset fan surfaces account for the unusually large (7 m) and fresh-looking scarps still visible at the main site.

The alluvial fan deposits offset by the fault at the main site are Qfy and Qfi (Figure 1); to the north Qfm deposits comprise the faulted piedmont. The large scarp across the wash in the parking area cuts Qfy deposits, and the high fan surfaces into which the drainages are deeply incised are all of Qfi age, containing strong argillic Bt and stage II-III Bk horizons. To the south, the scarp ascends a high Qfi ridgeline remnant which exhibits still visible 2-m right-lateral offset of the narrow ridge crest. Slemmons (1957) measured offset roots and striations at this location having a rake of 55E south.

Detailed surficial mapping of the faulting at the main site revealed no evidence for older scarps in the Qfi alluvium. In 1998 an exploratory trench was excavated across the 4-m Fairview Peak scarp south of the main site (Figure 2), and the trench provided verification that Qfi deposits were offset only by the 1954 rupture. At the distal end of the offset fan, Qfi deposits exposed in the road cut contain a 3-5 cm tephra layer identified as the Wilson Creek bed 19, radiocarbon dated in the Mono Lake area at 35.4 ka (A. Sarna-Wojcicki, unpub. data). The presence of the ash together with the lack of evidence for prior faulting in the Qfi deposits indicate that the Fairview fault had not ruptured for at least 35 ky prior to 1954.

Structural-chronostratigraphic relations at Bell Flat.

At this location in northern Bell Flat (no relation to the author), the 1954 rupture lies along a 1-km left-step in the Fairview fault zone (Figure 1). In contrast to the fault history at the main site, this segment of the Fairview fault exhibits evidence for one older paleo-event. Qfi and younger deposits are offset only by the 1954 rupture as at the main site, but here remnants of the older Qfo fan deposits are offset by the 1954 and one additional older event which form a compound scarp 5 m in height (Figure 2). Total-station topographic profiles of the scarp indicate that the earlier event was comparable in vertical displacement to that in 1954, with about 2.5 m of vertical separation. Caskey et al. (1996) described as much as 2.5 m of 1954 right-lateral offset at this location, but comparable lateral offsets related to the older event are not evident.

Based on trenching and fault-stratigraphic relations at the main site, the penultimate event predates Qfi deposits containing the 35.4 ka tephra bed. Although no numerical ages are

available for Qfo deposits along Fairview Peak, regional stratigraphic and soils relations suggest that these deposits are probably on the order of at least 100-200 ka, providing an approximate maximum limiting age for the event. In the 1932 Cedar Mountain area 50 km to the south, alluvial-fan deposits intermediate in age between Qfi and Qfo (Qf2a) contain a 60-90 ka tephra (the Negit Causeway bed; Bell et al., 1999). A typical pedon profile for Qfo deposits can be observed in a soil pit near the location of the compound scarp profile (Figure 2) where a 30 cm argillic Bt horizon overlies a 1 m thick stage IV Bqkm horizon. Such pedons are commonly thought to be of at least interpluvial stage 5 age (cf., Machette, 1985). The Bqkm is partially exposed locally along the 1954 scarp face at this location, and has also engulfed the fault zone and numerous rhizoliths are visible in the carbonate-cemented shear zone.

In contrast to the Rainbow Mountain and Dixie Valley faults, the Fairview fault does not exhibit an earlier Holocene rupture. The lack of pre-1954 faulting in Qfi deposits and the evidence for a single paleo-event in Qfo deposits indicate that the Fairview fault is a low slip rate fault (≤0.1 mm/yr), illustrating that even low-slip-rate faults have measurable seismic potential in the western Basin and Range. The results of studies in this portion of the central Nevada seismic belt indicate that this is a complex structural-tectonic region consisting of single and multiple, interconnected and overlapping fault segments. The pattern of historical faulting is complicated and not dependent upon paleoseismic history or pattern. The widely differing slip histories of the separate fault zones strongly suggest that conventional paleoseismic parameters, such as slip and recurrence rate, may not be reliable criteria for distinguishing the CNSB from other seismically active areas of the western Basin and Range.

References

Bell, J.W., dePolo, C.M., Ramelli, A.R., Sarna-Wojcicki, A.M., and Meyer, C.E., 1999, Surface faulting and paleoseismic history of the 1932 Cedar Mountain earthquake area, west-central Nevada, and implications for modern tectonics of the Walker Lane: Geological Society of America Bulletin, v. 111, no. 6, p. 791-807.

Caskey, S.J., Wesnousky, S.G., Zhang, P., and Slemmons, D.B., 1996, Surface faulting of the 1954 Fairview Peak (Ms7.2) and Dixie Valley (Ms6.8) earthquakes, central Nevada: Seismological Society of America Bulletin, v. 86, p. 761-787.

Machette, M.N., 1985, Calcic soils of the southwestern United States, *in* Weide, D.L., ed., Soils and Quaternary geology of the southwestern United States: Geological Society of America Special Paper 203, p. 1-21.

Slemmons, D.B., 1957, Geological effects of the Dixie Valley-Fairview Peak, Nevada, earthquakes of December 16, 1954: Seismological Society of America Bulletin, v. 47, no. 4, p. 353-375.

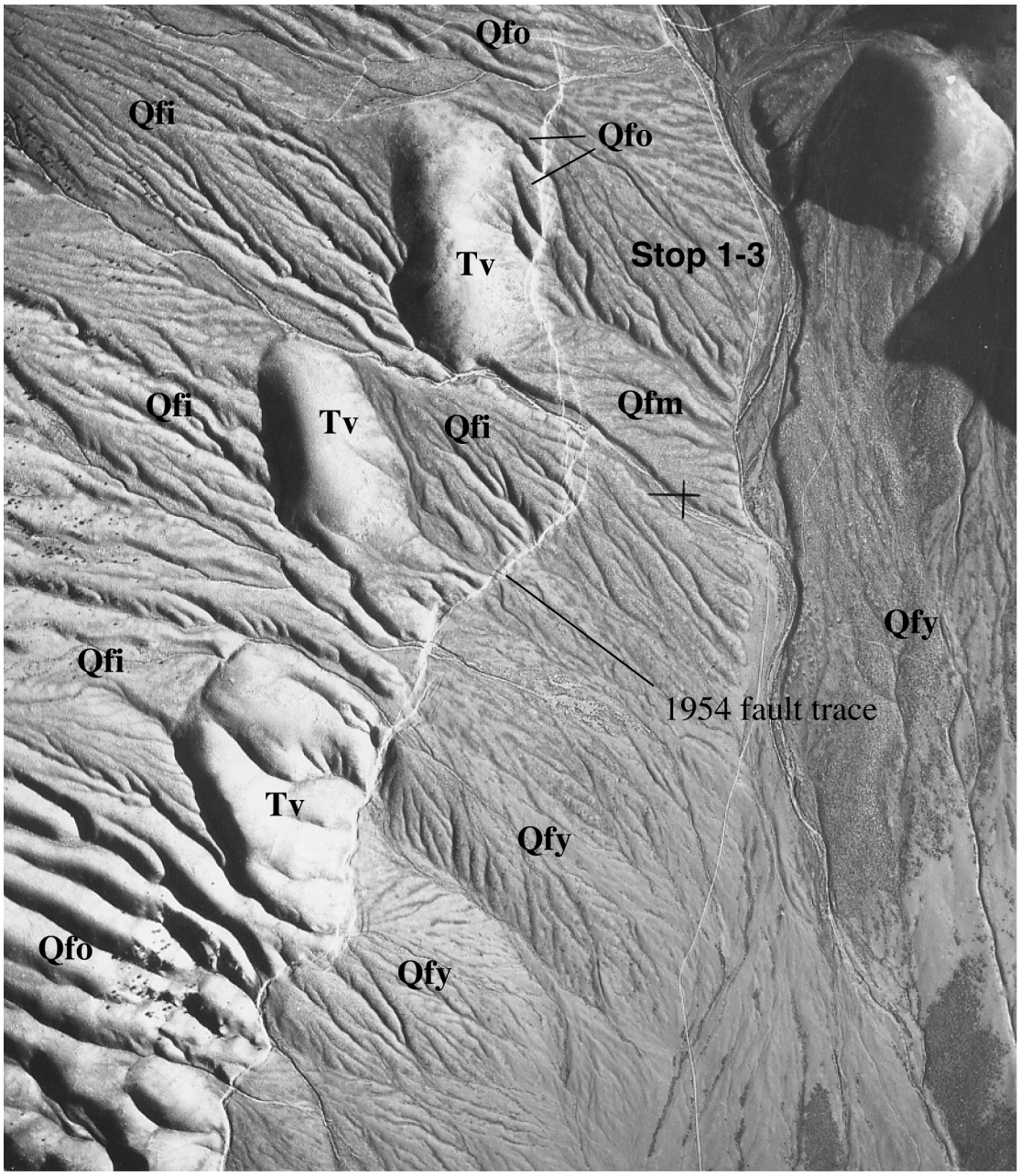

Figure 1 - 1:12,000 scale low-sun-angle-photograph of the northern part of Bell Flat (Stop 1-3) showing 1954 ruptures and fan units. Units refer to those in Figure 2 (except Tv, Tertiary volcanic rocks) and are described in the text. North is up.

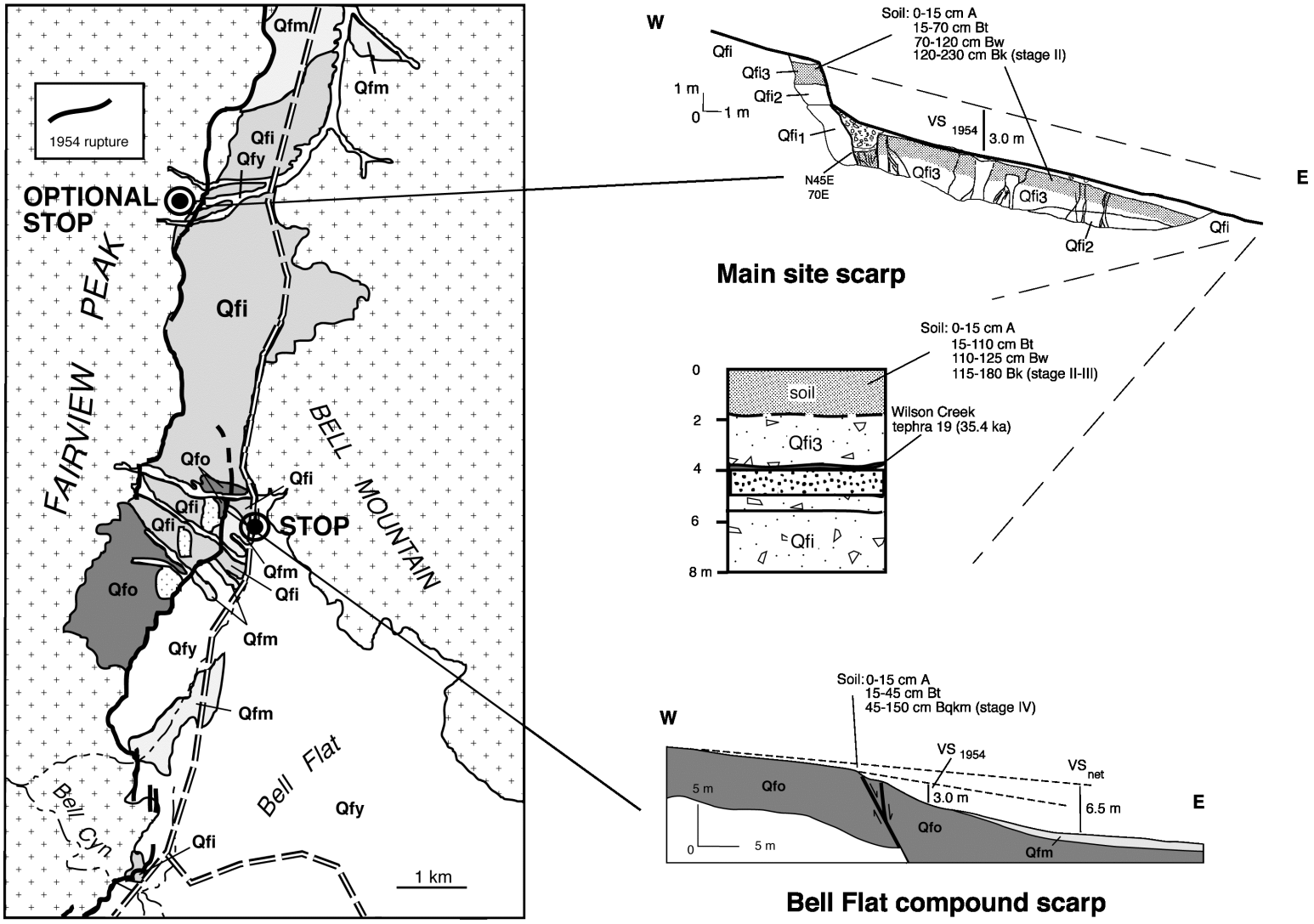

Figure 2 -Surficial map and trench logs for the Fairview fault in the vicinity of the main site and the north end of Bell Flat

APPENDIX 1-4

Overview of Large, Pre-late Pleistocene Pluvial Lakes in Nevada

Marith Reheis

The following summary is extracted verbatim from Reheis et al. (in press):

> "During the Pliocene to middle Pleistocene, pluvial lakes in the western Great Basin repeatedly rose to levels much higher than those of the well-documented late Pleistocene pluvial lakes, and some presently isolated basins were connected. Sedimentologic, geomorphic, and chronologic evidence indicates that Lakes Lahontan and Columbus-Rennie [Fish Lake and Columbus valleys] were as much as 70 m higher at about 650 ka than during their late Pleistocene high stands. Lake Lahontan at its 1400-m shoreline would submerge present-day Reno, Carson City, and Battle Mountain, and would flood other now-dry basins. To the east, Lakes Jonathan (new name), Diamond, Newark, and Hubbs also reached high stands during the early-middle(?) Pleistocene that were 25-40 m above their late Pleistocene shorelines; at these very high levels, the lakes became temporarily or permanently tributary to the Humboldt River and hence to Lake Lahontan."
>
> "The implications of a 1400-m shoreline of Lake Lahontan, here estimated to have been at about 650 ka (within isotope stage 16), are staggering: for example, such a lake would inundate Granite Springs and Kumiva Valleys, would back up the Truckee and Carson Rivers to submerge all or part of present-day Reno and Carson City, would back up the Humboldt River at least to present-day Battle Mountain, and would extend 60 km southeast from Walker Lake to Rhodes Salt Marsh. If allowances are made for local tectonics and sedimentation in the past half-million years, the lake would have flooded into Dixie and Fairview Valleys and inundated many other flat-lying valleys whose floors are now only a few tens of meters above the 1400-m level."
>
> "Such projections permit specific hypotheses to be proposed and tested. For example, Hubbs and Miller (1948) postulated an "early pluvial" connection between Lake Dixie and Lake Lahontan on the basis of a subspecies of *Gila bicolor obesa* that inhabits a present-day spring in Pleasant Valley, between Dixie Valley and Grass Valley (an arm of Lake Lahontan). The modern distribution of the springsnail *Pygulopsis gibba* also supports this connection (Hershler and Sada, this volume). … the 1400-m level of Lake Lahontan would probably have flooded Dixie, Fairview, and Pleasant Valleys (the present lowest sill height is only 8 m above this lake level; Reheis and Morrison, 1997), providing easy access for migrating fish."

Late Pleistocene pluvial lakes in Fairview (Lake Labou) and Dixie (Lake Dixie) Valleys were separate from Lake Lahontan (Sehoo highstand ~1335 m (4380 ft). Lake Labou reached a highstand of 1264 m (4180 ft) and overflowed into Lake Dixie, which reached about 1097 m (3600 ft) (Mifflin and Wheat, 1979). If Lake Lahontan were again to reach its highest known level of 1400 m, it would lie only about 8 m below the present lowest point in Sand Springs Pass on US 50. Because both sides of the Stillwater Range are bounded by active normal faults, it is quite likely that the area of Sand Springs Pass is now higher in elevation than it was in the early

to middle Pleistocene, and may well have served as a conduit for overflow from Lake Lahontan into Fairview and Dixie Valleys.

At STOP 1-4, we will view, discuss, and debate possible evidence for such an overflow. The long ridge topped by the radar station is dissected on the east by Dixie Valley Wash. Deposits exposed here, 45-50 m thick, are distinctly different in bedding, sorting, and rounding from the fan gravels that crop out at similar altitudes to the east, derived from the Clan Alpine Mountains, and also from those to the west flanking the Stillwater Range. Deposits at Stop 4 consist of tan to brown, loose to weakly cohesive, monotonously interbedded mud, silt, sand, and pebble to cobble gravel. Commonly each bed is laterally extensive, moderately well sorted, and thinly bedded. Locally exposed are steeply dipping beds and truncations of beds. A few beds are calcareous and porous, suggesting marshy conditions, but the overall appearance is similar to fluvial-deltaic deposits in a rapidly rising lake. The loose, weakly cemented nature of the deposits suggests a relatively young age (they are much less indurated than the Miocene lake beds to the northeast, described in the road log).

References

Hershler, R., and Sada, D. W., in press, Biogeography of Great Basin freshwater snails of the genus Pyrgulopsis, *in* Currey, D., Hershler, R., and Madsen, D., eds., Great Basin Aquatic Systems History: Washington, D.C., Smithsonian Institution.

Hubbs, C. L., and Miller, R. R., 1948, The Great Basin. II. The zoological evidence: University of Utah Bulletin, v. 38, p. 17-166.

Mifflin, M. D., and Wheat, M. M. (1979). Pluvial lakes and estimated pluvial climates of Nevada. Nevada Bureau of Mines and Geology Bulletin 94, 57 p.

Reheis, M. C., and Morrison, R. B. (1997), High, old pluvial lakes of western Nevada, *in* Link, P. K., and Kowallis, B. J., eds., Proterozoic to recent stratigraphy, tectonics, and volcanology, Utah, Nevada, southern Idaho and central Mexico: Brigham Young University Geology Studies, Provo, v. 42, pt. 1, pp. 459-492.

Reheis, M. C., Sarna-Wojcicki, A. M., Reynolds, R. L., Repenning, C. A., and Mifflin, M. D., in press, Pliocene to middle Pleistocene lakes in the western Great Basin: Ages and connections, *in* Currey, D., Hershler, R., and Madsen, D., eds., Great Basin Aquatic Systems History: Washington, D.C., Smithsonian Institution.

APPENDIX 2-1

Alluvial Chronostratigraphy and Active Faulting at Terrace Creek

John Caskey

(largely a summary of Chadwick et al. 1984)

Terrace Creek is an informal name for the drainage between Cottonwood and Hare canyons to the south and north, respectively. This site is geologically interesting because of the prominent flight of alluvial terraces that reflect active uplift of the footwall of the Dixie Valley fault. At this site, Chadwick et al. (1984) examined soil profiles, geomorphic characteristics of terrace and fan surfaces, and relationships to local time-stratigraphic features such as pluvial Lake Dixie shorelines and Mazama ash beds to develop a soil chronosequence for the area and to constrain the timing of faulting at Terrace Creek. Soil processes in this area are of particular interest because of the rapid (i.e., post-mid-Holocene) development of thin, natric (Btn) horizons (Alexander and Nettleton, 1977) which are generally defined as soil horizons of illuviated clay and high levels of exchangeable sodium.

At this stop we will observe and discuss geomorphic and pedologic aspects of the chronostratigraphy and structural relations bearing on the rates of fault activity. None of the trip leaders have conducted detailed studies at this site, so the hope is to have an open discussion that draws from everyone's ideas and expertise. Oliver couldn't make the trip.

Stratigraphic units and faulting

Chadwick et al. (1984) defined four alluvial terraces, T1-T4 (youngest to oldest), west of the fault, and two fan units (F1 and F2) to the east, which correlate across the fault to terraces T1 and T2 (Figure 1).

- The T1/F1 surface is the smooth, bouldery, and sparsely vegetated surface that most of us are camped on. This surface is offset only along small (<25-cm-high) 1954 scarps. These small, delicate scarps are still well-preserved at the fan head. The age of the T1/F1 surface is not known, but it must be very young because wood that came down with the F1 debris flow (from higher elevations) has not yet decomposed and vanished from the fan surface.
- The T2/F2 surface is offset along both the small 1954 ruptures and a large, ~2-m-high Holocene fault scarp. Paleoseismic studies about 10 km to the north indicate that the age of the Holocene earthquake rupture that broke across this area is 2.0-3.4 ka (Caskey, Appendix 3-2). T2/F2 deposits are clearly younger than the 12-13 ka Lake Dixie high stand (Thomson and Burke, 1973; Bell, unpublished data) because there are no shorelines on the F2 surface at or below 1097 m (3600 ft.) (Figure 1).
- T3 is the next highest terrace. The T3 terrace defined by Chadwick et al. actually consists of an additional higher terrace that projects a couple of meters above the surface we can see from the fan head. The height of the scarp bounding T3 is about 10 m near the fan head, but increases markedly to 20-30 m just out of view to the north. The larger scarp probably represents a closer estimate of the vertical offset of T3 because the down-faulted T3 surface is presumably buried by a thinner section of F2 deposits to the north than near the fan head. The upper step along the fault scarp to the north appears (to me) to be a depositional contact

where F2 deposits are buttressed against the large preexisting scarp developed on T3. The large post-T3 scarp is among the largest alluvial scarps in the valley, so the age of the T3 surface and an understanding of the geomorphic and structural relations at Terrace Creek are important for determining a late Pleistocene slip rate for the Dixie Valley fault.

· T4 is preserved as small erosional remnants on both sides of the creek. T4 is mainly a strath (i.e., erosional) terrace characterized by a several-meter-thick mantle of alluvium over Tertiary lacustrine deposits. These terrace remnants appear to correlate with a much better preserved strath terrace (or terraces) several km to the south where they are capped by very well rounded gravel; much different material than the late Pleistocene to recent alluvial deposits characteristic of T1-T3. I have not looked at the T4 surfaces/deposits at Terrace Creek. Conventional thought is that pedimentation and strath terrace development (e.g., T4) along fault-bounded range fronts represents a period of tectonic stability. The age of T4 is not known.

Table 1. Geomorphic and soil characteristics of T1/F1, T2/F2, and T3 surfaces (mostly synthesized from Chadwick et al. (1984))

Surface	Geomorphic characteristics	General soil characteristics from representative pedon	Soil Classification
T1/F1	sparse vegetation (burrowbrush, cheatgrass), bouldery, moderate dissection of T1 at Terrace Creek, no desert pavement, incipient cryptogam, <25-cm-high1954 fault scarps	**A** (0 to18 cm) **Bw** (18 to 33 cm), a few clay films **BCn** (33 to 51 cm) **Ck** (51 to 140 cm)	Typic Camborthid
T2/F2	vegetation 40% of surface (greasewood, shadscale, cheatgrass), moderate dissection (T2), abundant cryptogam coverage , patchy-moderately-interlocking desert pavement, moderate desert varnish, ~2-m-high compound scarps	**Av** (0 to 13 cm) **Btn** (13 to 23 cm), moderate clay films on weak peds and in pores **Btkn** (23 to 36 cm). Stage I carbonate **Ckqn** (36 to 53 cm) **Ck** (53 to 152 cm)	Typic Natrargid
T3	vegetation 30% of surface (shadscale, greasewood, cheatgrass), deeply incised, moderate cryptogam coverage – primarily where vegetation traps thick eolian silt, well-developed interlocking desert pavement, strongly developed desert varnish, 10-30m-high fault scarps	**Av** (0 to 5 cm) **Btk** (5 to 38 cm) argillic, thick clay skins and bridges, mod. med. prismatic structure, Stage I-II carbonate **Ck** (38-117 cm)	Typic Paleargid

Table 2. Approximate surface ages for Terrace Creek chronosequence (modified after Chadwick et al. (1984).

Surface	Approximate age (yrs. B.P.)*
T1	30-6900
F1	30-6900
T2	6900-12,000
F2	6900-12,000
T3	>12,000
T4	?

*****Chadwick et al.'s (1984) age estimates for the surfaces were based, in part, from quantitative soil-development index (SDI) values calculated for each representative pedon following procedures described by Harden (1982). However, they assigned age ranges based mainly on cross-cutting relationships with 12-13 ka Lake Dixie shorelines and comparisons to soil development on post-Mazama aged (6.9 ka) surfaces.

<u>Some interesting topics for discussion at Terrace Creek include</u>:

- **Soil forming processes**, specifically the rapid development of Natrargids (T2/F2) due to the local abundance of eolian salt. Stop 2-4 is located at Alexander and Nettleton's (1977) study site where they described post-Mazama Typic Natrargids. Chadwick et al. suggested that the Natrargids characteristic of T2/F2 are better developed than those at Stop 2-4, hence the 6.9-12.0 ka age estimate (Table 2).

- **The apparent lack of exchangeable sodium in the T3 soil** (see soil profile, Table 1). Chadwick et al. interpreted the lack of sodium in the T3 soil to mean that the soil formed "during a period of greater effective moisture which enhanced leaching and weathering, and **playas were not present** to supply salts." This brings up the notion of soil forming intervals.

- **The age of T3 and the large scarps developed on T3**. If T3 is less than a few tens of thousands of years old, then the apparent structural relations imply a slip rate in excess of 1 mm/yr, which is considerably greater than our current estimates of 0.3-0.6 mm/yr for the Dixie Valley fault (Bell and Katzer, 1990; Bell et al., in review). Also, how do the surfaces at Terrace Creek fit into the more regional chronostratigraphic framework defined by Bell and Katzer (1990)?

- **Pedimentation**. If the strath terrace (T4) represents a period of relative tectonic stability, then are we seeing evidence for temporal variations in fault slip rate?

References

Alexander, E.B. and W.D. Nettleton, 1977, Post-Mazama Natrargids in Dixie Valley, Nevada, Soil Sci. Soc. Am. J., 41, 1210-1212.

Bell, J., and Katzer, T., 1990, Timing of late Quaternary faulting in the 1954 Dixie Valley earthquake area, central Nevada: Geology, v. 18, p. 622-625.

Bell, J. W., S. J. Caskey, A. R. Ramelli, L. Guerrieri, and A. M. Sarna Wojcicki, (in review Geology), Patterns and rates of faulting in the central Nevada seismic belt.

Chadwick, O.A., S. Hecker, and J. Fonseca, 1984, A soils chronosequence at Terrace Creek: studies of late Quaternary tectonism in Dixie Valley, Nevada, US Geol. Survey Open File Report OFR 84-90,

Harden, J.W., 1982, A quantitative index of soil development from field descriptions: examples from a chronosequence in central California, Geoderma, 28, 1-28.

Thompson, G.A., and D.B. Burke, 1973, Rate and direction spreading in Dixie Valley, Basin and Range province, Nevada: Geol. Soc. Am. Bull., v. 84, p. 627-632.

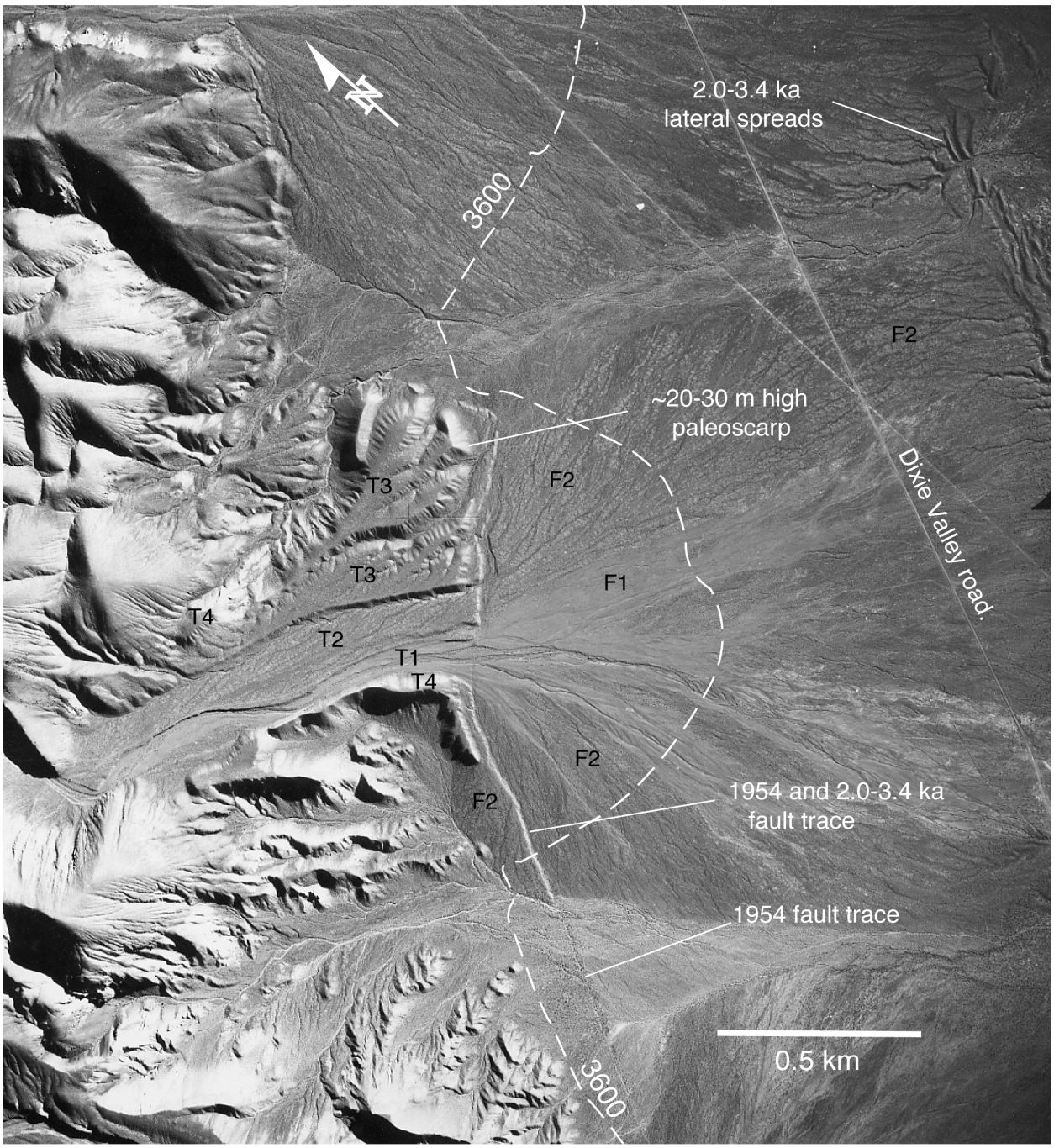

Figure 1 - Low-sun-angle photo of the Terrace Creek area (Stop 2-1, and camping area for Friday and Saturday nights) showing surfaces mapped by Chadwick et al. (1984), the 1954 fault trace, paleoscarps, and a small part of the area disrupted by 2.0-3.4 ka liquefaction. The lateral spreading that occurred at 2.0-3.4 ka will be the focus of discussion at Stop 2-4. The approximate location of the 3600 ft (1097 m) topographic contour is shown as reference to the 12-13 ka Lake Dixie

APPENDIX 2-2

Geological and Geophysical Evidence for Low Dip on the Dixie Valley Fault: Little Box to Big Box Canyons

John Caskey

Despite a growing body of geological and geophysical evidence arguing for the existence of active low-angle normal faults in seismogenic crust (e.g. McDonald, 1976; Johnson and Loy, 1992), the paradox of the near-complete absence of low-angle normal faulting events in the seismic record remains. Caskey et al. (1996) reported data and a number of observations that strongly suggest that at least a 15-20 km-long section of the 1954 Dixie Valley fault rupture broke along a low-angle fault (~25-30˚). This section of the fault lies between just north of Coyote Canyon and The Bend (see Appendix 1-3A, Figure 1). Some of the geologic features that indicate low-angle fault geometry are best expressed along the 1954 rupture zone between Little Box and Big Box canyons (Figure 1).

Abbott et al. (2001) conducted seismic reflection and gravity experiments near Willow Canyon, located several km north of Little Box Canyon, to test the low-angle fault hypothesis of Caskey et al. (1996). The results of both high and medium resolution reflection surveys show profiles of a smooth fault plane dipping at 25˚-30˚ to depths of 50 m and 500 m, respectively (Figure 2). The medium resolution profile (not included herein) also shows stratigraphic truncations, hanging wall rollovers, and a slightly listric fault geometry (shallowing to less than 25˚) at 1-2 km depths. Gravity profiles constrain a conservative maximum basin depth and define an identical low-angle fault geometry, defined by the alluvium-bedrock interface, to greater than 2 km depth (Figure 3). Unless the Dixie Valley fault becomes steeper at greater depths (which seems unlikely since it appears to show slightly listric geometry above 3 km depth), then the results appear to mark the first on-land example of a historical, large-magnitude earthquake rupturing on a low-angle normal fault.

At this stop, we will examine and discuss geologic features along the 1954 rupture trace between Little Box and Big Box canyons that express the low-angle geometry of this part of the Dixie Valley fault. The geologic features include:

- a prominent low-angle fracture set along the range front within Tertiary granitic rocks of the footwall. The low-angle fractures closely parallel the sinuous range-front fault from north of Coyote Canyon to just south James Canyon where competent granitic rocks lie in the footwall. The fractures are particularly well-expressed just north of Big Box, but also at Little Box and points in between.

- prominent V-shaped fault patterns where the surface rupture breaks across alluvial ridges. The best example of this is at Little Box Canyon, as viewed along-strike from the graben above the south side of the creek (Stop 2-2). Three-point solutions for fault line-elevation surveys at Little Box Canyon, and also James Canyon 7 km to the north, indicate fault dips between 20˚-30˚ (Figure 4).

There are also very intriguing structural relationships across some of the graben that strongly, though qualitatively suggest a low fault dip. The narrow graben that form in alluvium along normal faults result from a slight (or not-so-slight) upward steepening of the fault near the ground surface (Figure 5). At several locations, both north and south of Little Box Canyon, profiles across graben show almost no vertical separation (Figure 6). At face value, such a relationship would require that fault dip shallows in the subsurface to an angle no greater than the slope of the faulted fan surfaces (<10˚, which does not appear to be reasonable). The apparent lack of vertical separation across the graben can be explained by a slight left-lateral shift across the graben along the northeast-trending and northeast-sloping range front south of Little Box Canyon and a slight right-lateral shift across the graben along the northwest-trending and southeast-sloping range front north of Little Box Canyon. (*The lateral components of slip are indicated by the en echelon patterns of Riedel shears along the graben trace (Figure 1)).* Nevertheless, a case can be made that vertical separation across the graben appears to be very small, and almost certainly less than the heave (i.e., the horizontal component of fault-normal extension). If so, then this relation requires fault dip to be less than 45˚, since a 45˚ dipping normal fault would show equal components of vertical separation and heave. There will undoubtedly be some interesting discussion about the structural relations across graben on the traverse.

References

Abbott, R. E., Louie, J. N., Caskey, S. J., and Pullammanappalli, S., 2001, Geophysical confirmation of low-angle normal slip on the historically active Dixie Valley fault, Nevada: Journal of Geophysical Research, v. 106, no. B3, 4169-4181.

Caskey, S. J., Wesnousky, S. G., Zhang, P., and Slemmons, D. B., 1996, Surface faulting of the 1954 Fairview Peak (Ms7.2) and Dixie Valley (Ms6.9) earthquakes, central Nevada: Bulletin of the Seismological Society of America, v. 86, no. 3, p. 761-787.

Gilbert, G. K., 1890, Lake Bonneville, U.S. Geol. Surv., Monograph 1.

Johnson, R. A., and Loy, K. L., 1992, Seismic reflection evidence for seismogenic low-angle faulting in southeastern Arizona: Geology, v. 20, no. 7, p. 597-600.

McDonald, R. E., 1976, Tertiary tectonics and sedimentary rocks along the transition: Basin and Range province to plateau and thrust belt province, Utah, *in* Symposium on geology of the Cordilleran hingeline, Denver, p. 281-317.

Slemmons, D. B., 1957, Geological effects of the Dixie Valley-Fairview Peak, Nevada, earthquakes of December 16, 1954, Bull. Seism. Soc. Am. 47, 353-375.

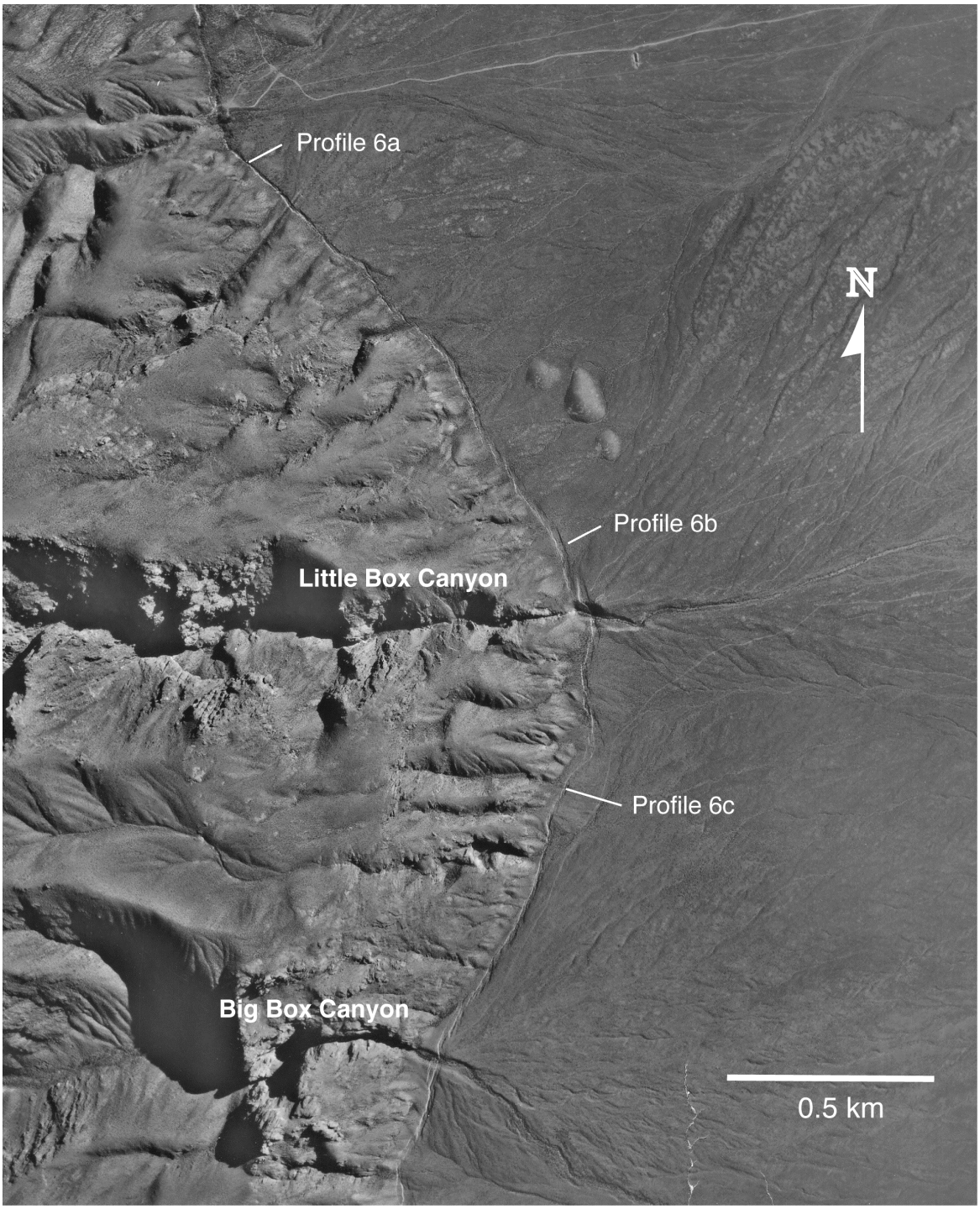

Figure 1 - 1:12,000-scale, low-sun-angle, 1970 photograph of the Little Box-Big Box canyon area along the 1954 Dixie Valley fault (Stop 2-2). Photo taken in early morning sunlight. Note the continuously developed graben and the right-and left-stepping *en echelon* pattern to fault ruptures along the northeast- and northwest-striking sections of the fault, respectively, reflecting components of left- and right-lateral slip. Locations of graben profiles (Figure 6) are shown along the fault trace

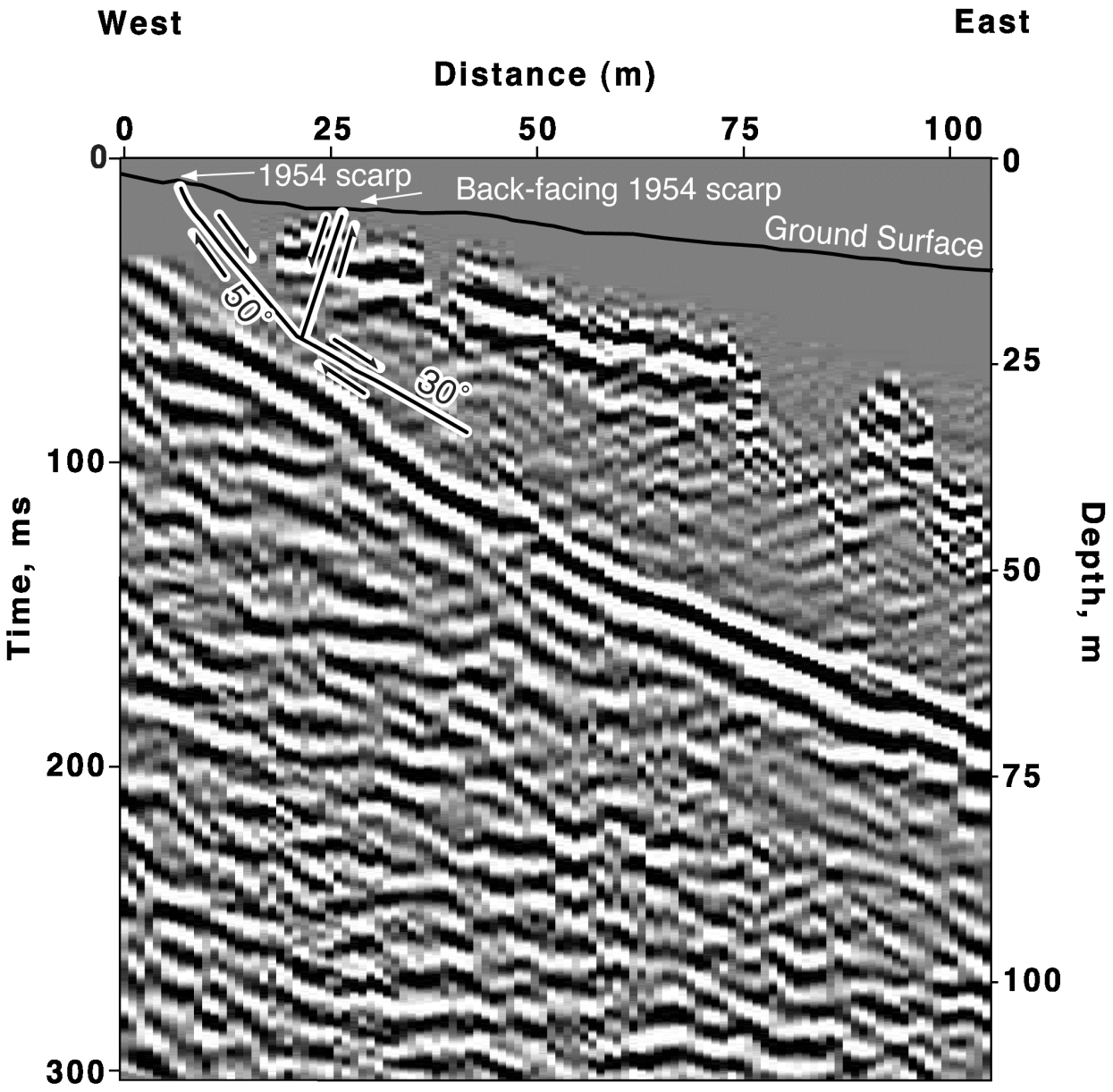

Figure 2 - Common depth point (CDP) stack of high resolution reflection data across the 1954 Dixie Valley fault near Willow Canyon, located 1 km north of Little Box Canyon. The prominent reflection represents the granite-alluvium contact along the fault. The graben cross section (shown for reference)is from a balanced cross-sectional model of subsurface fault geometry at East Job Canyon located ~1.5 km north of the survey line (Caskey et al., 1996). Figure is modified from Abbott et al., 2001.

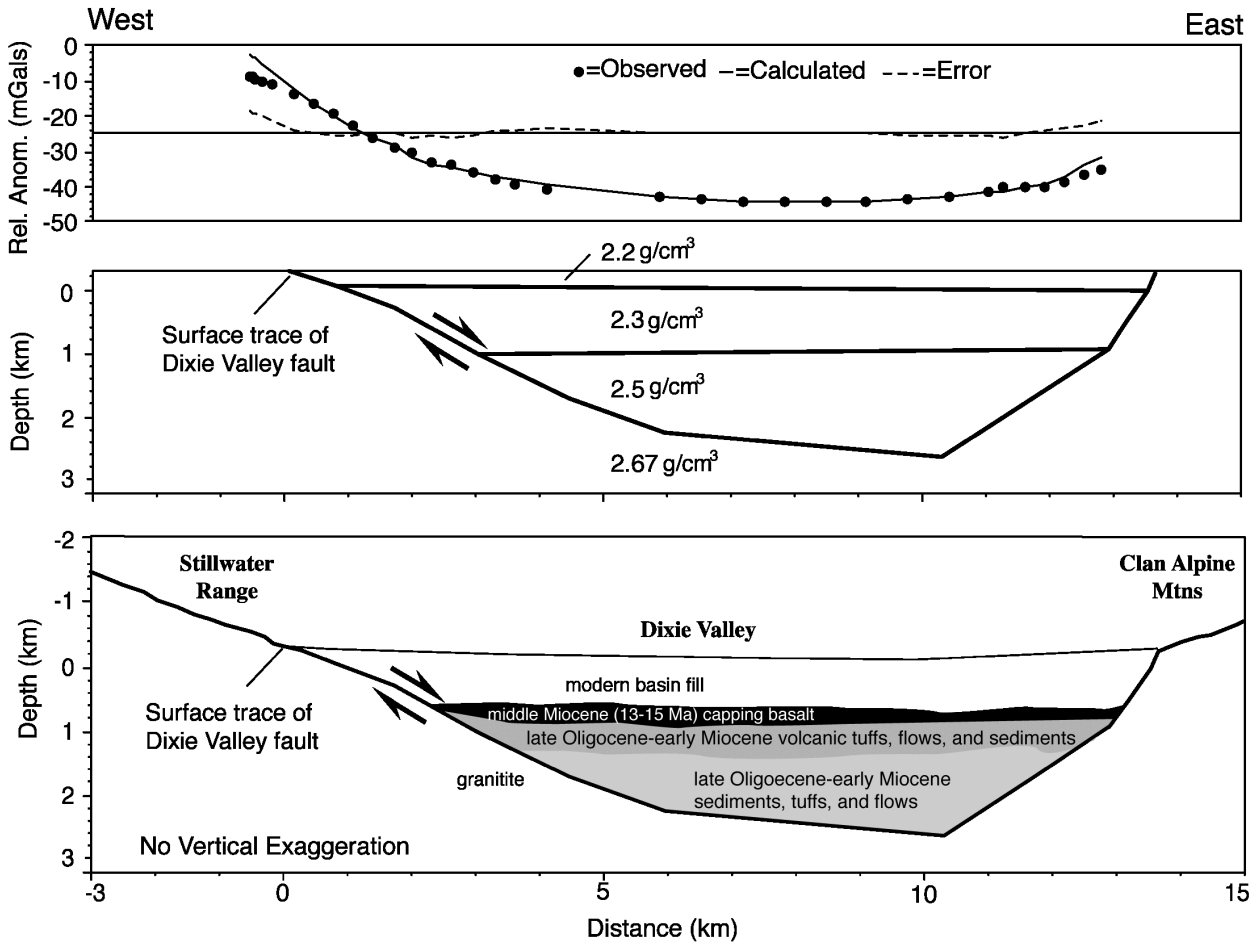

Figure 3 - Gravity model (top two figures) of Dixie Valley at the latitude of Willow Canyon and Cattle Road, a few km north of Little Box Canyon (see Road Log). Circles are observed gravity, and dashed line is model misfit. The model supports a fault dip of ~26˚E if the bedrock-basin fill interface represents the fault. Bottom figure is a schematic showing fault geometry and interpretation of basin fill materials based on the gravity model and medium resolution seismic reflections (modified after Abbott et al., 2001)

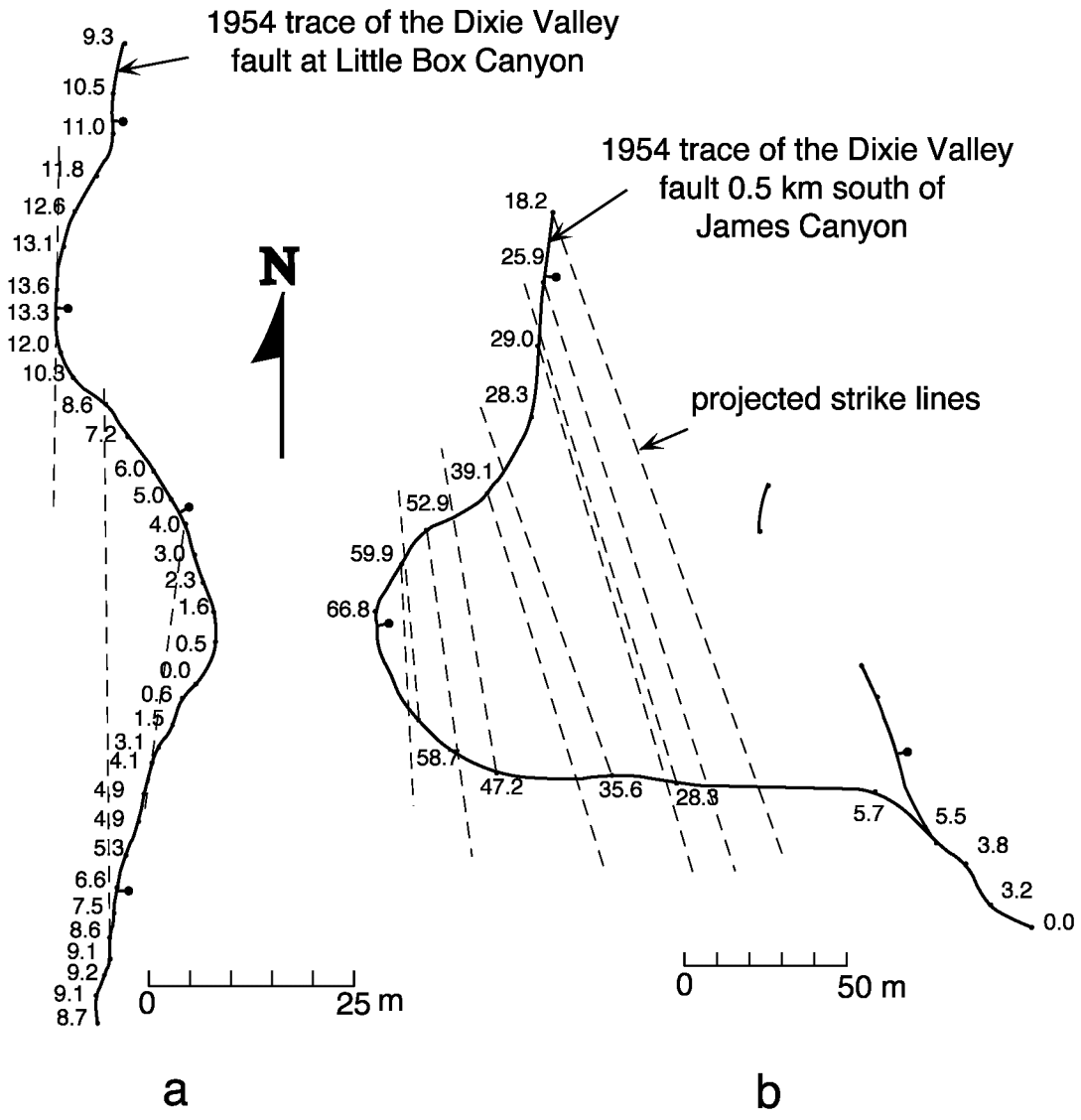

Figure 4 - Fault line surveys of V-shaped fault patterns where the 1954 surface rupture breaks across **a)** an alluvial ridge at Little Box Canyon, and **b)** a bedrock ridge near James Canyon. Survey points are shown with respective relative elevations in meters. Light dashed lines are inferred strike lines. Three point solutions suggest a fault dip of ~32˚E at Little Box Canyon and ~25˚E near James Canyon. Figure modified after Caskey et al., 1996.

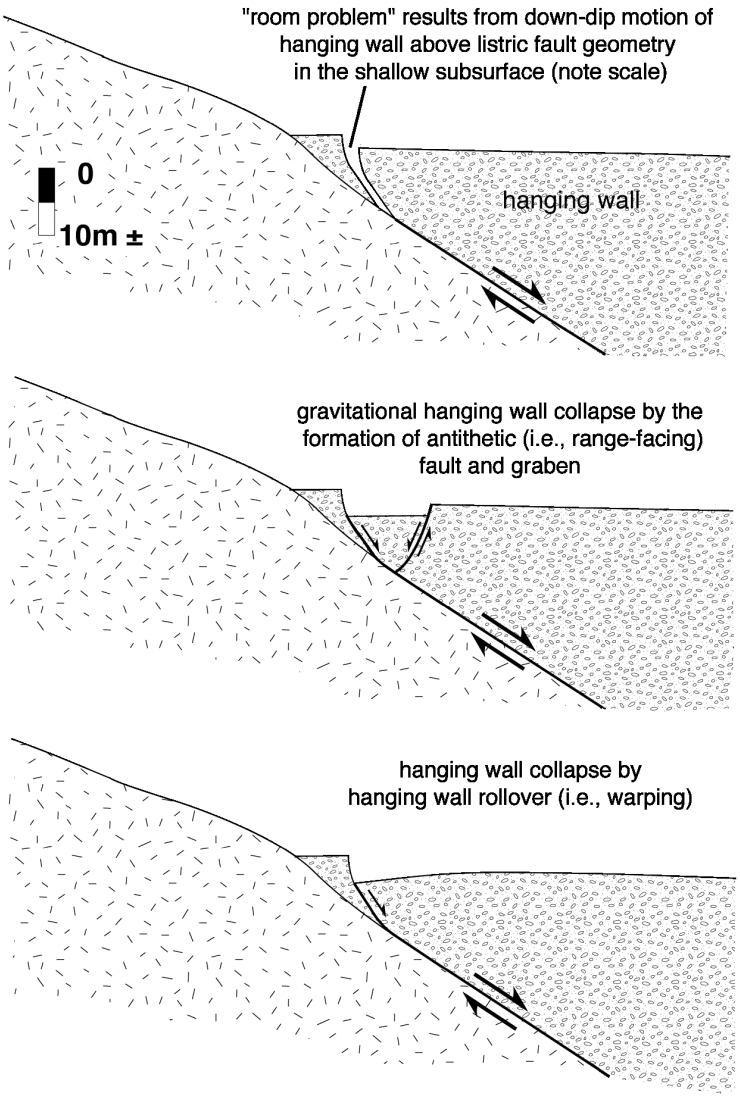

Figure 5 - Model for graben formation and hanging wall rollover along normal fault rupture traces (after Gilbert, 1890). Note that the large fissure or void produced by the "room problem" (top figure) is only shown conceptually since hanging wall collapse (lower two figures) primarily occurs during ground rupture. However, significant ground settling often takes place in the collapsed area after the earthquake, presumably due to the compaction of material that loosely or gradually fills the "room" produced by movement on the listric fault. Possible evidence of this occurred along the Dixie Valley fault near Willow Canyon where the synthetic (i.e., valley facing) scarps of the graben increased in height by as much as a meter in the days following the earthquake (Slemmons, 1957), and at East Job Canyon where a hanging wall rollover and numerous fissures eventually evolved and subsided into a well-developed graben.

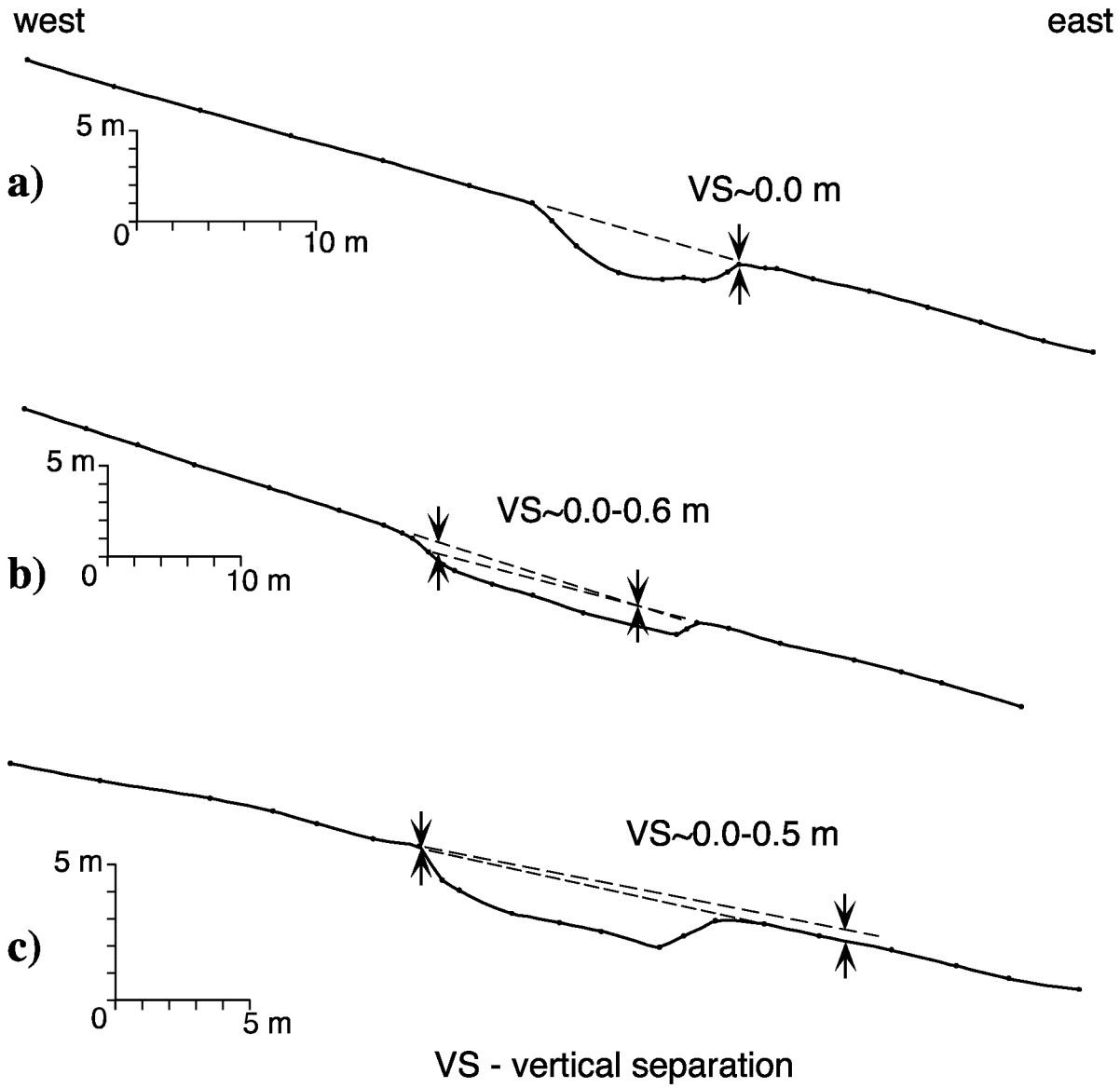

Figure 6- Graben profiles in the vicinity of Little Box Canyon showing little or no apparent vertical separation. See Figure 1 for profile locations.

APPENDIX 2-3

Structural-chronostratigraphic relations of the Dixie Valley fault in The Bend

John W. Bell

The Stillwater Range is uplifted along a normal fault, here called the range-front fault, and along a series of synthetic, antithetic, and nested graben faults lying a few kilometers to the east, collectively called the piedmont fault zone (Bell and Katzer, 1987, 1990). From the turnoff at Settlement Road, the dirt road to IXL Canyon crosses the piedmont fault zone about 0.9 km east of the range front where prominent scarps and graben as much as 15 m in height cut Qfo alluvial fan surfaces (Figures 1 and 2). The 1954 event produced 3.5-4.0 m-high scarps on the range front fault (1.5-2.5 m of vertical separation; Caskey et al., 1996) and 0-50 cm of offset on the piedmont scarps.

Paleoseismic studies in the Bend area indicated that late Quaternary faulting has migrated several times between the range-front and piedmont fault zones. The most recent event prior to 1954, termed the Bend event, occurred on the piedmont fault zone, and it produced 3 m high scarps comparable to those formed in 1954. In contrast to the 1954 rupture, however, surficial evidence indicated that no displacement occurred on the range-front fault during the Bend event. Other older events are preserved along the range-front fault, such as at IXL Canyon where Qfo deposits are offset about 12 m by pre-1954 faulting. North of IXL Canyon, Qfi fan deposits are offset by a single event which produced a 2.5-3.0 m-high scarp; this event, which preceded the Bend event, is called the IXL event and is the oldest mappable rupture in central Dixie Valley, extending the length of the 1954 rupture zone to where it overlaps with the 1954 Fairview Peak zone. Collective offsets on the range-front and piedmont faults associated with all events which cut Qfo and younger fan deposits indicate that late Quaternary slip rates are between 0.2-0.5 mm/yr.

At this stop, remnants of beach gravel associated with pluvial lake Dixie are cut by several traces of the piedmont fault zone (Figure 1). These deposits lie slightly below the 12-13 ka highstand elevation of Lake Dixie (1097 m); a 14C date on tufa coatings from the gravels yielded an age of 15,180 ± 220 yrs BP suggesting that the gravel beach bars were deposited as the lake ascended.

Between here and the range front fault to the west, the piedmont is composed almost entirely of Qfm deposits containing the Mazama ash, and Qfy deposits deposits containing the 1.5 ka Turupah Flat or younger tephra. Looking to the southwest toward IXL and East Job Canyons, the piedmont fault zone can be seen cutting higher Qfo alluvial-fan surfaces where 10-15 m high compound scarps are visible, particularly in late afternoon lighting conditions.

Bend-event scarps

The 2-3 m-high scarps visible along much of the piedmont fault zone from 1.5 km north of Little Box Canyon to about 6 km north of the gravel quarry (Stop 2-3) where the piedmont fault zone joins the range-front fault at the north end of the The Bend. These scarps are principally related to faulting produced by the Bend event, though up to 60 cm of the 2-3 m offsets were produced by 1954 faulting. The Bend event scarps also extend north into the Stillwater seismic gap, with an end-to-end length of about 46 km. The Bend event rupture trace

overlaps the 1954 rupture zone by about 25 km. Exploratory trenching on the scarp near Willow Canyon and about 5 km north of the quarry revealed that Qfm, Qbg, and lower Qfy deposits are offset 1.5-2.5 m by a single pre-1954 event (Bell and Katzer, 1987, 1990). The event produced much larger displacements in the Stillwater gap area where it represents the only surface rupture along the range front in the last 12 ka. Surficial mapping by Bell and Katzer (1987) demonstrated that the age of the Bend event was bracketed by the Mazama and Turupah Flat ash beds in faulted Qfm and unfaulted Qfy deposits at between 1.5-6.9 ka.

References

Bell, J.W., and Katzer, T., 1987, Surficial geology, hydrology, and late Quaternary tectonics of the IXL Canyon area, Nevada: Nevada Bureau of Mines and Geology Bulletin 102, 52 p.

Bell, J.W., and Katzer, T. 1990, Timing of late Quaternary faulting in the 1954 Dixie Valley earthquake area, central Nevada: Geology, v. 18, p. 622-625.

Caskey, S.J., Wesnousky, S.G., Zhang, P., and Slemmons, D.B., 1996, Surface faulting of the 1954 Fairview Peak (Ms7.2) and Dixie Valley (Ms6.8) earthquakes, central Nevada: Seismological Society of America Bulletin, v. 86, p. 761-787.

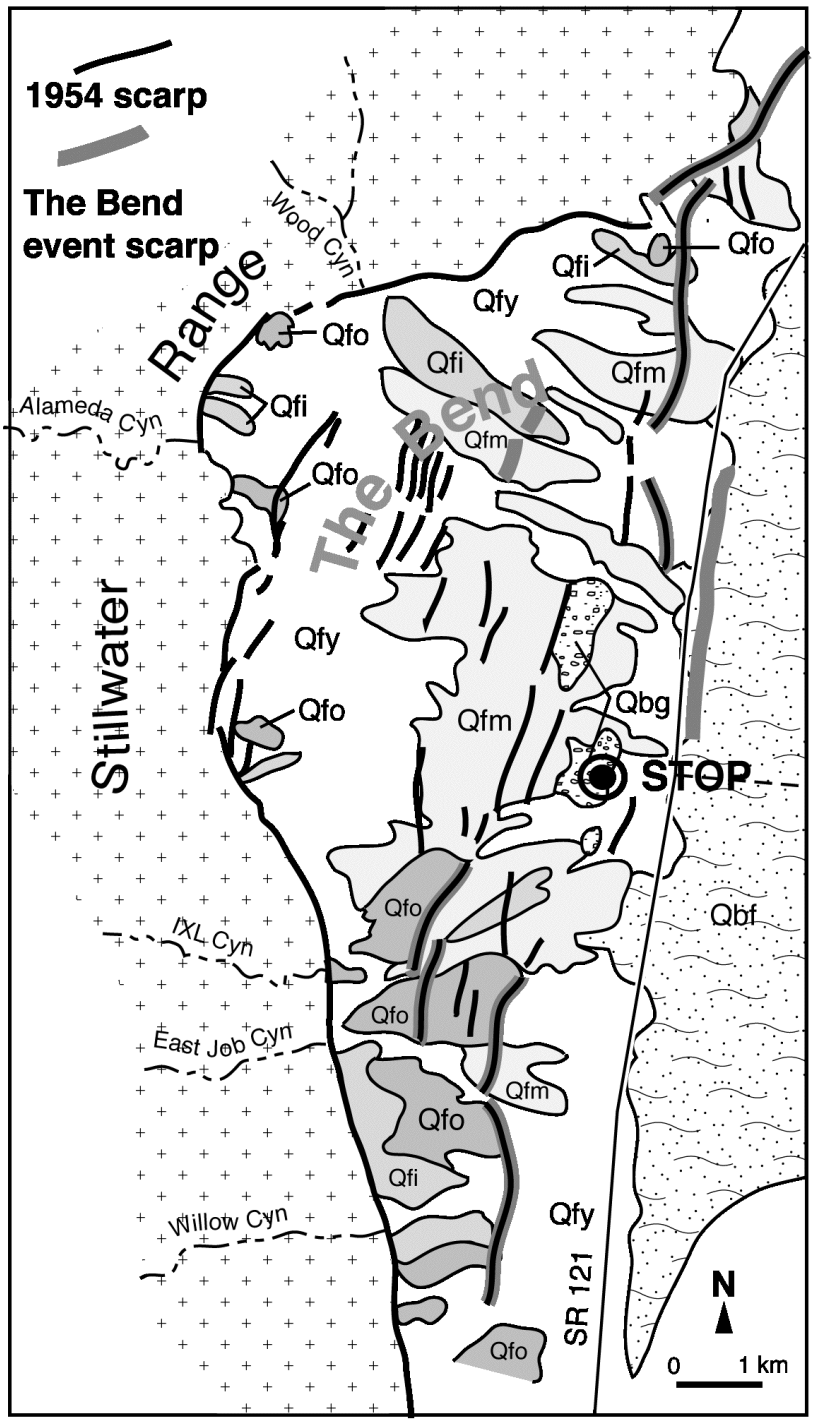

Figure 1 - Surficial map in the vicinity of The Bend in Dixie Valley

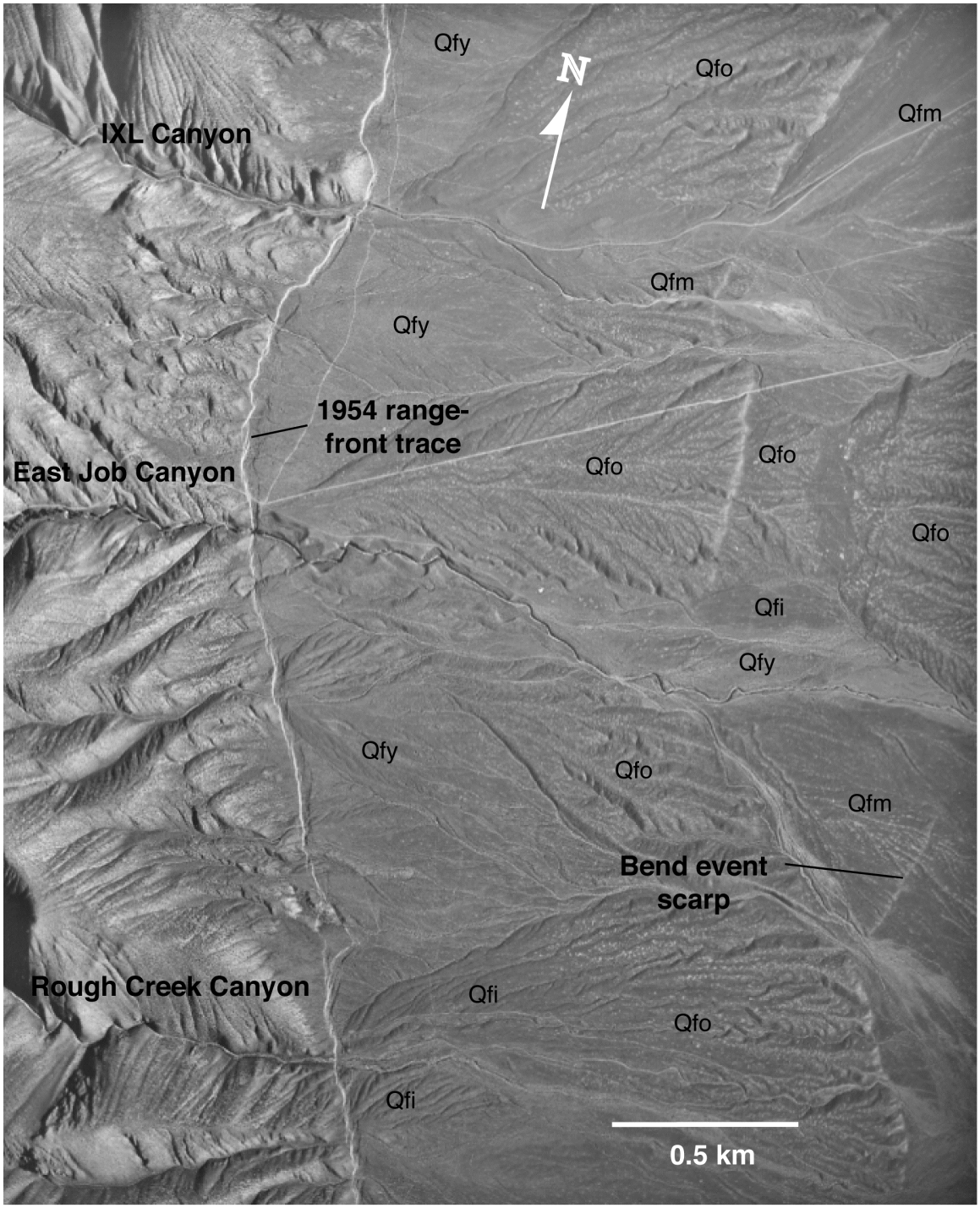

Figure 2 - 1:12,000 scale low-sun-angle photograph showing the 1954 Dixie Valley range-front fault ruptures, the piedmont fault zone, and general distribution of fan units described in Appendix 1-3B (text and Figure 1). Area is located a few km southeast of the gravel quarry (Stop 2-3). Note the large (~10-12-m-high) compound scarps developed on Qfo deposits along the piedmont fault zone.

APPENDIX 2-4

Large-scale Lateral-spread Paleoscarps and Mazama-age Lacustrine Deposits at Dixie Hot Springs

John Caskey

Neotectonic setting: the Stillwater seismic gap

This stop lies at the latitude of the north end of the 1954 rupture zone and the south end of the Stillwater seismic gap, a 45 km-long section of the Dixie Valley fault that lies between endpoints of the 1915 Pleasant Valley and 1954 Dixie Valley earthquakes (Wallace and Whitney, 1984; Figure 1). The 2.0-3.4 ka fault ruptures discussed at previous stops overlap with the 1954 rupture zone to the south by about 20 km and continue northward into the Stillwater gap for a total distance of at least 46 km (Figure 1). Vertical offsets across the 2.0-3.4 ka fault ruptures average ~2-3 m and reach a maximum of 5-6 m about 4 km north of this location. The size of the late Holocene earthquake is estimated to be ~M_w7.3.

Lateral-spread paleoscarps

The large scarps at this location (Figure 2) are interpreted to have formed by severe ground failure (i.e., lateral spreading) related to liquefaction during the 2.0-3.4 ka earthquake. This area is only part of a more extensive zone of paleoliquefaction-related lateral spreading that disrupted the area along the fan piedmont-basin floor boundary for a distance of greater than 30 km (Figure 1). The lateral-spread interpretation of these features is based on: 1) the scalloped-shaped nature of the scarps; 2) an abundance of large fissure-like features along the zone, 3) the distribution of fragmented blocks or mounds that emanate from the head scarp in raft-like fashion (Figure 2); 4) the close proximity of the disrupted zone to the playa margin where the water table is shallow; 6) soft-sediment (liquefaction) features expressed locally on cleaned exposures of the disrupted sediments; and 6) the graben form of the structures and lack of net vertical offset across the graben. *Note that the lateral-spread features here at Dixie Hot Springs lack the graben form expressed at most of the other lateral spread areas*.

Age constraints are similar for the range-front fault ruptures and the lateral spread scarps (i.e., post-3.4 ka, and post 3.7-ka, respectively) (Caskey, Appendix 3-2; Lutz et al., 2002). Additionally, both the range-front and lateral spread scarps exhibit similar geomorphic expression with scarp slopes commonly holding up at the angle of repose (~30˚). These relations together with the observation that the liquefaction zone is centrally positioned along the late Holocene rupture trace (Figure 1) indicate that the fault ruptures and lateral spreads formed during the same 2.0-3.4 ka earthquake. Much smaller lateral spreads also formed locally along the base of the paleo-liquefaction features during the 1954 earthquake (Figure 1; also see Road Log descriptions between Stops 2-3 and 2-4).

Folded and imbricated lacustrine deposits

Other fascinating structural features which appear to be associated with the 2.0-3.4 ka liquefaction and lateral spreading are the intensely folded and “thrust” imbricated (i.e., shingled) lacustrine deposits found along the west margin of the playa (Figures 2 and 3). These severely compressed zones are found only in areas that are down-slope from the most intense lateral

spread zones which suggests a causative relationship. I interpret the compressed zones along the playa margin as areas that accommodated the down-slope movement of relatively cohesive material from the lateral spread zones. At Stop 3-3 we will observe and discuss structural relationships that are well-expressed across one of these compressed zones.

Alluvial and Lacustrine Stratigraphy

The lateral spread paleoscarps at Dixie Hot Springs formed on Qfm fan deposits (Bell, Appendix 1-3B; Bell and Katzer, 1989, 1990) that overlie lacustrine strata. Lateral spreading in this area was undoubtedly accommodated by liquefaction within the lacustrine deposits. Lateral spread scarps ~400 m to the south expose a 1-2 m-thick mantle of Qfm gravel above lacustrine strata that contain the 6.9 ka Mazama tephra (Sarna-Wojcicki, personal communication). The Mazama tephra lies at an elevation of ~1046 m (3430 ft). Approximately 15 km to the south, the Mazama tephra lies within fluvial deposits at an elevation of ~1055 m (3460 ft) along Dixie Settlement Rd. (See Road Log Addendum). These relations indicate that a sizeable 6.9 ka lake, with a high stand elevation between 1046-1055 m, occupied Dixie Valley. This translates to a maximum water depth of 19-28 m (compared to the 70 m depth of the 12-13 ka Lake Dixie high stand at 1097 m). Evidence for the existence of a Mazama-age pluvial lake in Dixie Valley is intriguing since lakes of this age have not been recognized in Lake Lahontan sub-basins to the west.

This stop is located at Alexander and Nettleton's (1977) study area where they described rapid development of post-Mazama Typic Natrargids. Chadwick et al. (1984) suggested that the Natrargids on the T2/F2 surfaces at Terrace Creek are better developed than those here at Dixie Hot Springs. So it might be interesting to compare soil development for the two areas. It's also a good place to look at surface characteristics of some of the younger variety Qfm fans. Note the patchy, but fairly well-developed desert pavement. Also of interest is the classic spalling of boulders and cobles in this area, apparently enhanced by mechanical weathering related to salt precipitation.

An interesting structural relation at this location, is that Qfm deposits east of the lateral-spread scarps are only represented as small, isolated blocks or mounds of material, that don't appear to fully account for the original areal extent of Qfm deposits. At most other locations along the 30-km-long paleoliquefaction zone (Figure 1), the lateral spreads are expressed as graben, across which there is no net vertical separation of the broken fan surfaces. So, one possibility is that there is a vertical tectonic component of offset along this part of the liquefaction zone which has resulted in down-faulting and burial of the Qfm surface east of the fault. However, this would apparently require more than about 5 m of vertical offset. This offset added to the 3-4 m of vertical offset along the range front in this area would result in a combined offset of 8-9 m for the 2.0-3.4 ka event - an unreasonably large amount of offset when compared to known offsets along single-event, historical normal fault ruptures (Caskey et al., 1996). Alternatively, the highly fragmented nature of Qfm remnants may suggest that significant flow failure and subsidence may have accompanied liquefaction. The apparent large amount of shortening across the compressed zone along the playa margin in this area, also suggests that down-slope lateral spread movements were particularly large in the Dixie Hot Springs area.

References

Alexander, E.B. and W.D. Nettleton, 1977, Post-Mazama Natrargids in Dixie Valley, Nevada, Soil Sci. Soc. Am. J., 41, 1210-1212.

Bell, J., and Katzer, T., 1990, Timing of late Quaternary faulting in the 1954 Dixie Valley earthquake area, central Nevada: Geology, v. 18, p. 622-625.

Bell, J. W., S. J. Caskey, A. R. Ramelli, L. Guerrieri, and A. M. Sarna Wojcicki, (in review Geology), Patterns and rates of faulting in the central Nevada seismic belt.

Caskey, S. J., Wesnousky, S. G., Zhang, P., and Slemmons, D. B., 1996, Surface faulting of the 1954 Fairview Peak (Ms7.2) and Dixie Valley (Ms6.9) earthquakes, central Nevada: Bulletin of the Seismological Society of America, v. 86, no. 3, p. 761-787.

Chadwick, O.A., S. Hecker, and J. Fonseca, 1984, A soils chronosequence at Terrace Creek: studies of late Quaternary tectonism in Dixie Valley, Nevada, US Geol. Survey Open File Report OFR 84-90.

Dohrenwend, J. C., Schell, B. A., Menges, C. M., Moring, B. C., and McKittrick, M. A., 1996, Reconnaissance photogeologic map of young (Quaternary and late Tertiary) faults in Nevada, Open File Report, OFR 96-2: Nevada Bureau of Mines and Geology, in cooperation with the U.S. Geological Survey, scale 1:1,000,000.

Lutz, S. Juch, S.J. Caskey, D.D. Mildenhall , P.R.L. Browne, and S.D. Johnson, 2002, Dating sinter deposits in northern Dixie Valley, Nevada - the paleoseismic record and implications for the Dixie Valley geothermal system, Proceedings, Twenty-Seventh Workshop on Geothermal Reservoir Engineering, Stanford University, Stanford, California, January 28-30, 2002, SGP-TR-171.

Wallace, R.E., and R.A. Whitney, 1984, Late Quaternary history of the Stillwater seismic gap, Nevada, Bull. of the Seism. Soc. of America, v. 74, no. 1, 301-314.

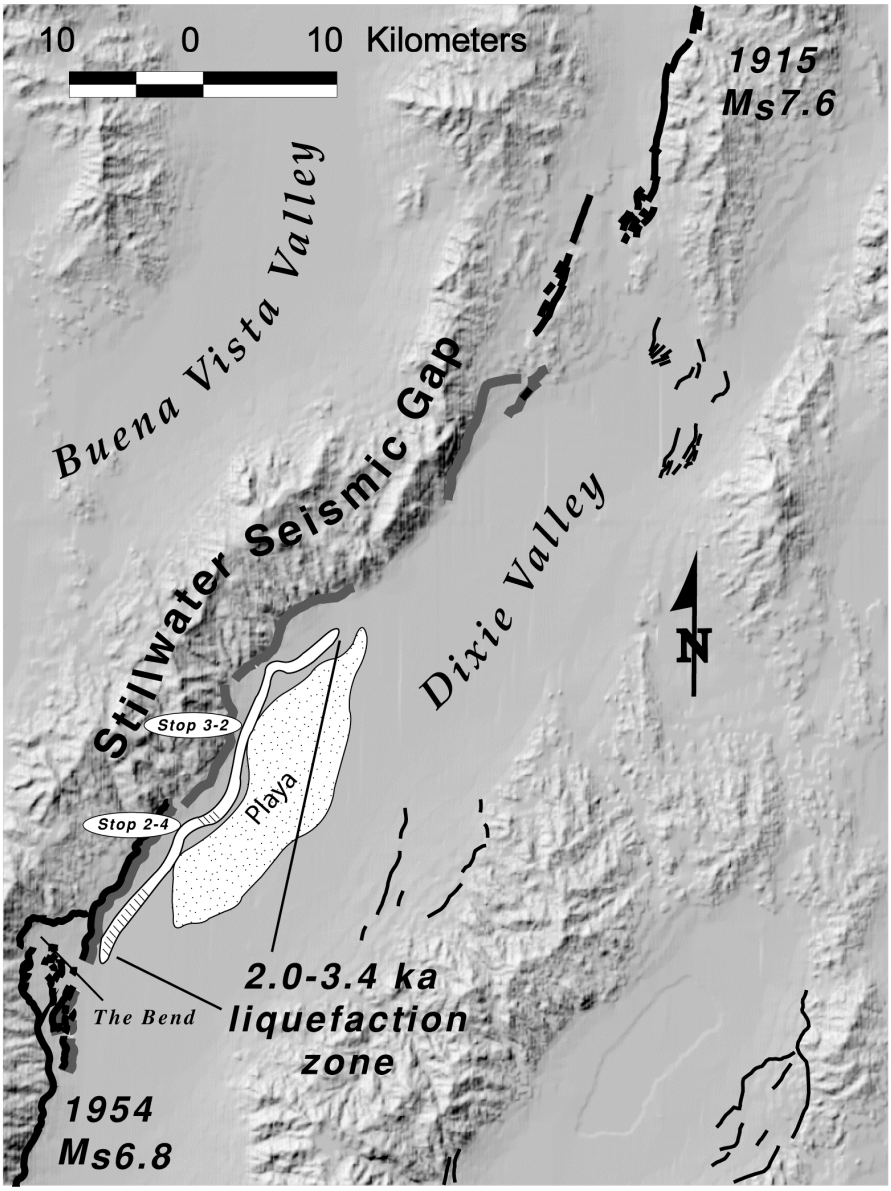

Figure 1 - Map of the Stillwater seismic gap region showing extensive zone of paleo-liquefaction formed during the 2.0-3.4 ka earthquake, and locations of Stops 2-4 and 3-2. 1915 Pleasant Valley and 1954 Dixie Valley earthquake ruptures are shown as thick black lines. Holocene ruptures along the Stillwater Range front are shown as thicker gray lines. The 2.0-3.4 ka fault ruptures overlap with the 1954 ruptures by about 20 km and extend for a total length of 46 km to just north of the playa. It is unknown whether the Holocene ruptures at the north end of the valley formed during the 2.0-3.4 ka event. Other late Pleistocene faults are shown as thin black lines (After Dohrenwend et al., 1996). Hatchered areas within the liquefaction zone show areas where 1954 liquefaction also occurred (Caskey et al., 1996).

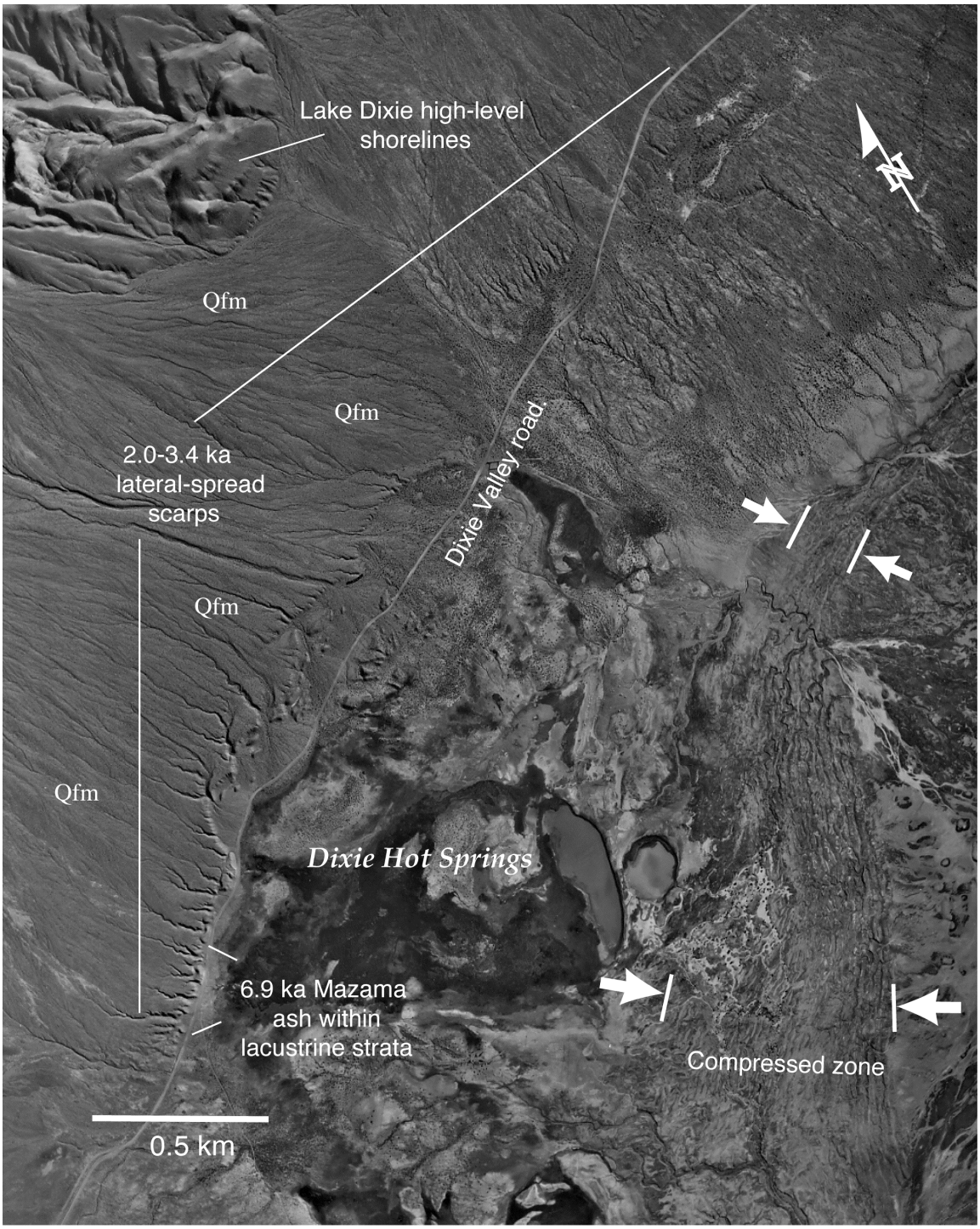

Figure 2 - Low-sun-angle aerial photograph of the Dixie Hot Springs area showing lateral spread paleoscarps developed on Qfm fan deposits and folded and thrust imbricated lacustrine deposits (compressed zone) along western margin of the playa. These features formed in response to liquefaction during the 2.0-3.4 ka Mw~7.3 earthquake that ruptured along the range-front fault. Note that the width and amount of the shortening within the compressed zone appears to relate to the intensity (amount(?) of the lateral spreading upslope.

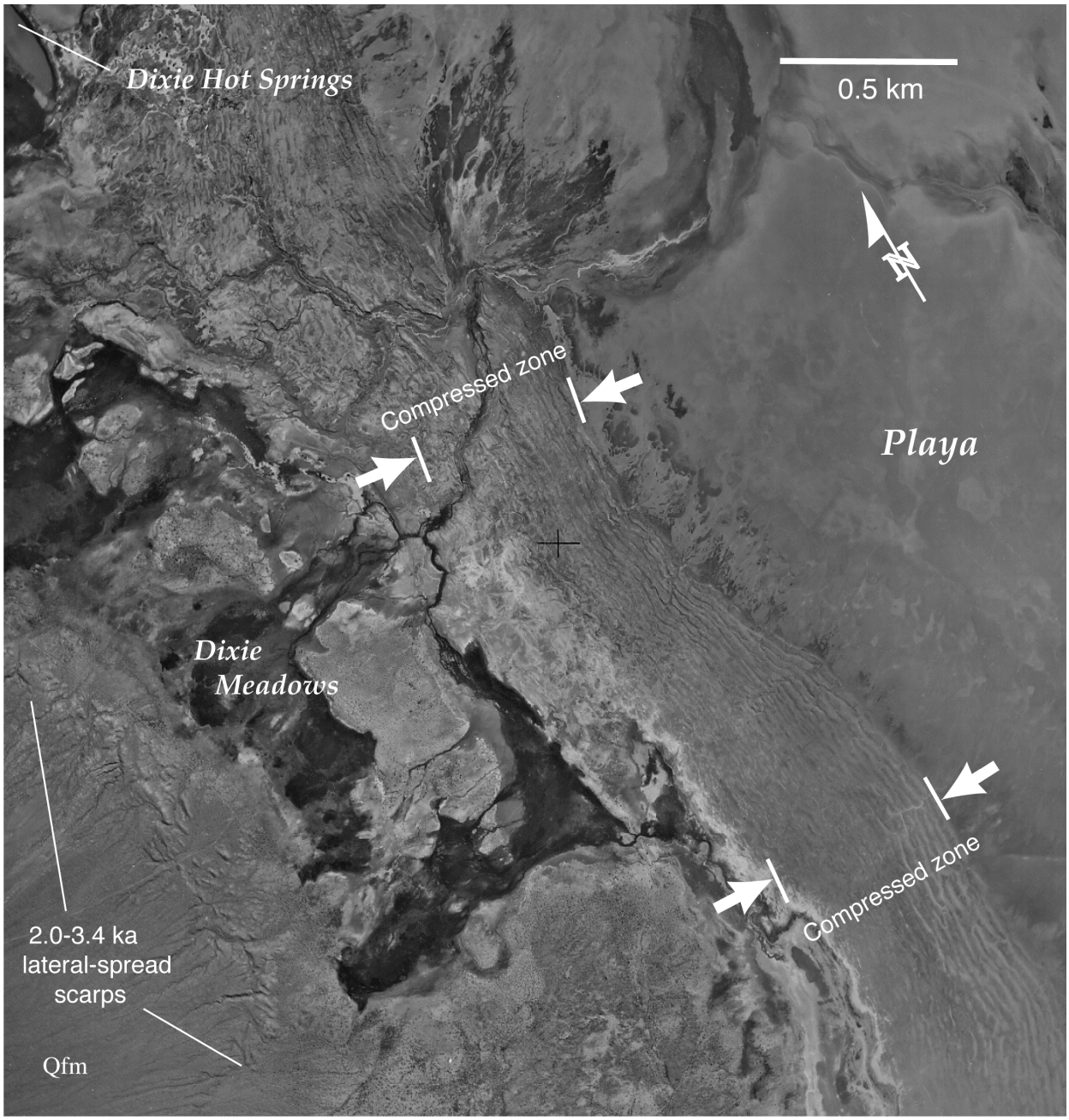

Figure 3 - Low-sun-angle aerial photograph of the area immediately south of the Dixie Hot Springs area showing lateral spread paleoscarps developed on Qfm fan deposits and folded and thrust imbricated lacustrine deposits (compressed zone) along western margin of the playa. These features formed in response to liquefaction during the 2.0-3.4 ka Mw~7.3 earthquake that ruptured along the range-front fault.

APPENDIX 3-1

Tectonic and Isostatic Deformation of Latest Pleistocene Lake Dixie Shorelines

John Caskey, Alan R. Ramelli, Eric W. Ford, Carolyn J. Domrose, Gary Schneider, Michael W. Goebel, Nathan W. Smith, Tandis S. Bidgoli, and Anne Marie Scherer

Dixie Valley, which is one of the topographically lowest tectonic depressions in the northern Great Basin (second only to the Pyramid Lake basin), was occupied by the latest Pleistocene pluvial Lake Dixie. Lake Dixie, at its highstand elevation of ~1097 m (3600 ft), had a surface area of 715 km^2, and had a maximum water depth of ~70 m (230 ft) (Mifflin and Wheat, 1979). The high shoreline has been radiocarbon dated from tufa at 12-13 ka (Thompson and Burke, 1973; Bell, unpublished data) indicating that the Lake Dixie highstand was approximately coeval with the Lake Lahontan highstand to the west (Broeker and Kaufman, 1965; Benson and Thompson, 1987; Adams and Wesnousky, 1998).

Lake Dixie shorelines

Lake Dixie highstand shorelines locally preserved along the west side of the valley generally occur on the steep frontal escarpment of the Stillwater Range (i.e., footwall of the Dixie Valley fault). Here they consist primarily of wave-cut strandlines and cemented beach-rock ledges (Figure 1). These types of high-level shoreline features approximate the highstand elevation, but it's possible that the lake rose higher than these levels without leaving an "indelible" record of the highstand. Further, Adams et al. (1999) found that high-level shoreline angles of wave-cut terraces in the Lahontan basin are consistently 1-3 m lower than the crests of adjacent constructional (i.e., depositional) beach ridges. Therefore, the high-level erosional strandlines and cemented beach-rock ledges on the west side of the valley represent only a minimum measure of the highstand elevation. In contrast, well-preserved high-level shorelines on the east side of the valley consist entirely of constructional beach gravel ridges developed on older alluvial fan surfaces. Elevations of these shorelines represent a more direct and maximum measure of the highstand. Adams et al. (1999) reported a natural, local variation in highstand beach-ridge elevations of up to 3 m in the Lahontan basin. The smaller fetch and lower maximum wave heights expected for the smaller Lake Dixie suggest that the natural variation of beach-ridge elevations in Dixie Valley should be considerably smaller than for Lake Lahontan. In any case, the high-level shorelines generally provide a paleo-horizontal datum from which to assess post-13 ka deformation in the valley.

Tectonic displacement of shorelines across the Dixie Valley fault

At Stop 3-1 (Figure 1), high-level shorelines are vertically displaced across the 2.0-3.4 ka fault scarps by up to 5 m (16 ft) (Figure 2). Thompson and Burke (1973) first recognized the offset shorelines. They mapped and conducted a survey of the shorelines using a hand level and altimeter (Thompson, personal communication) and concluded that the shorelines were offset vertically by ~9 m (30 ft). From this estimate, they calculated a post-highstand slip rate for the Dixie Valley fault of ~1 mm/yr. Because the 2.0-3.4 ka scarps exhibit a maximum vertical offset of only about 5 m, the 9 m of vertical offset measured by Thompson and Burke (1973) would

require multiple, post-12 ka faulting events. Recent mapping along the entire fault trace within the Stillwater gap (Caskey, in preparation) has revealed no evidence for multiple Holocene fault offsets such as beveled scarps or differing vertical offsets on surfaces of different ages at a given location. For this reason we resurveyed the shoreline elevations with a total station. We carefully identified the highest shoreline features at the locations mapped by Thompson and Burke (1973). The high-level shorelines are marked by cemented beach rock plastered on the range-front escarpment (southernmost site) (Figure 2), a shoreline angle of a wave-cut terrace (middle site), and high-shoreline gravel on a V-bar complex (northernmost site). Both the southernmost and middle sites lie in the uplifted footwall of the fault. The high shoreline gravel at the northernmost site lies in the down-dropped hanging wall block. We find that the high-level shorelines identified by Thompson and Burke are vertically offset by only ~5 m across the fault (Figure 1), identical to the offsets measured across fault scarps in this area (e.g., Figure 2). Our results indicate that the hand-level/altimeter technique used by Thompson and Burke did not provide accurate results and that the slip-rate estimate of ~1 mm/yr for the Dixie Valley fault based on their shoreline survey is too high.

Isostatic deformation of shorelines across Dixie Valley

Measurements of highstand shoreline elevations in the Lahontan Basin (Mifflin and Wheat, 1971; Adams et al., 1999) show that the region to the west of Dixie Valley has isostatically rebounded as much as 22 m due to crustal unloading related to post-13 ka desiccation of Lake Lahontan (Figure 3). The area of greatest upwarping corresponds to the Carson Sink area (Figure 3) where the largest volume of water produced the greatest crustal load in pluvial times. The pattern of isostatic rebound contours of Adams et al. (1999) suggests that we might expect to see 6 or more meters of eastward tilting across Dixie Valley. Because the lakes were coeval, it follows that the eastward tilting should be expressed by broad deformation of originally horizontal, Lake Dixie shorelines. To test this hypothesis and potentially provide peripheral data for details of the Lake Lahontan rebound signal, we collected elevation measurements at 16 sites along the Lake Dixie highstand shoreline (Figure 4). Along the west side of the valley we were able to accurately survey elevations with a total station by utilizing the numerous National Geodetic Survey benchmarks established along Dixie Valley Road. A lack of benchmarks on the east side of the valley required us to measure shoreline elevations using a differential GPS array tied to a known elevation on the west side of the valley. We employed Trimble 4000Ssi GPS receivers which enabled us to achieve centimeter-level vertical and horizontal accuracy. The largest source of uncertainty in the GPS measurements comes from the estimated geoid separation (i.e., difference between GPS height and elevation above mean sea level), which is likely on the order of a few decimeters.

The distribution of high shoreline elevations show convincingly that broad regional-scale deformation, likely related to isostatic rebound of Lake Lahontan, is recorded by Lake Dixie shorelines. This is expressed by ~6 m of difference in shoreline elevations between the northeast (~1092 m) and west shores (~1098 m) and ~4 m of difference between the north and southeast shores (1092 m and 1096 m, respectively). Shoreline elevations along the east shore show a distinct, gradual trend of increasing elevation to the southeast, consistent with significant eastward tilting across the region.

An understanding of the details of the rebound recorded across Dixie Valley is complicated by at least two factors:

1) We are comparing constructional shoreline features on the east side with strandlines and erosional features on the west side. Because the constructional features on the east shore represent maximum highstand elevations and the strandline elevations on the west shore represent minimum highstand elevations, we consider the differences in shoreline elevations across the valley to be a minimum estimate of the amount of deformation.

2) Comparisons of shoreline elevations across the valley are also complicated by the large Holocene fault ruptures that offset shorelines along the west shore. The high shorelines along the west shore generally lie in the uplifted footwall of the 2.0-3.4 ka fault ruptures in an area where vertical offsets average about 4-5 m. The east shore lies in the hanging wall. An obvious question is: How much of the vertical offset measured across the fault (i.e., 4-5 m) would be expressed as changes in relative elevation (between points on the footwall and hanging wall) in the far field, say across distances equal to the width of Dixie Valley (~15 km)? Detailed geodetic leveling across the 1983 Borah Peak, Idaho earthquake rupture (Figure 5; Stein and Barrientos, 1985; Barrientos et al., 1987) shows that a point on the footwall near the fault exhibits a small change in elevation relative to a point on the hanging wall 15 km away from the fault rupture. In this example, the change in relative elevation (at 15 km) is equal to only about 20% of the amount of offset across the fault. This would equate to only about 1 m of elevation change across Dixie Valley (i.e., 20% of 5 m). It's important to note that the far-field displacement signal is contingent upon fault geometry. However, the Lost River fault, which ruptured during the Borah Peak earthquake, and the Dixie Valley fault in the Stillwater gap area both dip 45-50˚, supporting the use of the Borah Peak earthquake as an analogue.

In conclusion, we suggest that the ~6 m of difference in high shoreline elevations mainly reflects eastward tilting of the Dixie Valley region in response to isostatic rebound of the Lake Lahontan basin. We are able to generally project Adams et al.'s (1999) rebound contours across Dixie Valley (Figure 4) with only minor alterations.

References

Adams, K.D. and S.G. Wesnousky, 1998, Shoreline processes and the age of the Lake Lahontan highstand in the Jessup embayment, GSA Bulletin, 110, no. 6, p. 1318-1332.

Adams, K.D., S.G. Wesnousky, and B.G. Bills, 1999, Isostatic rebound, active faulting, and potential geomorphic effects in the Lake Lahontan basin, Nevada and California, GSA Bulletin, v. 111, no. 12, 1739-1756.

Barrientos , S.E., R.S. Stein, and S.N, Ward, 1987, Comparison of the 1959 Hebgen Lake, Montana and the 1983 Borah Peak, Idaho, earthquakes from geodetic observations, Bull. of the Seism. Soc. Am., v. 77, no. 3, 784-808.

Benson, L.V. and Thompson, R.A., 1987, Lake-level variation in the Lahontan basin for the past 50,000 years: Quaternary Research, v. 28, p. 69-85.

Broecker, W.S. and Kaufman, A., 1965, Radiocarbon chronology of Lake Lahontan and Lake Bonneville II, Great Basin: Geological Society of America Bulletin, v. 76, p. 537-566.
Mifflin, M. D., and Wheat, M. M., 1971, Isostatic rebound in the Lahontan basin, northwestern Great Basin, GSA Abstracts with Programs, v. 3, p.647.
Mifflin, M. D., and Wheat, M. M., 1979, Pluvial lakes and estimated pluvial climates of Nevada. Nevada Bureau of Mines and Geology Bulletin 94, 57 p.
Reheis, M., 1999, Extent of Pleistocene lakes in the western Great Basin, U.S. Geol. Surv. Misc. Field Studies Map MF 2323, (online version).
Stein, R.S., and S.E. Barrientos, 1985, Planar high-angle faulting in the Basin and Range: geodetic analysis of the 1983 Borah Peak, Idaho earthquake, Jour. of Geophys. Res., 90, 355-366.
Thompson, G.A., and D.B. Burke, 1973, Rate and direction of spreading in Dixie Valley, Basin and Range province, Nevada, GSA Bull., 84, 627-632.

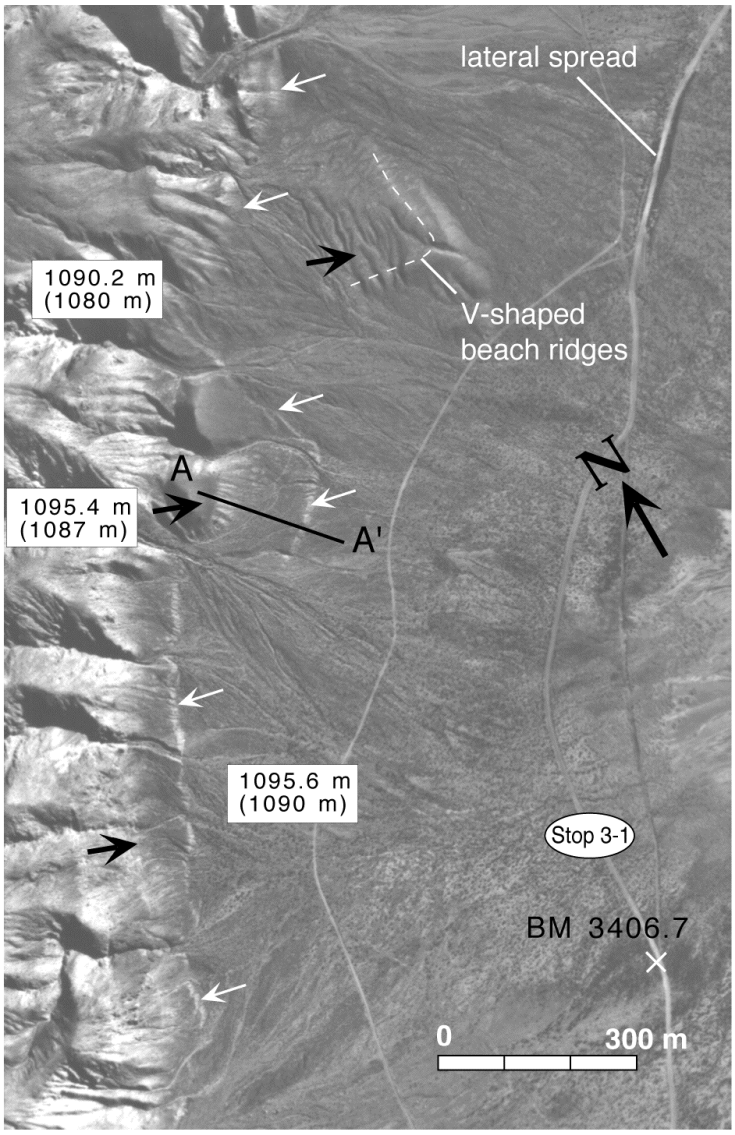

Figure 1 - Low-sun-angle photograph showing Thompson and Burke's (1973) shoreline survey site (Stop 3-1) and high-level pluvial Lake Dixie shorelines (black arrows) (see Road Log, Figure 1 for location). Also note the location of Profile A-A' (Figure 2). Elevations resurveyed using a total station are shown in comparison to Thompson and Burke's altimeter elevations (in parentheses). Elevations are calibrated to the NGS benchmark (elevation 3406.7 ft) shown along the old Dixie Valley road. White arrows show the trace of the 2.0-3.4 ka fault rupture. The modern Dixie Valley road is not on the photo.

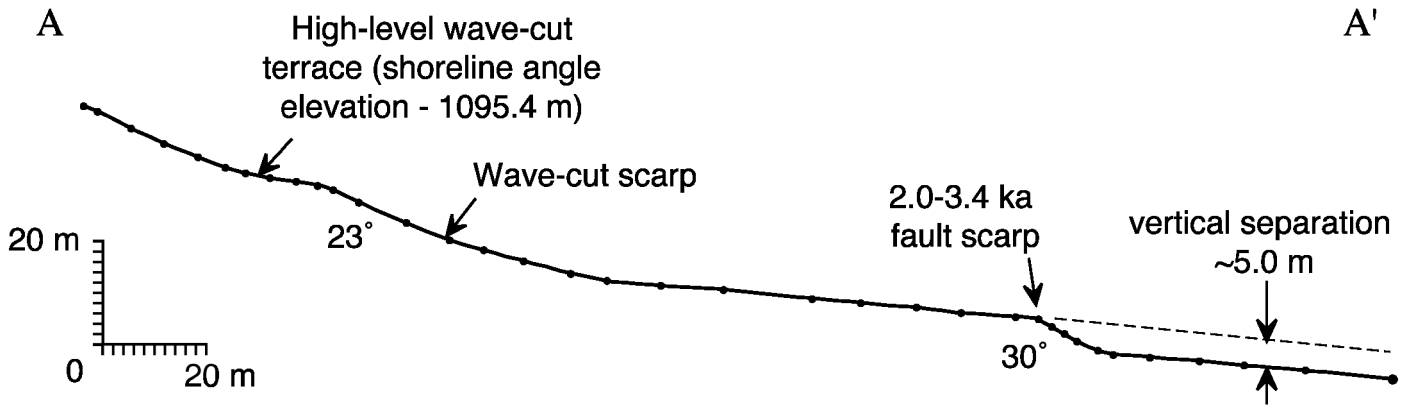

Figure 2 - Total Station profile A-A' across the wave-cut terrace and late Holocene fault scarp (middle survey site, Figure 1). Scarp-slope angles are shown for both the 12-13 ka wave-cut scarp and the 2.0-3.4 ka fault scarp.

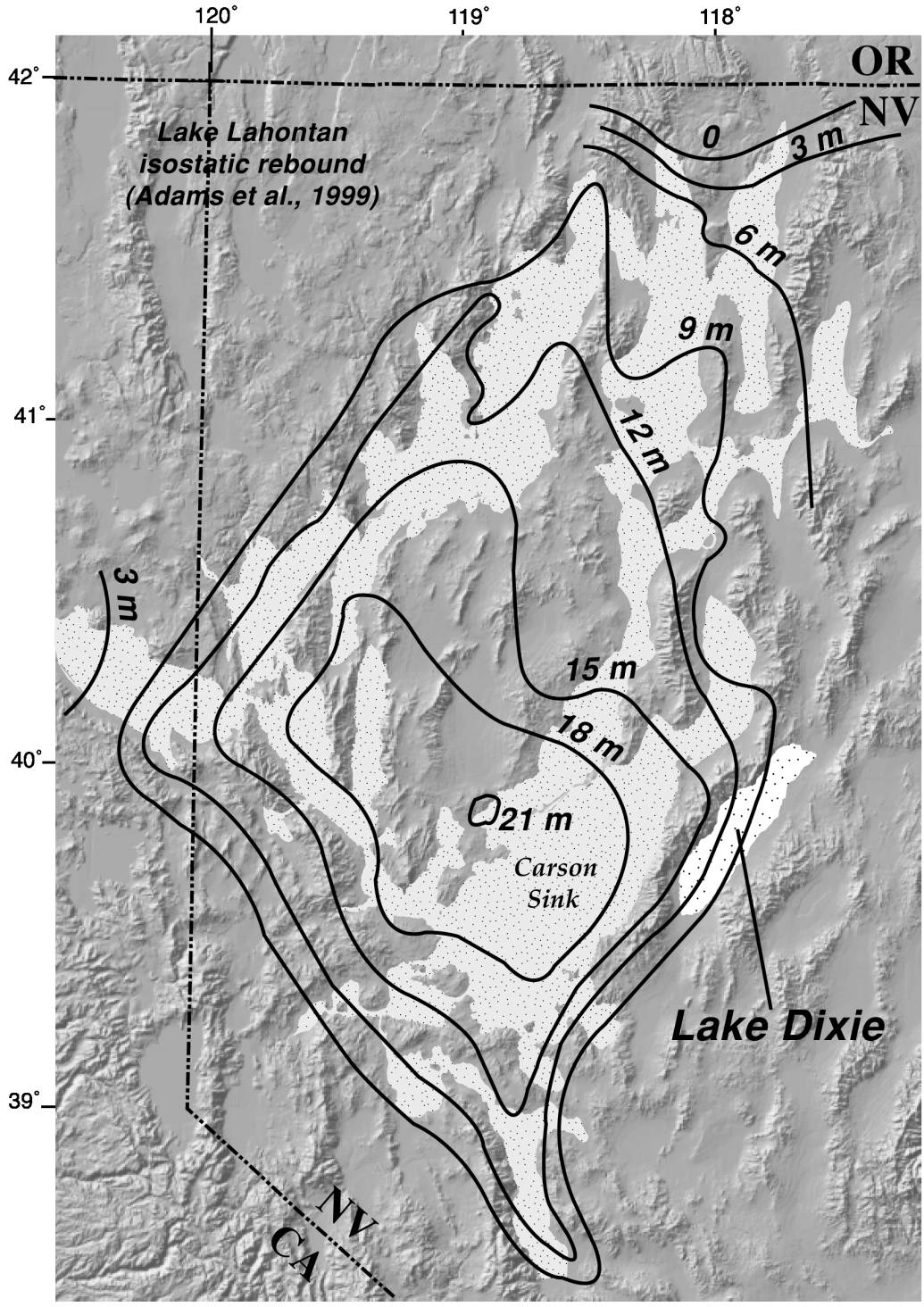

Figure 3 - Contours of estimated isostatic rebound from post-13 ka desiccation of Lake Lahontan. (adapted from Adams et al., 1999). Coutour interval is 3 meters. Based on projections of the rebound contours east of the Lahontan basin, 6 or more meters of rebound might be expected across Dixie Valley. Base map and lake outlines from Reheis (1999).

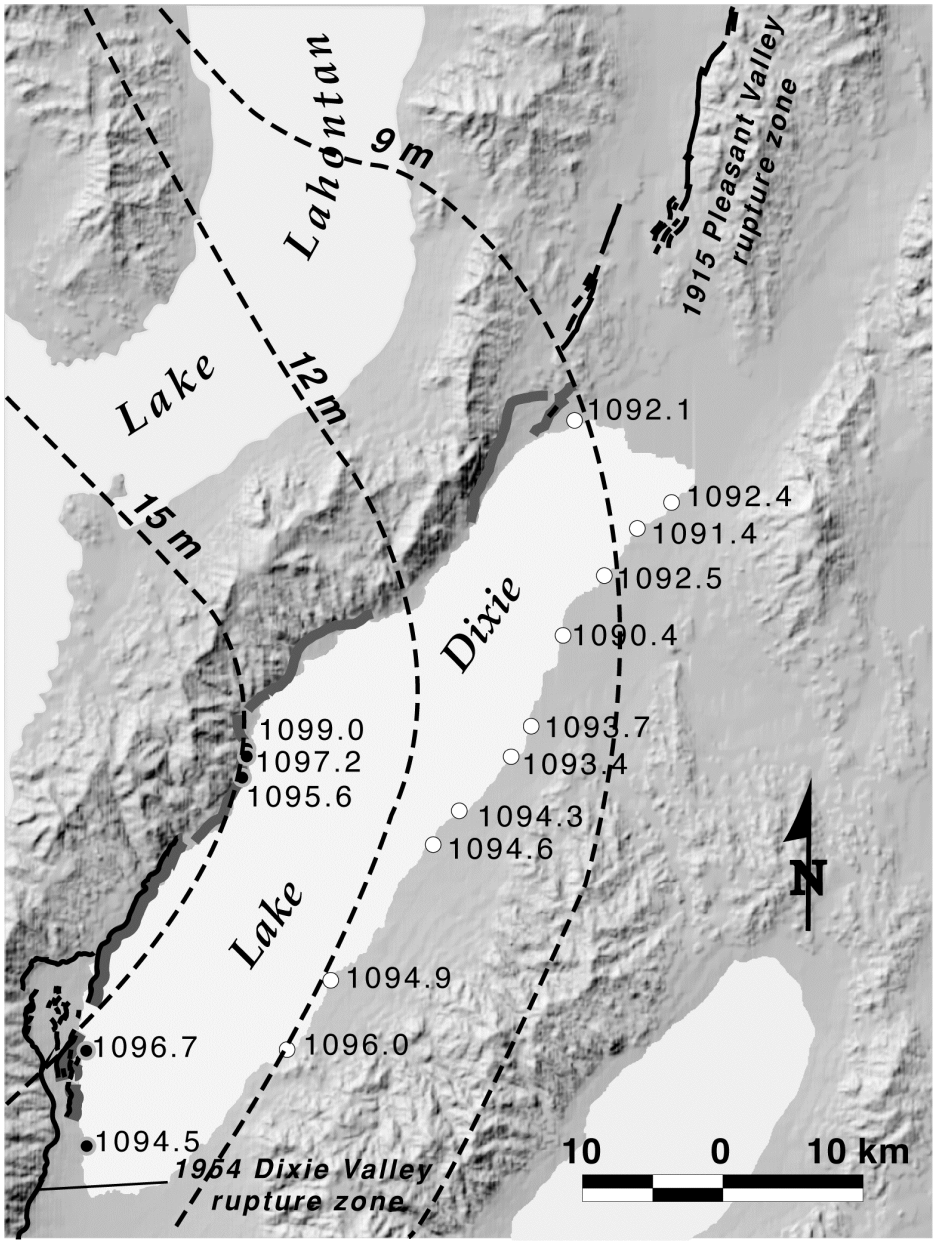

Figure 4 - High-level shoreline elevations for Lake Dixie and partial contours of estimated post-13 ka isostatic rebound of the Lake Lahontan basin (modified after Adams et al., 1999). Coutour interval is 3 meters. Shoreline elevations on the east and north shore (white circles) are from beach ridges deposited on older alluvial fans. Those on the west shore (gray and black circles) represent the highest identified shorelines at those locations, but consist of cemented beach rock, erosional strandlines, high shoreline gravel, and a high-level beach ridge (southernmost elevation) that don't necessarily record the maximum highstand elevation. Rebound contours of Adams et al. (1999) are modified to reflect about 4 m of difference in shoreline elevations along the east side of the valley, and a ~6 m difference between shorelines on the northeast and west shores. Base map and lake outlines from Reheis (1999).

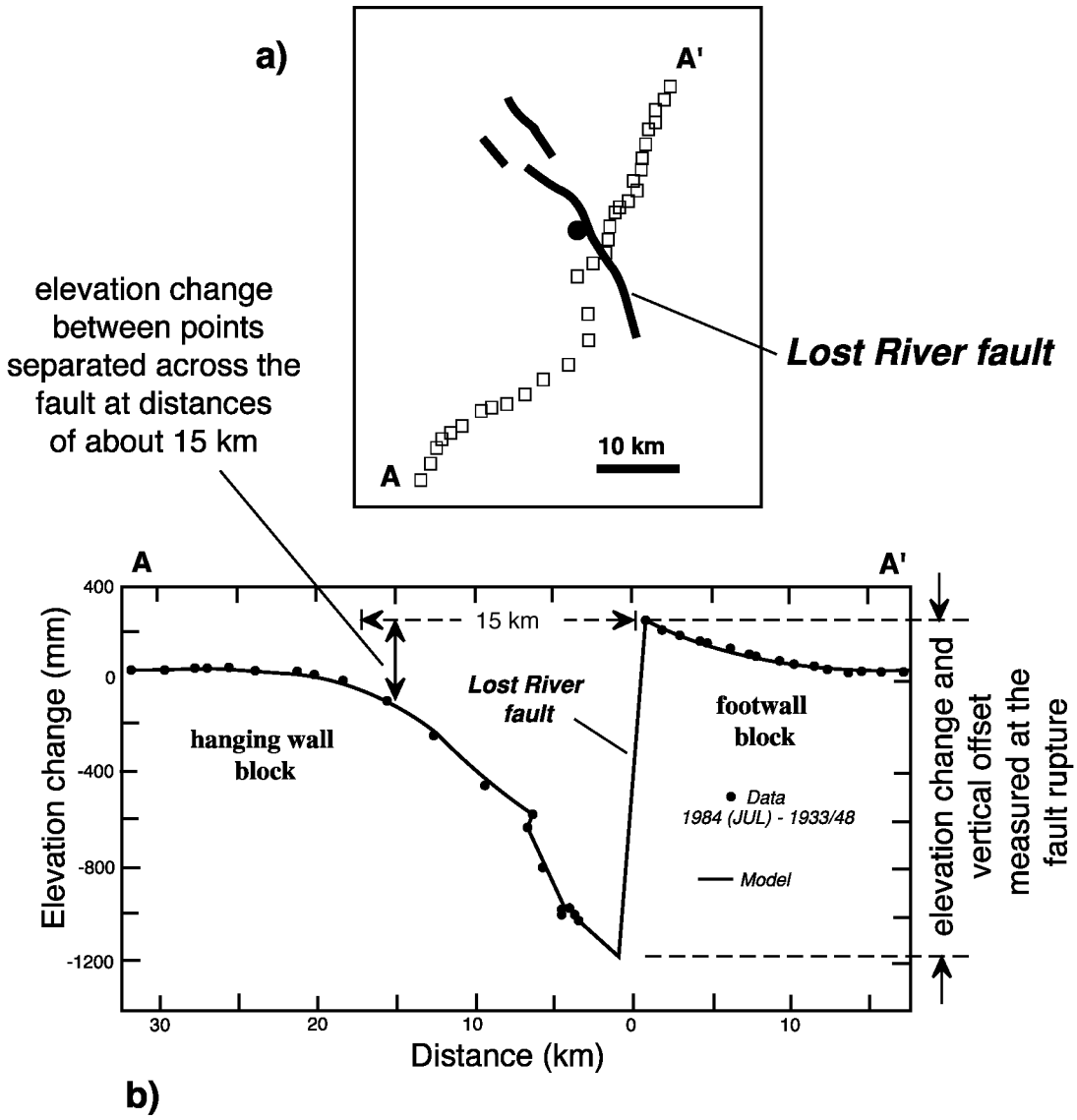

Figure 5 - a) Map view of the geodetic leveling route (A-A') across the 1983 Borah Peak earthquake rupture on the Lost River fault, central Idaho. b) Elevation changes along leveling route A-A'. Solid circles represent the leveling data. The plot shows that relative elevation change between points separated across the fault by about 15 km is only equal to a small percentage of the vertical offset measured at the fault rupture. Lake Dixie is only about 15 km wide, so we would expect one meter or less in the the change in elevation of the high shorelines due to the Holocene rupture on the west side of the valley. Figures modified after Stein and Barrientos (1985), and Barrientos et al. (1987).

APPENDIX 3-2

Age of Faulting in the Stillwater Gap and Lateral-spread-induced Contraction along the Playa Margin

John Caskey

The large graben at Stop 3-2 (Figure 1) is interpreted as a lateral spread formed by seismically-induced liquefaction of subsurface, water-saturated sediments – most likely pluvial lacustrine deposits. The liquefaction features in this area are just part of the nearly continuous, 30 km-long zone of lateral spreading that extends from The Bend area to about 10 km north of this site (Appendix 2-4, Figure 1). As discussed at Stop 2-4, it is fairly certain that the severe ground failure along this 30 km-long zone formed during the M_w~7.3 earthquake that ruptured along the piedmont fault zone in The Bend and northward into the Stillwater gap for a minimum total distance of 45 km. Because the Stillwater gap marks one of only two significant seismic gaps within the central Nevada seismic belt (the other being the White Mountains seismic gap), the paleoseismic history of faulting in this area has drawn the attention of many geologists, most noteably Wallace and Whitney, 1984.

Bell and Katzer (1987, 1990) bracketed the age of Holocene faulting in The Bend area from stratigraphic relations at 1.5-6.9 ka. Hecker (1985) used morphologic scarp dating techniques and 27 scarp profiles along the Holocene rupture trace between The Bend and Dixie Comstock (Figure 1) and determined a range of mean scarp ages of 2.6-2.9 ka with a more conservative age range of 1.1-7.5 ka. Similarly, Pearthree (1990) using 24 scarp profiles determined a range of mean scarp ages in this area at 2.4-3.0 ka. Although these more tightly bracketed, late Holocene age estimates are consistent with the youthful expression of the scarps, the age of faulting has previously not been as tightly constrained by direct stratigraphic and structural relations. For this reason, an exploratory trench was excavated across the graben at this site (Figure 1). The hope was to find a well-stratified and well-preserved record of pre- and post-seismic deposition that would enable us to determine the age of faulting. In this sense, the lateral-spread graben is used as a proxy indicator for the age of faulting at the range front.

Trench results

The trench was excavated across part of the 45 m-wide graben, and exposed a 9 m-thick section of Qfm alluvium truncated by the lateral-spread head scarp on the west side of the graben (Figure 2). Depositionally overlying the head scarp is a large colluvial wedge that extends and thins eastward across the width of the exposure. The wedge shows distinct eastward-inclined layering where it laps onto the head scarp. A 3 m-thick section of graben fill overlies the colluvial wedge. The graben fill consists primarily of well-stratified silty material with thin intertongues of gravel colluvium that thicken toward the scarp. The well-stratified silty deposits likely represent eolian material that has been slightly reworked or modified during wet periods. The silty deposits are overlain by ~1 m of alluvial gravel that is probably derived from the deep incisions into Qfm alluvium adjacent to the trench. *It's interesting to note that the scarp on the west side of the graben, prior to infilling of the graben, was about 10 m high! You can get a feel for the scale of the structure when standing on the floor of the trench while looking up to the scarp crest.*

The fine grained graben fill consists of numerous burn layers with locally abundant charcoal and a 2-3 cm-thick Mono Craters tephra layer that extends across the entire section of graben fill and laps onto scarp-derived colluvium to the west. Radiocarbon ages from four of the burn layers range from 1.8-1.0 ka, with all ages in correct stratigraphic sequence. The 1.0 ka date is from charcoal sampled just below the tephra layer indicating an age for the tephra that is similar to other Mono Craters tephra found in this region. Organic-rich sediment sampled from the distal, westernmost exposure of the colluvial wedge yielded an age of 2.0 ka. A hand excavation at the bottom of the trench exposed a 0.5 m section of moderately oxidized gravel with distinct, partially decomposed roots, some of which are up to 1 cm thick. These partially decomposed roots are absent in the overlying colluvial gravel. I interpret the oxidized gravel in the lowermost part of the trench as Qfm alluvium that is buried beneath scarp derived colluvium. A bulk sample from the buried Qfm alluvium, which contained some of the partially decomposed roots, yielded and a radiocarbon age of 3.7 ka. Based on these interpreted stratigraphic relations and radiocarbon ages, the earthquake that produced the lateral spreading occurred after 3.7 ka (age of the buried Qfm alluvium) and before 2.0 ka (age of scarp-derived colluvium).

A more recent study by Lutz et al. (2002) along the range front fault, 15 km to the north, provides an additional constraint on the age of faulting in this area. A radiocarbon age from faulted alluvium, which is interbedded with opaline sinter, yielded a radiocarbon age of 3.4 ka, thus providing a slightly lower maximum age of faulting than determined at the trench site. We are currently in the process of trying to date minor amounts of organic material that is present within the dense impermeable sinter deposits to provide additional and perhaps more reliable age constraints than bulk sample ages generally allow.

In conclusion, the 2.0-3.4 ka age of faulting, constrained by radiocarbon ages and stratigraphic and structural relations in the trench and along the range-front fault, is very consistent with the morphological scarp ages (2.4-3.0 ka) determined by Hecker (1985) and Pearthree (1990).

Lateral-spread-induced contraction along the playa margin (Stop 3-3)

As discussed at Stop 2-4, the “compressed zone” along the playa margin is interpreted as being caused from the catastrophic, basinward movement of material from the lateral-spread zone. At Stop 3-3 (Figure 1), the compressed zone is not as dramatically expressed as it is at other locations. However, at this location the playa margin is easily accessible, and the exposures reveal some great structural and stratigraphic relations.

At the edge of the playa, lacustine strata are severely buckled up along folds and imbricate “thrusts” that parallel the edge of the playa across a width of ~100 m. Cleaned exposures across the 100 m transect (Cross section A-A’, Figure 1 and 3b) revealed 14 different exposures of deformed Mazama ash. The ash bed, at most locations, dips to the east indicating that the strata is repeated along multiple west-vergent “thrusts” and folds. The ash bed is overlain almost everywhere by a thick, well-indurated salt layer that has apparently given rigidity to the lake sediments and allowed for the development of the somewhat regular “fold and thrust belt” geometry of the compressed zone. Bedding attitudes at each of the 14 tephra exposures, a total station profile accurately marking each exposure, and a hand dug pit that revealed the depth to the Mazama ash east of the deformed zone provided constraints for a detailed, reconstructable

cross section along the transect (Figure 3b). The cross section was constructed in such a way as to minimize the amount of shortening represented by the folds and thrusts. Although the cross section does not represent a unique solution for the observations, it appears to be reasonable.

The cross section indicates a minimum of 27 m of shortening across the compressed zone at this location. It stands to reason that the amount of shortening across the compressed zone should approximately balance with the amount of down-slope spreading across graben directly upslope from the playa. Although lateral spreads formed across the entire area between the playa margin and the large graben at the trench site, the greatest spreading probably occurred across the largest graben. At the trench site, the graben width is ~43 m. The 27 m of (minimum) shortening across the playa margin suggests that a significant portion of the graben width was produced by actual down-slope movement of the "detached" alluvium (Figure 3a). It's quite mind boggling to picture huge areas of the piedmont simultaneously sliding basinward for distances of tens of meters. The areal extent of severe ground failure related to liquefaction during the 2.0-3.4 ka earthquake is estimated at 20-30 km^2.

References

Bell, J.W., and Katzer, T., 1987, Surficial geology, hydrology, and late Quaternary tectonics of the IXL Canyon area, Nevada: Nevada Bureau of Mines and Geology Bulletin 102, 52.

Bell, J.W., and Katzer, T. 1990, Timing of late Quaternary faulting in the 1954 Dixie Valley earthquake area, central Nevada: Geology, v. 18, p. 622-625.

Hecker, S., 1985, Timing of Holocene Faulting in Part of a Seismic Belt, MS thesis, University of Arizona, 41 pp.

Lutz, S. Juch, S.J. Caskey, D.D. Mildenhall , P.R.L. Browne, and S.D. Johnson, 2002, Dating sinter deposits in northern Dixie Valley, Nevada - the paleoseismic record and implications for the Dixie Valley geothermal system, Proceedings, Twenty-Seventh Workshop on Geothermal Reservoir Engineering, Stanford University, Stanford, California, January 28-30, 2002, SGP-TR-171.

Pearthree, A.P., 1990, Geomorphic Analyses of Young Faulting and Fault Behavior in Central Nevada. PhD thesis, University of Arizona, 211 pp.

Wallace, R.E., and R.A. Whitney, 1984, Late Quaternary history of the Stillwater seismic gap, Nevada, Bull. of the Seism. Soc. of America, v. 74, no. 1, 301-314.

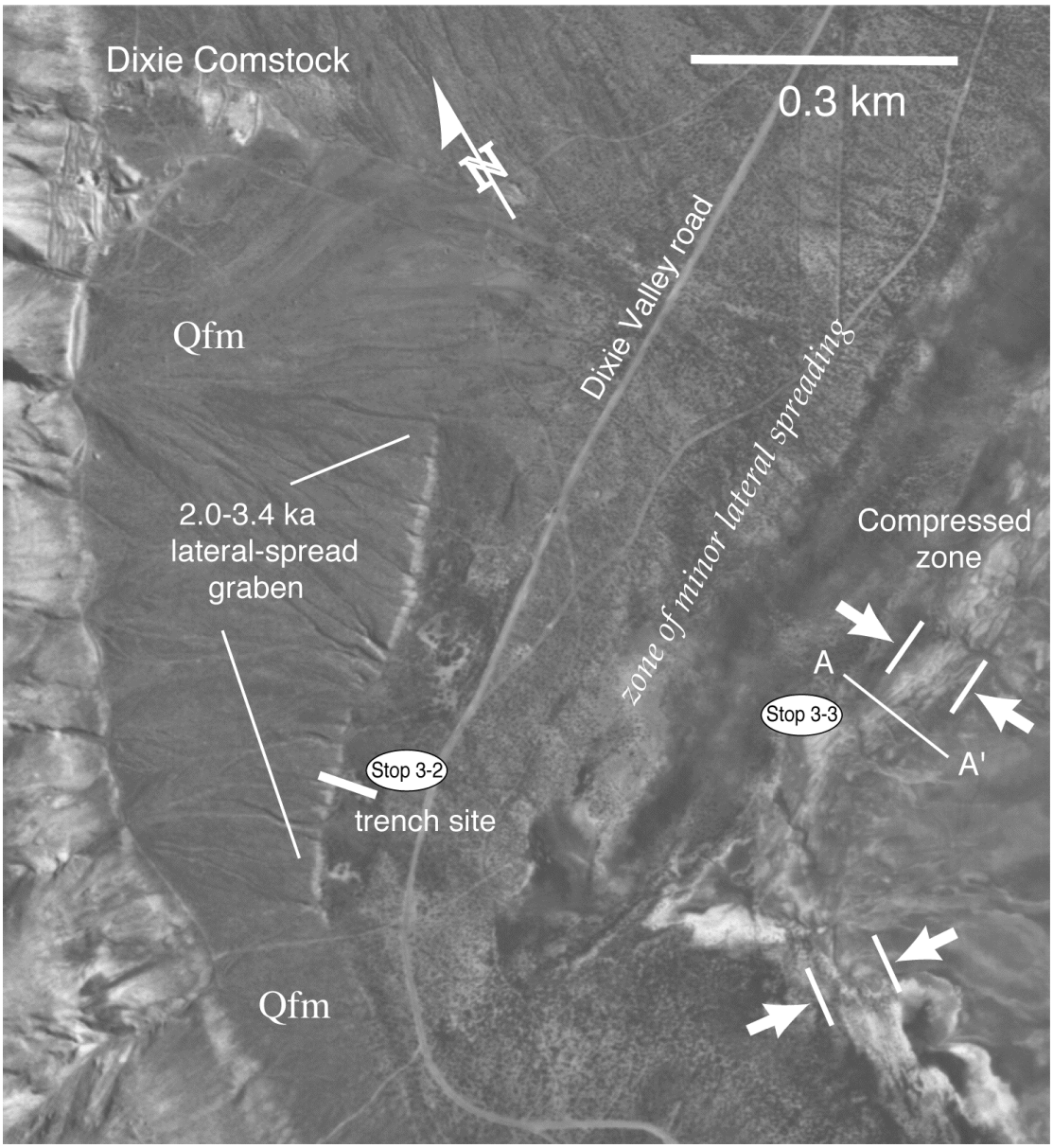

Figure 1 - Low-sun-angle photograph of the Stillwater gap trench site area (Stop 3-2; see Road Log, Figure 1 for location). The trench was excavated across a large lateral-spread graben (Figure 2). Note location of cross section A-A' across the compressed zone on the playa margin (Figure 3).

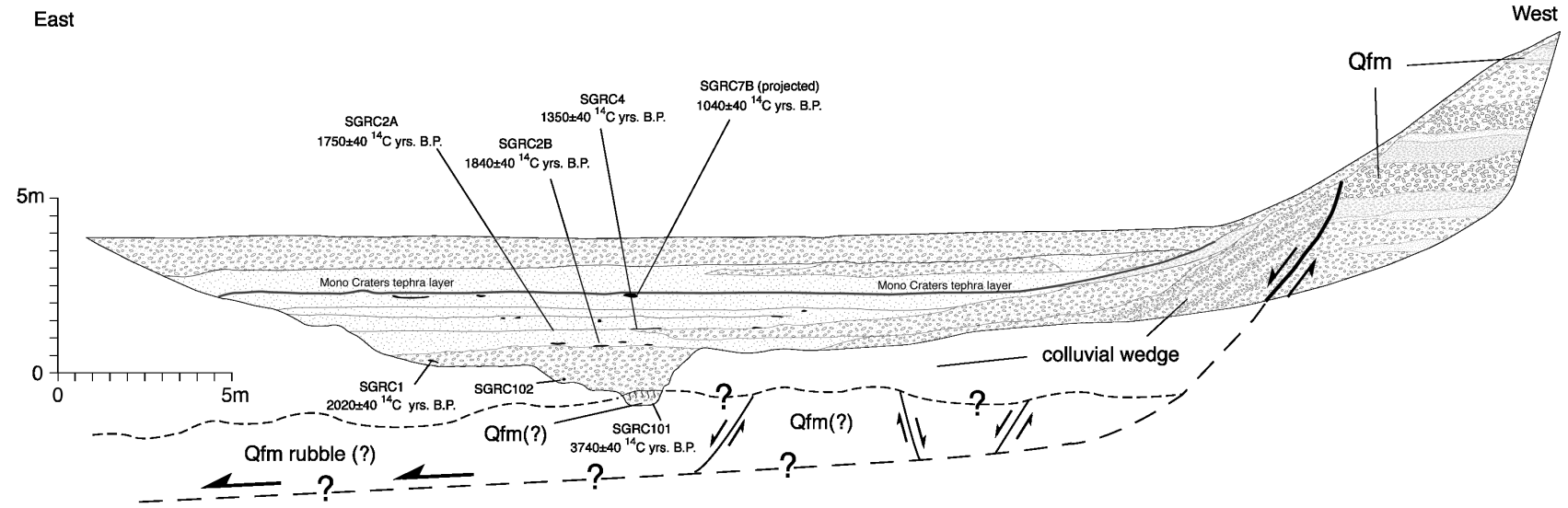

Figure 2 - Trench log across part of the lateral-spread graben south of Dixie Comstock (Figure 1). The age of the earthquake that produced the lateral spread is bracketed between 3.7 ka, a bulk radiocarbon age of a paleo-root zone in deposits inferred to be Qfm fan gravel beneath the large coluvial wedge (sample SGRC101)), and 2.0 ka, the radiocarbon age of organic material sampled from the easternmost exposure of the coluvial wedge (sample SGRC1). The structure shown beneath the trench log is conceptual, but based on similar structure exposed in a trench across a large lateral-spread graben located about 10 km to the north.

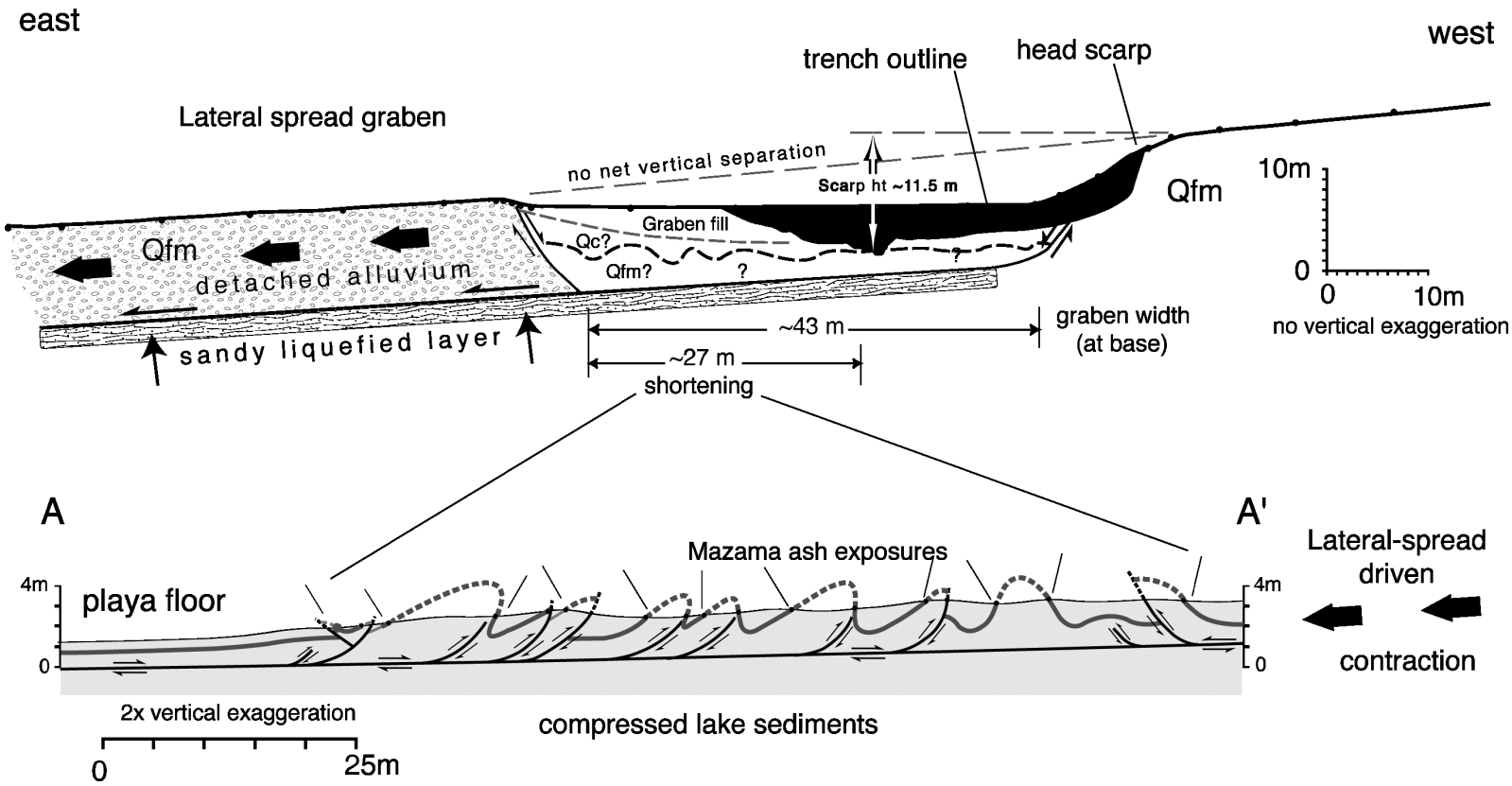

Figure 3 - a) Conceptual cross section across the lateral-spread graben south of Dixie Comstock. b) Cross section A-A' across the playa-margin compressed zone located down-slope from the lateral spread graben in a) (see Figure 1 for location). Cross section is constrained from attitudes of 14 repeated beds of 6.9 ka Mazama ash exposed across the zone of folded and thrust-imbricated lacustrine sediments and a test pit excavated into the playa floor east of the disrupted zone (note east is to the left). The deformed beds are interpreted to be the result of accomodation of the down-slope movement of relatively cohesive Qfm fan deposits above a liquefied zone of water-saturated lacuctrine sand. Cross section A-A' suggests approximately 27 meters of shortening across the zone. (Note that shortening was calculated from a non-vertically exaggerated version of the cross section). The graben width is about 43 meters, suggesting that much of that width represents actual down-slope movement of the detached alluvium east of the graben. Note that both figures are shown at the same horizontal scale. The two cross sections are separated by a down-slope distance of about 300 m.